Aus dem Bereich Physiologie

Theoretische Medizin und Biowissenschaften

der Medizinischen Fakultät

der Universität des Saarlandes, Homburg/Saar

Influence of the strength of the initial cytotoxic synapse T cell receptor trigger on subsequent synapse formation and cytotoxic granule fusion

Dissertation zur Erlangung des Grades eines Doktors der Medizin

der Medizinischen Fakultät

der UNIVERSITÄT DES SAARLANDES

2020

vorgelegt von

Michael Estl

geb. am 23.06.1996 in Salzburg

Tag der Promotion:	02.12.2020
Dekan:	Univ.- Prof. Dr. Michael Menger
Berichterstatter:	Univ.- Prof. Dr. Jens Rettig
	Univ.- Prof. Dr. Markus Hoth
	Univ.- Prof. Dr. Nils Brose

List of contents

Abbreviations

°C	Degrees Celsius
AP	Adaptor protein
APC	antigen-presenting cell
ATP	Adenosine triphosphate
βME	β-Mercaptoethanol
CD	Cluster of differentiation
CD3ε	epsilon subunit of CD3
ClathrinLC	Clathrin light chain
CNS	central nerve system
CTL	cytotoxic T lymphocyte
CG	cytotoxic granule
DAG	diacylglycerol
DNA	Desoxyribonucleic Acid
DPBS	Dulbecco’s phosphate buffered saline
ER	endoplasmic reticulum
Granzyme	Granule associated enzyme
HEPES	4-(2-Hydroxyethyl)-1-piperazineethanesulfonic acid
ICAM-1	Intercellular adhesion molecule 1
IP3	inositol-1,4,5-trisphosphate
IMDM	Iscove's Modified Dulbecco's medium
IS	immunological synapse
KI	knock-in
LAMP	Lysosomal associated membrane proteins
LFA	lymphocyte function associated antigen
MHC	major histocompatibility complex
min	minutes
ml	milliliters
MTOC	microtubule-organizing center
MVB	multivesicular body
NK	natural killer cells
PCR	Polymerase chain reaction
PD-L1	programmed death-ligand 1
PFA	Paraformaldehyde
pH	Potential Hydrogen
PIP3	phosphoinositide 3-kinases
PLC	phosphoinositide-specific phospholipase C

RNA	Ribonucleic Acid
RPMI	Roswell Park Memorial Institute
s	seconds
SIM	structured illumination microscopy
SIRPα	signal regulatory protein α
SMAC	supramolecular activation cluster
SNAP-25	Synaptosomal-associated protein-25
SNARE	soluble N-ethylmaleimide-sensitive factor attachment protein (SNAP) receptor
Syb2	Synaptobrevin 2
t-SNARE	target-SNARE
TCR	T cell receptor
TIRFM	total internal reflection fluorescence microscopy
VAMP	Vesicle-associated membrane protein
v-SNARE	vesicular-SNARE

1 Summary

1.1 Summary

When a cytotoxic T lymphocyte is activated by a target cell, it is forming a very close contact to this cell, called the immunological synapse [35]. As a result, cytotoxic granules are polarized towards the immunological synapse where they secret their cargo such as cytotoxic proteins like Granzyme B ultimately leading to the apoptosis of the target cell [20,80]. Different SNARE proteins are necessary for the exocytosis of a cytotoxic granule and Synaptobrevin 2 was shown to be part of the SNARE complex for that in murine cytotoxic T lymphocytes [67]. Additionally, proteins involved in this process are endocytosed [13] and depending on the strength of stimulus on the T cell receptor, different modes of endocytosis of Synaptobrevin 2 have been suspected. To address this scientific question cytotoxic T lymphocytes from Granzyme B mTFP knock-in mice were transfected with Synaptobrevin 2 pHuji, which is a pH-dependent fluorophore and would light up when the cargo of a cytotoxic granule would be secreted through an opening of the fusion pore. These cytotoxic T lymphocytes were analyzed on lipid bilayers containing ICAM protein at a concentration of (0.55 mg/ml) but three different concentrations of anti-CD3ε antibody, to represent different stimulus strengths on the T cell receptor (5, 10 and 20 µg/ml). The result was that the Synaptobrevin 2 would either diffuse within three seconds into the plasma membrane after Granzyme B secretion, or it would stay at the same place of Granzyme B secretion and would be endocytosed within more than five minutes. These two event types occurred almost equally distributed among different concentrations of anti-CD3ε antibody used as TCR triggers. However, the fusion efficiency and upon further investigation of the immunological synapse formation also the size and the stability of the immunological synapse turned out to be significantly different when the strength of stimulus at the T cell receptor is varied. This study suggests that there is an optimal strength of stimulus for immunological synapse formation and secretion of cytotoxic granules. In this study it was 10 µg/ml anti-CD3ε antibody on lipid bilayer, because it triggers the lowest latency of cell adhesion to the lipid bilayer the highest secretion rate per cell, the largest size and the longest dwell time of CD3ε TFP clusters and the highest stability of the dSMAC ring.

1.2 Zusammenfassung

Wenn ein zytotoxischer T-Lymphozyt von einer Target-Zelle über dessen T-Zell-Rezeptor aktiviert wird, bildet sich eine immunologische Synapse aus [35]. Dies initiiert den Transport von zytotoxischen Vesikeln zu dieser Synapse und deren Inhalt wird sezerniert, wie zum Beispiel das zytotoxische Protein Granzyme B, welches zur Apoptose der Zielzelle führt [20,80]. Verschiedene SNARE Proteine sind am Sekretionsprozess eines zytotoxischen Vesikels beteiligt und es wurde nachgewiesen, dass Synaptobrevin 2 ein Teil des SNARE Komplexes in zytotoxischen T Lymphozyten der Maus ist [67]. Darüber hinaus, werden diese Proteine nach dem Prozess der Sekretion wieder in die Zelle aufgenommen [13] und es wird vermutet, dass es verschiedene Varianten gibt wie Synaptobrevin 2 wieder in das Zytoplasma der Zelle aufgenommen wird abhängig vom Stimulus am T-Zell-Rezeptor. Um diese Fragestellung zu beantworten wurden in dieser Studie Granzyme B mTFP knock-in zytotoxische T-Lymphozyten von der Maus mit dem Konstrukt Synaptobrevin 2 pHuji transfiziert. „pHuji“ ist ein Fluorophor das sensibel auf pH-Wert Erhöhungen (Deprotonierung) reagiert, daher leuchtet es hell auf, wenn das zytotoxische Vesikel seinen Inhalt durch die Fusionspore sezerniert, weil sich dann der pH-Wert von 6.1 auf 7.4 neutralisiert. Diese zytotoxischen T-Lymphozyten wurden auf einer künstlichen Doppellipidschicht mit derselben ICAM-1 Konzentration (0.55 mg/ml), aber mit drei verschieden anti-CD3ε Antikörper Konzentrationen (5, 10 und 20 µg/ml), um verschieden hohe Stimuli am T-Zell-Rezeptor zu imitieren, mit dem TIRF-Mikroskop untersucht. Es stellte sich heraus, dass Synaptobrevin 2 pHuji entweder innerhalb von drei Sekunden nach der Granzyme B Sekretion lateral in die Plasmamembran diffundiert oder an derselben Stelle verbleibt nach der Sekretion und in mehr als fünf Minuten in das Zytoplasma aufgenommen wird, aber diese beiden Modi wurden gleich verteilt unabhängig von der anti-CD3ε Antikörper Konzentration beobachtet. Die Sekretionseffizienz von zytotoxischen Vesikeln und durch genauere Untersuchung der Bildung der immunologischen Synapse, auch die Größe und die Stabilität der immunologischen Synapse waren zwischen den drei verschiedenen anti-CD3ε Antikörper Konzentrationen signifikant unterschiedlich. Aufgrund dieser Ergebnisse, wird vorgeschlagen, dass es ein Stimulusoptimum am T-Zell Rezeptor gibt. In dieser Studie liegt es auf der künstlichen Doppellipidschicht bei 10 µg/ml anti-CD3ε Antikörper, denn mit dieser Konzentration wurden die meisten zytotoxischen Vesikel sezerniert, die Latenzzeit zur Ausbildung einer immunologischen Synapse war am geringsten, die immunologische Synapse war am stabilsten und die größten und die am längsten verweilenden CD3ε TFP Cluster wurden mit dieser Konzentration im cSMAC beobachtet.

2 Introduction

2.1 The Immune System

The immune system protects the organism from invasions by pathogens or other damages. It consists of a specific and an unspecific part, which in synergy effectively recognize and eliminate pathogenic organisms. Cells and various other fluid substances, like macrophages or defensins, recognize pathogens and are part of the early onset answer and represent the unspecific part of the immune system, because they are not limited to a receptor antigen. The specific part is the late onset answer of the immune system and consists for example of plasma cells, which synthesize antibodies, or cytotoxic T lymphocytes (CTLs), which can eliminate pathogenic organisms, virus-infected cells or tumorigenic cells. The substantial difference between these two parts is that the specific part of the immune system has higher variability in its answer and the immunological memory, which ensures that the immune system can recognize specific antigens over decades and the highly specific antibodies to these antigens [2].

2.2 Cytotoxic T lymphocytes and the immunological synapse

Cytotoxic T lymphocytes (CTLs) are part of the specific immune system. They eliminate mutagenic or virus infected cells and spot their targets with their T cell receptor (TCR) and co-receptor CD8, which attaches to the MHC class I molecule of antigen presenting cells (APCs) [2]. This close link between a CTL and a target cell is known as the immunological synapse (IS) [35] (figure 1). The formation of an IS leads to the polarization of cytotoxic granules (CGs) to the IS, after which the content of the CG (perforin and granzymes) is emptied out into the synaptic cleft, which causes the apoptosis of the target cell [20,80].

There are two known types of immunological synapses, the initial long lasting IS (signaling synapse) for the activation of a naïve CD8+ T cell that induces CTL differentiation and the second IS that forms between a completely activated CTL and a target cell, lasting for up to 30 min. The second IS induces polarization of CGs towards the IS and leads to the secretion of the content of CGs. The two types of IS consist of three different areas, a central supramolecular activation cluster (cSMAC), a peripheral SMAC (pSMAC) and a distal SMAC (dSMAC) (figure 1) [28,35,72].

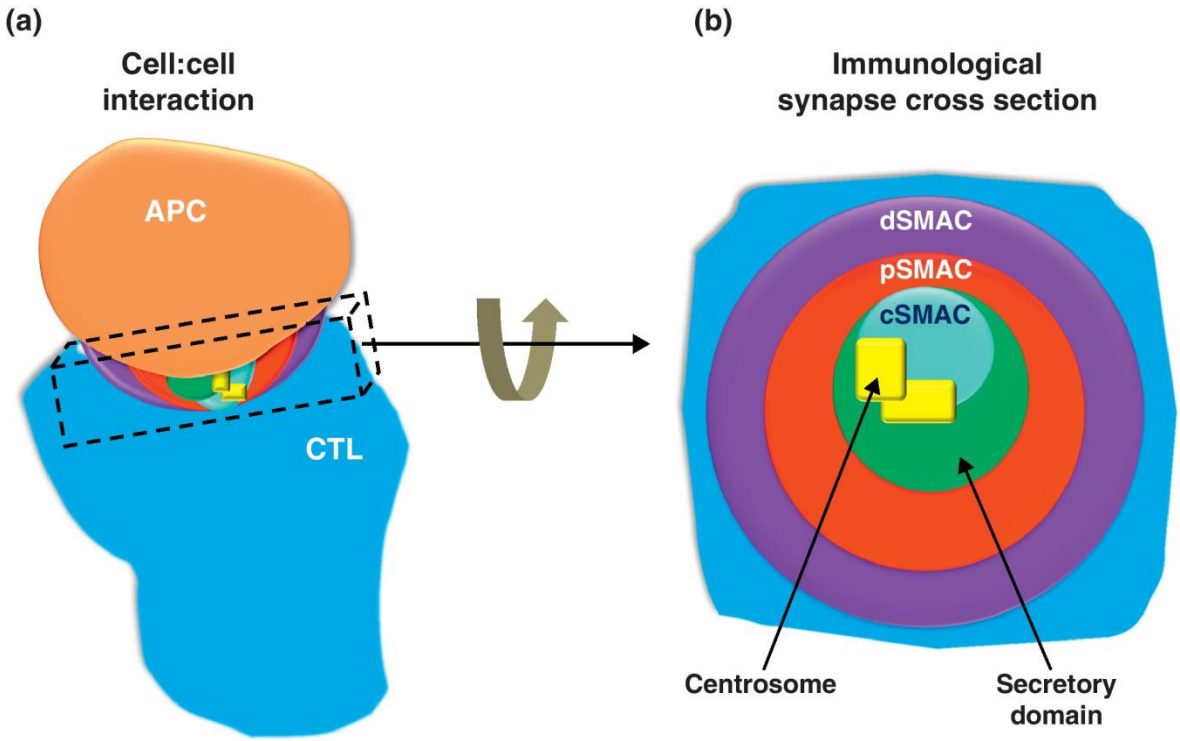

Figure 1 The immunological synapse. Image A shows a scheme of the immunological synapse (IS) between a T cell and a target cell. Image B shows the organization of the cSMAC, pSMAC and dSMAC in an IS [86].

During the initial contact of the CTL with a target cell, actin polymerizes within the first minute at the contact zone and then moves towards the periphery of the IS, while in the center of the IS TCR microclusters arrive after the reorganization of actin [11,90,100]. The polarizing centrosome leads to more TCR microclusters and induces the transport of CGs towards the functional secretory domain within the cSMAC of the IS, where the CGs also fuse with the plasma membrane [19,31,79,87,95,96]. In addition, proteins of the Src-kinase-family are found mostly in the cSMAC and appear in the first minutes of the IS formation [5]. The pSMAC consists mainly of adhesion molecules like lymphocyte function-associated antigens 1 (LFA-1), which are expressed on the T cell surface and interact with Intercellular Adhesion Molecules 1 (ICAM-1) on the target cell membrane. This interaction leads to a close contact between the CTL and the target cell [72,83]. In the dSMAC area of the IS actin clusters and the phosphatase CD45 can be found, which induces signaling pathways [28]. A part of this thesis characterizes any differences in the IS when the CTL is stimulated with various

concentrations of anti-CD3ε antibody on the lipid bilayer, using lifeact mRFP as a dSMAC marker and CD3ε TFP as a cSMAC marker in murine wildtype CTLs.

2.3 Cytotoxic granules

CTLs are capable of killing a target cell with their cytotoxic granules (CGs) [80]. The membrane proteins of CGs are the Fas-ligand (FasL), the V-type H+ ATPase, the lysosomal associated membrane proteins (LAMP-1, LAMP-2 and LAMP-3) and the v-SNARE Synaptobrevin 2 (Syb2) [6,22,29,67,80]. The membrane protein FasL of CGs diffuses into the CTL membrane during CG fusion and after activation by extracellular proteases producing a soluble FasL, which is inducing apoptosis of target cells when it binds to their Fas receptor (CD95) [6,22]. The V-ATPase is responsible for the stable acidic pH of CGs and is pivotal for their function, because it keeps the cytotoxic proteins inside the vesicle in an inactive state [53]. Furthermore, Syb2 is required as a v-SNARE for CG fusion in murine CTLs [67]. Inside the lumen of CGs are cytotoxic proteins (perforin and granzymes), lysosomal hydrolases (cathepsins) and chondroitin sulfate proteoglycans (serglycin). Serglycin is responsible for the dense core structure of the content of CGs and keeps the cytotoxic proteins inside the vesicle in an inactive state [6,20]. Furthermore, approximately eight different granzymes are already known in mouse CTLs (A, B, C, D, E, F, G and H), they are all serine esterases [66]. Perforin forms a pore in the target cell plasma membrane and therefore eases the penetration of the granzymes into the target cell [82,92].

2.4 Exocytosis of CGs in CTLs

SNARE proteins and several other proteins are pivotal for the exocytosis of CGs in CTLs, a process which is divided into three distinct steps namely docking, priming and fusion [40,62]. The docking step places the CG very close to the plasma membrane and proteins of the sec1/Munc18 family are required for this process [39]. After the ternary SNARE complex is formed, composed of one R-SNARE and two or three Q-SNAREs, the Munc13 proteins are activated, which are necessary for the priming process [23,24,88]. Munc13-1 is responsible for the release of Munc18-1 which enables syntaxin-1 to assemble properly with the other SNARE proteins [88,91]. The most critical step to initiating the fusion of CGs with the plasma membrane is the formation of a coiled-coil complex of the associated SNARE proteins especially of Syb2 and syntaxin, which provides the energy for the deformation of the plasma

membrane to enable fusion [49,93,94]. One of the aims of this study was to detect if Syb2 behaves differently after CG fusion when the CTL is stimulated with various anti-CD3ε antibody concentrations on the lipid bilayer with murine Granzyme B mTFP knock-in CTLs transfected with the Syb2 pHuji construct.

2.5 TCR signaling pathway

The TCR is expressed on the surface of T cells and is a multi-protein complex which consists of an alpha and a beta chain linked to the CD3 chain molecules (CD3 gamma, CD3 delta and CD3 epsilon), the zeta chain molecules intracellularly and the CD8 chain molecules, which are specific to the MHC1 complex (figure 2) [106].

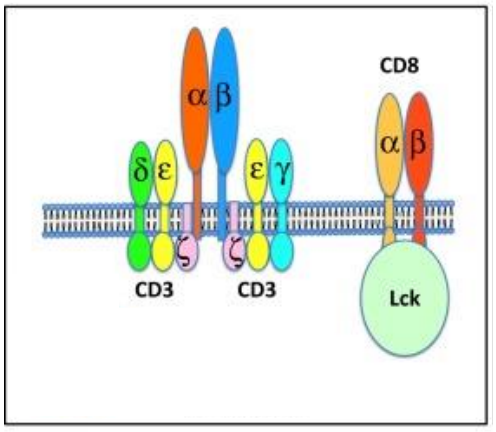

Figure 2 The CD8+ T cell receptor. This image shows all subunits of the T cell receptor of CTLs [42].

If an antigen is presented to the TCR, the Src kinase leukocyte-specific tyrosine kinase (Lck) phosphorylates the immunoreceptor tyrosine-based activation motifs (ITAMs) of CD3 subunits and after that, Zap70 is activated, which phosphorylates the linker for the activation of T cells (LAT) [12,32,52,97]. The phosphorylated LAT induces the phospholipase C-γ (PLCγ), which produces the second messengers inositol trisphosphate (IP3) and diacylglycerol (DAG), which then activates mitogen-activated protein kinase (MAPK) signaling pathways [57]. The CD28 receptor of APCs binds to the TCR and improves the signaling pathway through increased activation of Src-family proteins [1].

Furthermore, upon antigen presentation to the TCR actin-related protein 2/3 (Arp2/3), Wiskott–Aldrich syndrome protein (WASP) and WASP family verprolin- homologous protein (WAVE) complexes are activated, which in synergy stimulate actin polymerization at the IS [33,58]. The LAT-Slp76 complex and the activated PLCγ also recruit integrin to the IS, which leads to a stable T cell - target cell contact. Also, MTOC polarization towards the IS can be observed, which is mediated by Dynein, the formins (Diaphanous (Dia) and FMNL1) and the IQ-motif-containing GTPase-activating protein homolog (IQGAP) [3,18,33,34].

TCR stimulation leads to an upregulation of the transcription of the interleukin 2 gene mediated by the transcription factors activator protein 1 (AP1, a heterodimer of Fos and Jun), nuclear factor of activated T cells (NFAT) and nuclear factor-κB (NF-κB) [75,76]. Interleukin 2 is a cytokine, which is responsible for the proliferation, differentiation of CD8+ T cells and furthermore for the synthesis of other cytokines in CTLs [8,64,89].

2.6 Endocytosis

In general, three different endocytic pathways are known, either clathrin-mediated endocytosis (CME), which is always dynamin-dependent, or clathrin-independent endocytosis (CIE), which can be dynamin-dependent or dynamin-independent [7,61,71]. Clathrin is a protein that is involved in the trafficking steps of cargo. It consists of 3 light chains and 3 heavy chains, which interact at their C termini to form a triskelion [55,56,78]. AP180 is necessary to recruit clathrin to the area where synaptic vesicle protein reuptake occurs [99]. After that, AP2 is responsible for the polymerization of clathrin and the formation of a clathrin coated vesicle [54]. The role of clathrin in terms of endocytosis is already well established, but where the clathrin molecules come from is not yet known. One of the aims of our study investigates the localization of clathrin before CG endocytosis and also addresses its potential co-localization with cytotoxic granules upon IS formation. High resolution live and fixed-cell imaging such as Total internal reflection fluorescence (TIRF) and Structured illumination (SIM) microscopy on murine CTLs was used to address this question.

2.7 The endocytic pathway

Rab proteins play an important role in vesicle transport in CTLs. When GTP is bound to them, they are in an active state and bind membranes. If GDP is bound, Rab proteins are inactive and released from membranes. Guanine nucleotide exchange factors (GEFs) manage the

exchange of GDP to GTP [21]. Endosomes are characterized by an acidic pH and a V-type H+ ATPase is responsible for maintaining the stable acidic pH inside these vesicles [27]. Furthermore, accessory proteins, such as dynamin and epsin are necessary to pinch off clathrin-coated vesicles and to bend the lipid bilayer [25,26,98].

In general, the early endosome is the starting point for a vesicle in the endocytosis pathway and it is characterized by a pH of 6.5 at which there is a dissociation of the ligands and receptors during signaling receptor endocytosis [69,70,107,108]. Rab5 and the early endosomal antigen 1 (EEA1) are typical markers of the early endosomes, which are responsible for the fusion of vesicles with early endosomes and for sorting proteins to the different compartments of the cell [9,17]. Furthermore, Rab11, as a marker of recycling endosomes, is needed for the recycling process of proteins to the plasma membrane [37].

MVBs are formed on early endosome membranes to either generate secretory exosomes or Rab7 linked late endosomes that lead to lysosomes [36]. During this process Rab5 dissociates and is replaced by Rab7 and the pH inside late endosomes is typically 6, because of the increased activity of the V-ATPase. The low pH level inside late endosomes leads to further degradation of pathogen organisms and catalyzes the sorting of proteins [47,59,68,85]. Figure 3 shows a scheme of endocytic pathways.

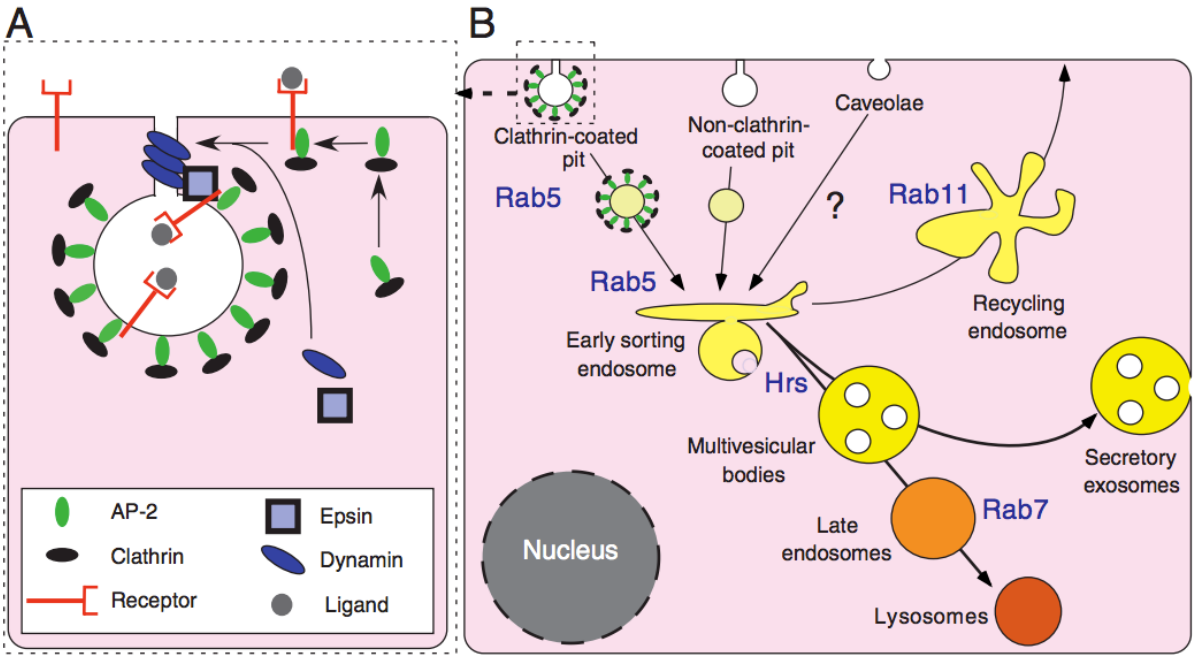

Figure 3 The endocytic pathway. Image A shows a clathrin-coated pit carrying the adaptor protein AP2. Image B shows a scheme of endocytic pathways that are either clathrin-independent, clathrin-dependent or caveolae-dependent [43].

3 Material

3.1 Used commercial kits

Dynabeads® FlowComp™ Mouse CD8 Kit (Invitrogen)

Nucleofection kit for mouse T cells (Lonza)

EndoFree Plasmid Maxi Kit (Qiagen)

EndoFree Plasmid Mini Kit (Qiagen)

QIAprep Spin Miniprep Kit (Qiagen)

QIAquick Gel Extraction Kit (Qiagen)

QIAquick PCR Purification Kit (Qiagen)

3.2 Commercial antibodies

Anti-CD3ε antibody (clone145-2C11) (Biolegend)

3.3 Media and solutions

Solutions for CD8 positive cell isolation

RPMI Medium (+ L-glutamine and phenol red) (Lifetechnologies)

IMDM Medium (Lifetechnologies)

BD Roundfilter (70 µm) (Becton Dickinson)

Erylysis buffer (adjust pH to 7.3)	NH_4Cl	155 mM
	$KHCO_3$	10 mM
	EDTA	0.13 mM

Isolation Buffer (adjust pH to 7.4)	DPBS 14190-094 (Lifetechnologies)	1x
	BSA 0.1% 0.5 g A 7906 (Sigma Aldrich)	
	EDTA	2 mM

Trypan Blue (Sigma)

Dynabeads FlowComp™ Mouse CD8 kit (Invitrogen)

includes:

- FlowComp™ Dynabeads (~1 × 10 (~10 mg) beads/ml in phosphate buffered saline (PBS), pH 7.4, with 0.1% bovine serum albumin (BSA) and 0.02% sodium azide as a preservative)

- FlowComp™ Mouse CD8 antibody (monoclonal anti-mouse CD8 antibody in PBS and 0.02% sodium azide)

- Release Buffer (modified biotin in 0.1% BSA and 2 mM EDTA)

Dynabeads mouse T-activator CD3/CD28 for T cell expansion and activation (Thermo Fisher)

Solutions for Transfections

Phosphat Buffered Saline (PBS) pH 7.4 (gibco by life technologies)

Nucleofection Solution (Lonza)

Transfection Medium	Mouse T Cell NucleofectorTm Medium	9.1ml
	Component A (Lonza)	100 µl
	Component B (Lonza)	100 µl
	FCS	500 µl
	Glutamax	200 µl

Medium for cellculture

AIM V Medium (ThermoFisher Scientific) + 50 µM Betamercaptoethanol + 10% FCS

Solutions for die anti-CD3ε antibody coated coverslip

Poly-L-ornithine solution (Sigma Life Science)

H_2O (Sigma)

Dulbeccos Phosphat Buffered Saline (DPBS) pH 7.4 (gibco by life technologies)

Anti-CD3ε Antibody (clone 145-2C11) (Biolegend)

Solution for anti-CD3ε antibody coated lipid bilayer

HBS/HSA buffer	HEPES pH 7.2	20 mM
	NaCl	137 mM
	KCl	5 mM
	Na_2HPO_4	0.7 mM
	D-Glucose	6 mM
	HAS	25x
	$CaCl_2$	1 mM
	$MgCl_2$	2 mM
Piranha solution	H_2O_2	30%
	Sulfuric acid	70%

Solutions for TIRF- and SIM- microscopy

0 Calcium solution	NaCl	155 mM
	KCl	4.5 mM
	HEPES	5 mM
	$MgCl_2$ x 6 H_2O	3 mM
	$C_6H_{12}O_6$	10 mM
10 mM Calcium solution	NaCl	140 mM
	KCl	4.5 mM
	HEPES	5 mM
	$MgCl_2$ x 6 H_2O	2 mM
	$CaCl_2$	10 mM
	$C_6H_{12}O_6$	10 mM

Solutions for fixation

Paraformaldehyde (15% in H_2O)	Paraformaldehyde	1.5 g
	H_2O (Sigma)	10 ml
	NaOH (1mM)	20 µl
0.1 M Glycine solution	PBS	50 ml
	L-Glycine	0.375 g
Mounting medium (pH 8.5)	Mowiol 4-88	2.4 g
	Glycerol	6 g
	H_2O double distilled	6 ml
	Tris-Buffer	12 ml

3.4 Plasmids

pMax Syb2 pHuji

pHuji was amplified from a previously described VAMP7 pHuji DNA using the forward primer 5’ ATG_TAT_ACC_CAA_GCT_TAT _GGT_GAG_CAA_GGG_CGA_G 3’ to add Hind111 site and the reverse primer 3’ ATG_TAT_ACG_CGG_ATC_CTT_ACT_TGT_ACA_GCT _CGT_C 5’ to add the Bamh1 site. The PCR product was digested and ligated into an optimized pMax-vector containing Synaptobrevin2 as previously described [15].

Lifeact mRFP

Lifeact mRFP was kindly provided by Dr. Ronald Wedlich-Söldner (University Münster, Germany).

Lifeact eGFP

Lifeact eGFP was kindly provided by Dr. Ronald Wedlich-Söldner (University Münster, Germany).

pMax CD3ε TFP

CD3 epsilon TFP was recently described [38].

pMax ClathrinLC mcherry/TFP

ClathrinLC mcherry was obtained from addgene (# 27680; Reference: Taylor et al. PLoS Biol. 2011 Mar. 9(3):e1000604). ClathrinLC mTFP was obtained by replacing the mcherry with TFP. TFP was amplified from a previously described Syb2-TFP DNA using the forward primer 5’ ATA_TAC_TAG_CTA_GCG_CCG_CCA_CCA_TGG_TGA_GCA_AGG_GCG_AGG _AG 3’ to add Nhe1 site and the reverse primer 5’ ATA_TAC_CGG_AAT_TCG_AGC_TAC _CGC_CGC_TTC_CGC_C 3’ to add the EcoR1 site. The PCR product was restriction digested and ligated to the restriction digested ClathrinLC mcherry according to standard molecular biology procedures.

Rab11a-mcherry

Rab11a-mcherry was previously described [38].

4 Methods

4.1 Mice

4.1.1 Granzyme B mTFP knock-in mouse

The Granzyme B mTFP knock-in mouse was generated with the CRISPR CAS9-D10A_mRNA (Nickase) system in cooperation with the Max Planck Institute in Göttingen. As a guide RNA the GranzymeB-protospacer-sgRNA2 sequence 5' GTC_CAG_GAT_TGC_TCT _AGG_AC-3' was used and as a Homology-Directed-Repair fragment the Granzyme B mTFP1 HDR1 fragment with the mTFP fluorophore with 3228 base pairs of length was inserted. Afterwards the genome of the mouse was fully sequenced to exclude side effects.

4.1.2 Wildtype mouse

All wildtype mice were obtained from Charles River Laboratories and belonged to the C57Bl/6N (Black 6) strain. The wildtype mice used for experiments were between 8 and 12 weeks old. All animal experiments were approved by the state of Saarland (Landesamt für Gesundheit und Verbraucherschutz; animal license number 41-2016) and were in accordance with German law and European animal healthcare guidelines (FELASA).

4.2 Cell isolation and cell culture

4.2.1 Positive isolation of CD8+ T Lymphocytes

The animal killing was performed according to the Animal Welfare Act (permission number K110/180-07 by the state of Saarland).

Splenocytes were prepared from 8- to 12-week old knock-in Granzyme B mTFP or C57Bl/6N wildtype mice. The isolation of CTLs was performed by positive isolation using Dynabeads® FlowComp Mouse CD8+ kit (Invitrogen).

The spleen was smushed on a 70 µm filter that was placed in a petridish filled with warm RPMI medium using the inner plunger side of a syringe. Cells were then collected from the petridish into a 15 ml falcon and the volume was filled up to 10 ml using the medium. Cells were spun at 1100 rpm without any brake or special settings for 10 min. The cell pellet after the first wash was subjected to erythrolysis by resuspending the cells in 1 ml of erythrolysis buffer for 30 s following which the reaction was stopped again by adding 9 ml of Isolation

buffer. The cells were washed again for 10 min. Cells were counted and 50 million splenocytes were taken for the positive isolation. Following this the supernatant was discarded and the pellet re-suspended in 500 µl Isolations buffer and incubated with 25 µl FlowComp™ Mouse CD8 antibody for 10 min on ice following which the cells were washed once by adding 6 ml of isolation buffer and centrifuging the cells at 328xg for 8 min. The cell pellet was re-suspended in 1 ml isolation buffer and the cells were incubated with 75 µl of pre-washed FlowComp™ magnetic Dynabeads for 15 min on a rocker at 4 °C. After adding 4 ml of isolation buffer, the suspension was placed on a magnet for 2 min to positively obtain the bead bound CD8 T cells by discarding the supernatant while the tube is in the magnet. The cell bound beads were washed twice this way using Isolation buffer. The cell suspension was incubated with 1 ml of release buffer for 10 min on a rocker at room temperature. Next, the suspension was placed on a magnet for 2 min again and while the tube is still in the magnet the supernatant containing the CD8 cells that have been released from the beads were transferred to a new tube. This procedure was repeated three times, to remove all magnetic beads. Before centrifuging the cells a small aliquot was taken for counting to determine the cell concentration.

4.2.2 Cell culture and activation of CTLs

The cells were cultured at a concentration of 1 x 10^6 cells per ml of AIMV Medium and 2 million in total per well of a 24-well plate. Cells were activated with anti-CD3/anti-CD28 antibody coated beads at a ratio of 1:0.8 cells to beads. Cells were incubated at 37 °C and 5 % CO_2 for 7 or 8 days. Cells were counted every day and split as needed if the cell density exceeded 1 million per ml due to proliferation. Furthermore 10 U/ml of recombinant mouse IL-2 was added as supplement to every well every time during the splitting.

Cells activated for 7 or 8 days as described above were used for all experiments.

4.3 Coating of glass coverslips

Clean glass coverslips were coated with 90 µl of poly-L-Ornithine (0.1 mg/ml) and incubated at room temperature for 30 min after which the solution was sucked off. The coverslips were used immediately (in control experiments which required only poly-ornithine coating) or coated with anti-CD3ε (30 µg/ml) solution in PBS for 2 hours at 37°C with 5% CO_2. The antibody was then sucked off and then the coverslips were ready to use for experiments that required anti-CD3ε coated glass coverslips.

4.4 Lipid bilayer preparation (by MSc Pascal Blatt and Dr. Hsin-Fang Chang)

4.4.1 Preparation of proteins

Monobiotinylation of anti-CD3$^{\varepsilon}$ antibodies

0.05 µg/ml of biotin (EZ-link suffo-NHS-LC-LC-Biotin (Life technologies) diluted in DMSO) were supplemented to the pure anti-CD3$^{\varepsilon}$ antibody (1 mg/ml) solution and incubated for 30 min at room temperature. A dialysis cassette (Slide-A-Lyzer® Dialysis Cassettes, Thermo scientific) was used for 12 hours at 4 °C in PBS to purify the solution after which the concentration was calculated by photometry.

ICAM-1

Murine ICAM-1 was produced with the drosophila S2 cell line kindly provided by Prof. Dr. Michael Dustin.

4.4.2 Preparation of lipids

100% DOPC, 25% NTA and 2% capbio were dried by lyophilizer for 2 hours at -40 °C. After resuspending the lipids in lipid buffer, the suspension was extruded in avestin extruder (Lipofast®) 20 times to generate a homogenous particle size distribution and then the lipids were diluted to a concentration of 0.4 mM each with DOPC.

4.4.3 Cleaning of glass slides

Glass slides were maintained in the Piranha solution (containing 50 ml of sulfuric acid and 25 ml of hydrogen peroxide) for 20 min and then washed with milliQ water for 5 min. It was important to use freshly prepared milliQ water to circumvent contamination of the glass. Next, the glass was dried at room temperature and remaining organic contaminations were eliminated by plasma cleaning for 10 min.

4.4.4 Coating of lipids and proteins on glass slides

The chamber (Ibidi stickyslide® VI microscopy chamber) was stuck on the cleaned glass slide. Following this 33 µl DGS-NTA (0.4 mM stock), 10 µl Cap PE capbio (0.4 mM stock), 6.5 µl DOPC (0.4 mM stock) and 0.5 µl (required for 5 µg/ml lipid bilayers), 1 µl (required for 10 µg/ml lipid bilayers) or 2 µl (required for 20 µg/ml lipid bilayers) of biotinylated anti-CD3ε antibody (clone 145-2C11) (0.5 mg/ml) were added to the chamber. Next, 1000 µl Casein (5%) with 10 µl of $NiSO_4$ (100 µM) were added to each well for 20 min. Afterward, 3 µl of the ICAM His-tag solution (dilution 1:2000 (stock 0.55 mg/ml)) were added to each chamber. In general, the chamber was washed gently 3 times with 150 µl HBS/HSA buffer after every step. Before imaging, the buffer was removed from the well and 200.000 CTLs of day 7 or 8 activated T cells suspended in 50 µl of 0 mM calcium buffer were seeded freshly onto one well.

To verify that with this method different amounts of anti-CD3ε antibodies are bound to lipid bilayers, 18 lipid bilayers were prepared with Alexa 561 labeled and biotinylated anti-CD3ε antibody and then 5, 10 and 20 µg/ml anti-CD3ε antibody labeled lipid bilayers were analyzed with TIRF microscopy without cells (figure 4).

The result was that in an area of 660 µm² (25 µm x 25 µm) on the lipid bilayer with 5 µg/ml anti-CD3ε antibody the mean grey fluorescence was 116.7 ± 0.9, with 10 µg/ml 189.3 ± 0.5 and with 20 µg/ml 252.7 ± 0.7. A one-way ANOVA test showed that the data sets are statistically different from another (p-value < 0.001). This increase in mean grey fluorescence implies that with higher concentrations of anti-CD3ε antibody applied on the lipid bilayers more antibodies are bound to it and therefore more fluorescence can be detected in TIRF.

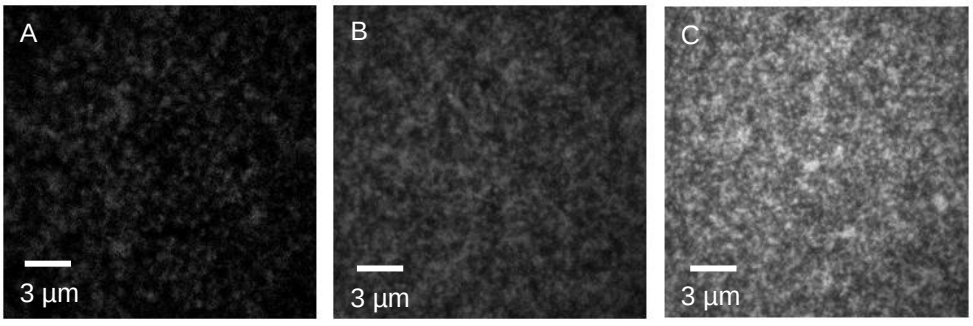

Figure 4 TIRF snapshots of lipid bilayers with 5, 10 and 20 µg/ml Alexa labeled and biotinylated anti-CD3ε antibody. Image A is with 5 µg/ml anti-CD3ε antibody, image B with 10 µg/ml anti-CD3ε antibody and image C with 20 µg/ml anti-CD3ε antibody.

4.5 Electroporation of CTLs

Anti-CD3/anti-CD28 beads were removed from day 7 or 8 activated CTLs by a magnet. CTLs were transfected overnight (12 hours) with 1.5 µg of either of the following constructs Syb2 pHuji, lifeact mRFP, lifeact eGFP, CD3ε TFP, ClathrinLC mcherry or Rab11a-mcherry.

Electroporation was performed using the Nucleofection kit (LONZA) according to the manufacturers protocol and recommendations. Briefly, 5 x 10^6 cells were spun for 7 min at 180xg then the supernatant was discarded and the cell pellet resuspended in 4 ml of Isolations buffer and spun again for 7 min at 180xg. After removing the supernatant, the cells were resuspended in 100 µl nucleofection solution and the corresponding plasmid DNA was added before subjecting the cells to electroporation. Following electroporation, the cells suspended and cultured in a special supplemented medium that is provided by LONZA overnight at 32°C with 5 % CO_2 in one well of a 12 well-plate. After 12 hours of incubation the cells were spun again for 7 min at 180xg and then resuspended in 3 ml of AIMV medium with 10 U/ml IL-2 and again placed in the incubator at 32°C with 5 % CO_2 till the end of the imaging experiments.

4.6 Structured illumination microscopy (SIM)

The setup used for super-resolution structured illumination microscopy (SR-SIM) is equipped with several different lasers (an HR Diode 405, 488 and 642 nm lasers and an HR DPSS 561 nm laser) as described previously [14]. The images were acquired using ZEN software. An oil-immersion plan-apochromat 63x objective with a NA of 1.4 was used for imaging. Fifty stacks were taken for each image with a z-step size of 0.2 µm to cover about 10 µm of the cell. Cells were settled for 7 min on either poly L-ornithine or anti-CD3ε antibody coated coverslips and fixed with PFA thereafter, washed and mounted on glass slides and then ready to be used for SR-SIM imaging.

4.6.1 Bleed through of constructs in SIM microscopy

Since we are using fluorophores with partial overlapping spectral profiles we performed single stained control experiments to correct for any bleed through. Granzyme B mTFP CTLs and wildtype CTLs transfected with ClathrinLC mcherry were fixed on separate anti-CD3ε antibody coated coverslips with PFA after letting them settle for 8 min on the coverslips. Cells were then imaged with the 445 nm laser (10 % laser power) and the 561 nm laser (30 % laser power) at the SIM microscope (figure 5).

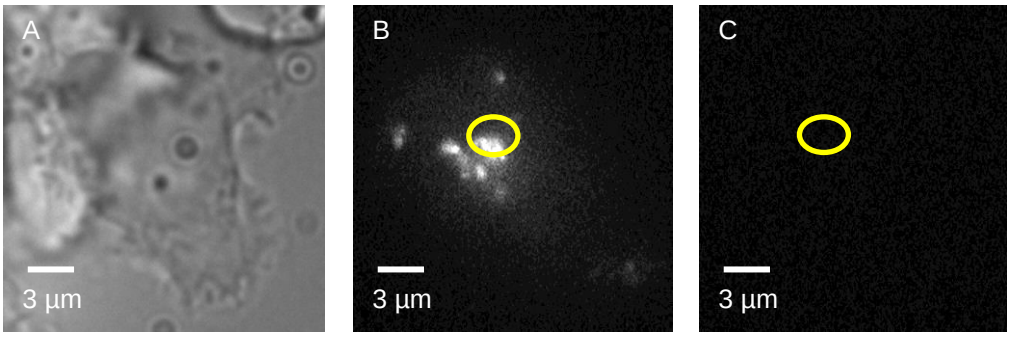

Figure 5 SIM image snapshots of a Granzyme B mTFP knock-in CTL. CTLs were fixed on an anti-CD3ε antibody coated coverslip and imaged in SIM by exciting at 445 and 561 nm. Image A shows the brightfield picture of the CTL, image B shows the 445 nm channel and image C shows the bleed through into the 561 nm channel.

The mean grey value was calculated at a particular position using the ROI (region of interest) manager in ImageJ in both the 445 and 561 nm excited images generated. The results are noted in the tables below. Thus, the first step of processing the image was to subtract the calculated bleed through of each fluorophore into the other channel (table 1 and 2).

If Granzyme B mTFP and ClathrinLC mcherry were used in the same cell and the ROI of a CG would have 10300 mean gray fluorescence for Granzyme B mTFP in the 445 nm laser channel then 1.3 % of this value is subtracted from the mean fluorescence value of the ROI in the 561 channel to get the unmixed ClacthrinLC mcherry signal.

construct:	**fluorescence emitted with 445 nm laser:**	**fluorescence emitted with 561 nm laser:**	**bleed through into the 561 nm channel in %:**
Granzyme B mTFP KI	10300	144	1.3

Table 1 Bleed through calculation of Granzyme B mTFP into the 561 nm channel.

construct:	**fluorescence emitted with 561 nm laser:**	**fluorescence emitted with 445 nm laser:**	**bleed through into the 445 nm channel in %:**
ClathrinLC mcherry	1932	92	4.7

Table 2 Bleed through calculation of ClathrinLC mcherry into the 445 nm channel.

4.7 Total internal reflection fluorescence microscopy (TIRFM)

The TIRFM setup used for the experiments to visualize the fluorescent proteins in the CTLs was basically as described previously [16] with specific changes mentioned further. The setup was based on an inverted Olympus IX83 microscope equipped with the Olympus autofocus module, a UAPON100XOTIRF NA 1.49 objective (Olympus), a 445 nm laser (100 mW) and a 561 nm solid state laser (100 mW), the iLAS2 illumination control system (Roper Scientific SAS, France). The 445 and 561 nm lasers were used for excitation along with a filter cube consisting of an emission filter ZET 442/514/568 and a dichroic beamsplitter ZT405/440/514/561 (Chroma Technology Corp, Olching, Germany). The pixel size of the camera was 160 nm. The setup was controlled by Visiview software (Version:4.0.0.11, Visitron GmbH). The acquisition frequency for all experiments was 5 Hz and the acquisition time was 15 min. In TIRF mode the penetration depth of the evanescent light for the 561 nm and the 445 nm laser was set at 150 nm through the iLAS2 illumination control system for all experiments.

4.7.1 Bleed through of constructs in TIRF microscopy

In the TIRF experiments again two different fluorophores were used to localize proteins in the same cell by exciting it with the 445 nm and 561 nm laser. Therefore, it was again essential to calculate the bleed through of each construct using cells that were transfected with only one of the fluorophores at a given time (figure 6).

For our control experiments wildtype CTLs were singly transfected with all the constructs used for the experiments or Granzyme B mTFP knock-in CTLs alone were imaged by exciting at 445 nm and 561 nm laser.

In Granzyme B mTFP knock-in CTLs, the bleed through of the TFP into the 561 channel was calculated similar to what is described in 4.6.1. Similarly, for the other 445 nm laser excitable and 561 nm laser excitable fluorophores the bleed throughs were calculated.

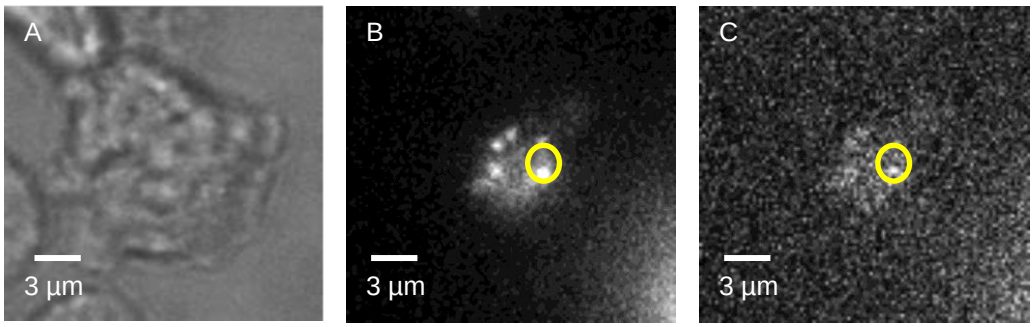

Figure 6 TIRF image snapshots of a Granzyme B mTFP knock-in CTL. CTLs were adhered on an anti-CD3ε antibody coated coverslip and imaged in TIRF by exciting at 445 and 561 nm. Image A shows the brightfield picture of the CTL, image B shows the 445 nm channel and image C shows the bleed through into the 561 nm channel.

For both constructs the mean grey value was calculated at a particular ROI with ImageJ, and and the bleed through in % was calculated as described in 4.6.1. The results are noted in Table 3 and 4 below. Thus, the first step of processing of the image was to subtract the calculated bleed through of a construct into the other channel. This procedure was necessary because most of the experiments of this thesis were done with cells which were marked with two different fluorophores.

If for example Granzyme B mTFP and Syb2 pHuji were used in the same cell and the ROI of a CG would have a mean fluorescent value of 3668 for Granzyme B mTFP in the 445 nm laser channel then 11.5 % of this value is subtracted from the mean fluorescence value of Syb2 pHuji in the 561 nm laser channel.

construct:	**fluorescence emitted with 445 nm laser:**	**fluorescence emitted with 561 nm laser:**	**bleed through into the 561 nm channel in %:**
Granzyme B mTFP KI	3668	424	11.55
CD3ε TFP	1808	131	7.2
lifeact eGFP	17564	1516	8.6

Table 3 Bleed through calculation of blue fluorophores into the 561 nm channel.

construct:	**fluorescence emitted with 561 nm laser:**	**fluorescence emitted with 445 nm laser:**	**bleed through into the 445 nm channel in %:**
Syb2 pHuji	41280	270	0.7
lifeact mRFP	3936	340	8.6
ClathrinLC mcherry	2652	142	5.3
Rab11a-mcherry	3601	102	2.8

Table 4 Bleed through calculation of red fluorophores into the 445 nm channel.

4.8 Fixation of CTLs

Transfected murine day 8 CTLs were counted in the Neubauer chamber and then 0.5 x 10^6 cells were taken out of the well-plate and spun down in a falcon tube at 180xg and resuspended in 50 µl of extracellular medium and incubated for 8 min on a poly L – ornithine or an anti-CD3ε antibody coated coverslip. The cells were then fixed with 4 % PFA for 20 min at room temperature. Afterward, the cells were washed three times with PBS and then incubated with 4 ml of 0.1 M Glycine in PBS for 10 min at room temperature after which the cells were washed again three times with PBS. Finally, the cells were very quickly dipped in H_2O to remove salts and then mounted on glass slides with 30 µl of mounting medium. The slides were incubated for 10 min at 37 °C. Following which in order to avoid further dehydration of the cells the coverslips were sealed with nail polish on the microscope slide and kept at 4 °C until imaging.

4.9 Software

ImageJ, National Institutes of Health, Federal Government of USA

Office 2013, Microsoft

Zeiss Efficient Navigator (Zen) 2012, Carl Zeiss

IGOR Pro 2018, WaveMetrics

SigmaPlot 14, Systat Software Inc.

4.10 Statistics

In this study the one-way ANOVA test and the Mann-Whitney-U-test were used to calculate if two populations or datasets are significantly different from another. In general, a p-value below 0.05 in the one-way ANOVA test means there is a significant difference among the data sets. An asterics sign (*) is used to depict the significance of the datasets in the figures. If the p-value obtained is less than 0.5 and more than 0.01 the significance is marked with - "*", if it is less than 0.01 and more than 0.001 it is marked with - "**" and if it is less than 0.001 it is marked with - "***". If there is no asterics sign at all the result of the one-way ANOVA test or the Mann-Whitney-U-test was higher than p 0.05, which means that the two datasets are not statistically different. This test was automatically done by the program SigmaPlot 14.

5 Results

5.1 Synaptobrevin 2 pHuji exhibits two types of behavior upon exocytosis of cytotoxic granules at the IS

In neurons and neuroendocrine cells Syb2 exhibits only fast endocytosis (which lasts for 1.8 s) with a low stimulus and fast and slow endocytosis (which lasts for 20 s) with a high stimulus on the plasma membrane [104]. Since Syb2 is the major v-SNARE in cytotoxic granules of murine CTLs we asked whether stimulus induced modes of exo-endocytosis also exist in murine CTLs. For our experiments CTLs isolated from a Granzyme B mTFP knock-in mouse were electroporated with Syb2 pHuji to visualize simultaneously the lumen and membrane of cytotoxic granules. Cells were then added to lipid bilayers containing different concentrations of anti-CD3ε antibody namely 5, 10 and 20 µg/ml and allowed to form an IS. Cells were imaged for 15 min by TIRF microscopy. The 445 nm laser was used for detecting the Granzyme B mTFP fluorophore and the 561 nm laser for Syb2 pHuji fluorophore.

pHuji is a pH-dependent fluorophore and would only be fluorescent in neutral pH which is around 7.4 and therefore this fluorophore would light up as soon as the fusion pore of a CG would open leading ultimately to Granzyme B secretion. In this study Granzyme B mTFP knock-in CTLs were electroporated with Syb2 pHuji to reveal any differences in the modes of fusion when stimulated with different concentrations of anti-CD3ε antibody. Thirty-one fusion events for the 5, thirty-four fusion events for the 10 and thirty-four fusion events for the 20 µg/ml anti-CD3ε stimulation conditions were analyzed.

Two different behaviors of Syb2 pHuji following Granzyme B mTFP secretion were typically seen and these behaviors were independent of the concentration of anti-CD3ε antibody on the lipid bilayer. In the first type of behavior the fluorescence of Syb2 pHuji would disappear within 3 seconds during a Granzyme B mTFP event (figures 7 and 9). We call these short fusion events. In the second type of behavior Syb2 pHuji would remain at the same place of Granzyme B mTFP secretion and the fluorescence would disappear slowly within or sometimes more than 5 min after the complete disappearance of Granzyme B secretion (figures 8 and 10). We call these long fusion events.

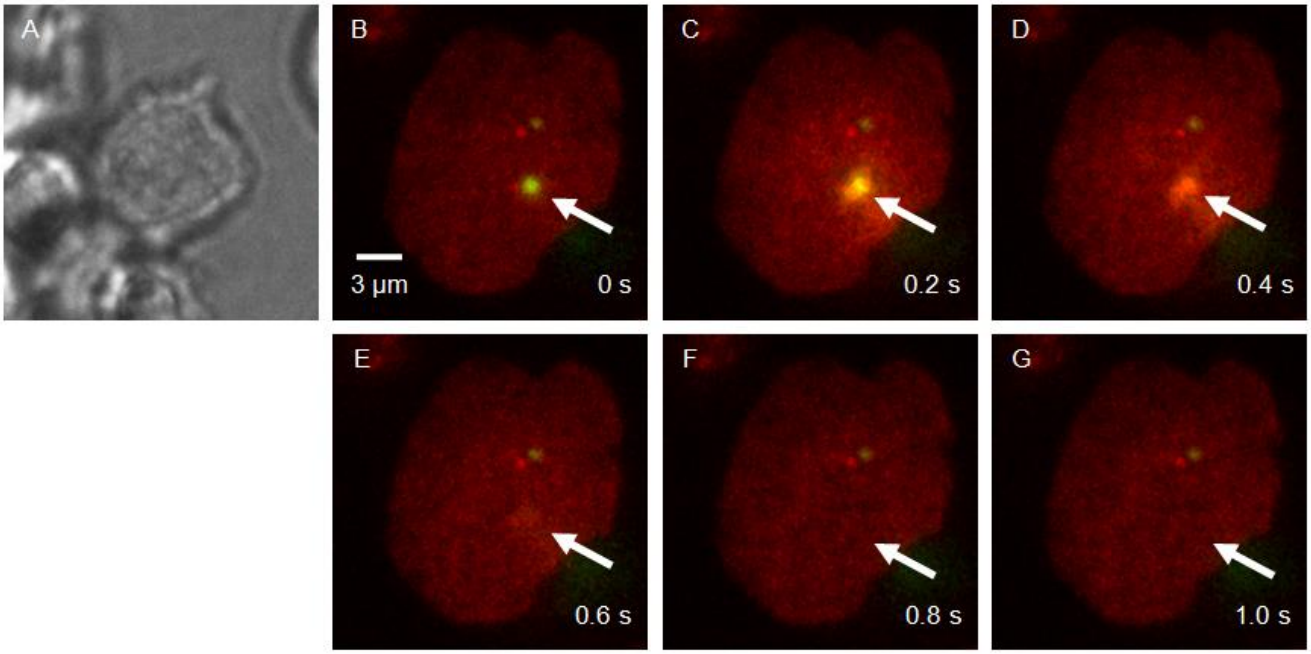

Figure 7 TIRFM snapshots showing Granzyme B mTFP and Syb2 pHuji fluorescence at the IS. Image A shows the brightfield picture of the CTL. Image B to G show the first type of fusion event where the Syb2 pHuji fluorescence would disappear within three seconds after Granzyme B mTFP secretion. Green: Granzyme B mTFP fluorescence, Red: Syb2 pHuji fluorescence and Yellow: co-localization of both fluorophores.

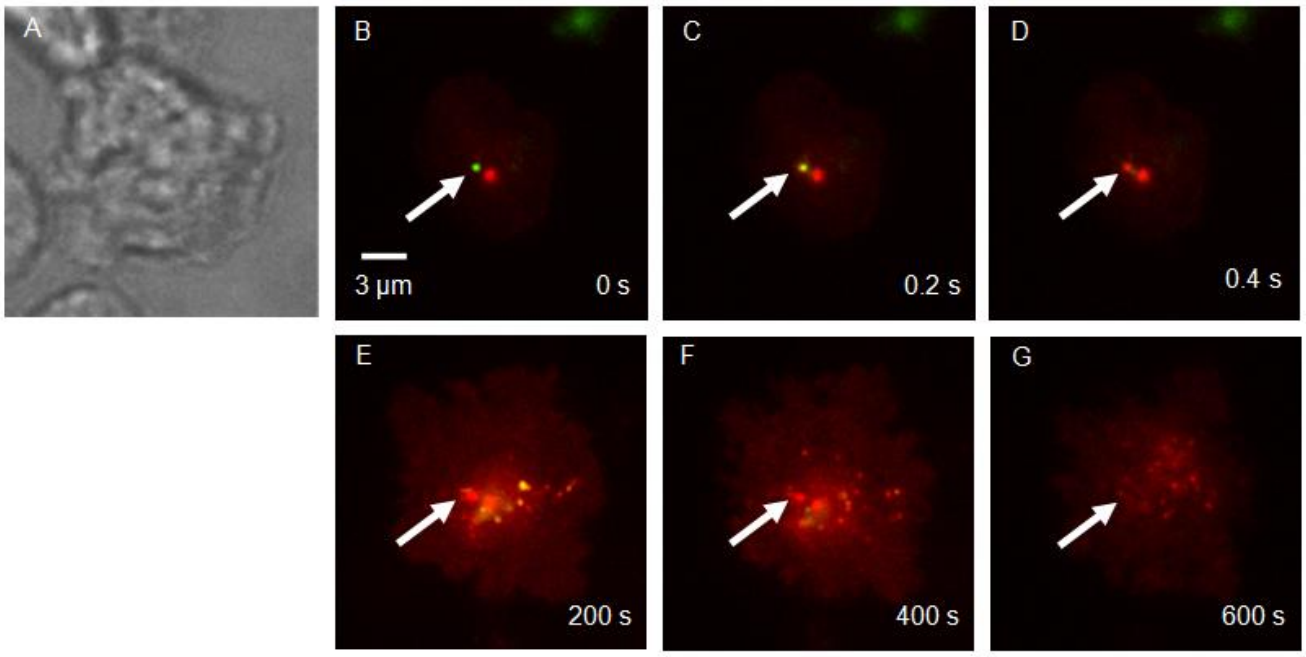

Figure 8 TIRFM snapshots showing Granzyme B mTFP and Syb2 pHuji fluorescence at the IS. Image A shows the brightfield picture of the CTL. Image B to G show the second type of fusion event where the Syb2 pHuji fluorescence would disappear within or more than 5 min after Granzyme B mTFP secretion. Green: Granzyme B mTFP fluorescence, Red: Syb2 pHuji fluorescence and Yellow: co-localization of both fluorophores.

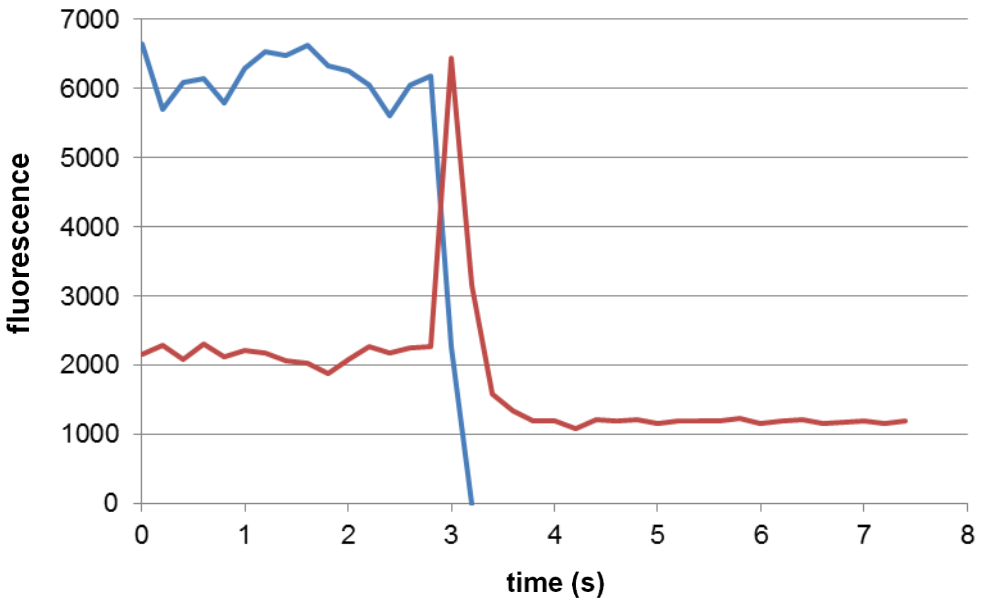

Figure 9 Changes in fluorescence of Granzyme B mTFP and Syb2 pHuji over time upon fusion of a short fusion event. Granzyme B mTFP signal disappears completely within 400 ms whereas Syb2 pHuji displays a sudden increase followed by a decrease in signal within 3 seconds in a short fusion event. Blue: Granzyme B mTFP fluorescence, Red: Syb2 pHuji fluorescence.

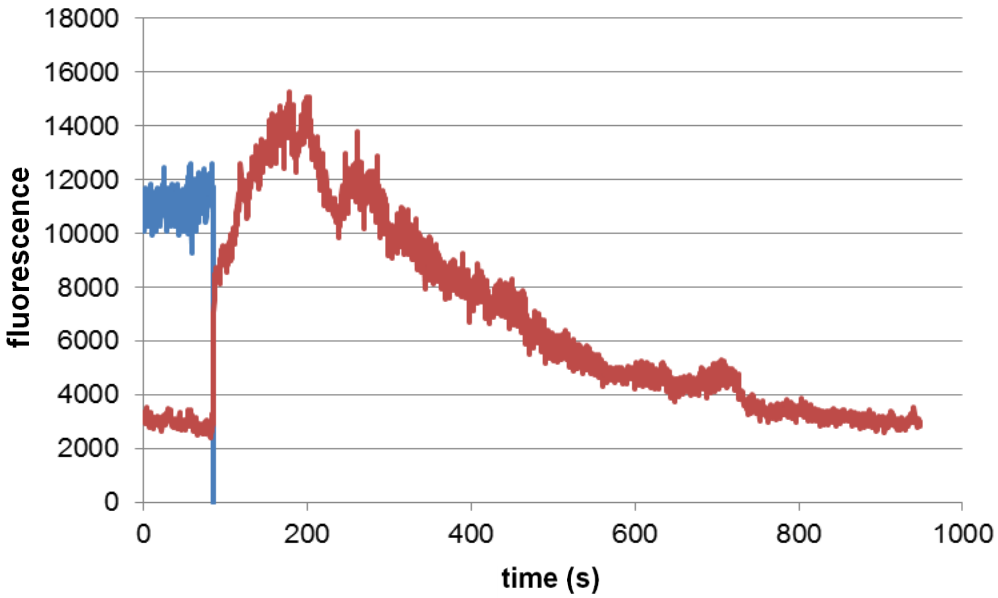

Figure 10 Changes in fluorescence of Granzyme B mTFP and Syb2 pHuji over time upon fusion of a long fusion event. Granzyme B mTFP signal disappears completely within 400 ms whereas Syb2 pHuji displays a sudden increase followed by a decrease in signal within 5 min or more in a long fusion event. Blue: Granzyme B mTFP fluorescence, Red: Syb2 pHuji fluorescence.

Out of the 31 fusion events analyzed for the 5 µg/ml anti-CD3ε conditions, 80.6% were short type fusion events and 19.4% were the long type fusion events. For the 10 µg/ml anti-CD3ε stimulation 82.4% of the 34 fusion events were short fusion events and 17.6% were long fusion events. Lastly for the 20 µg/ml anti-CD3ε 88.2% of the 34 fusion events were short fusion events and 11.8% were long fusion events.

The time for the complete short fusion events were 1.35 ± 0.06 s for the 5, 1.46 ± 0.07 s for the 10 and 1.48 ± 0.07 s for the 20 µg/ml anti-CD3ε stimulation conditions (figure 11). There were no significant differences in the timing required for the completion of short fusion events when the anti-CD3ε concentration was differed. Similarly, there were no significant differences in the timing required for the completion of long fusion events when the anti-CD3ε concentration was differed. The time for the complete long fusion events were 536.7 ± 81.6 s for the 5, 462.7 ± 122.5 s for the 10 and 570.6 ± 127.6 s for the 20 µg/ml anti-CD3ε stimulation conditions (figure 12).

For quantifying fusion pore opening times for the short and long fusion events a linear curve was fit for the uprise of Syb2 pHuji fluorescence of Syb2 pHuji from the base to the maximum fluorescence value using the program “IGOR Professional” and then the 10 to 90% rise time was calculated. For the 5 µg/ml anti-CD3ε condition this value was on average 0.55 ± 0.07 s, for the 10 µg/ml condition it was 0.66 ± 0.03 s and for the 20 µg/ml condition it was 0.65 ± 0.03 s (figure 13). Again, no significant differences were found in fusion pore opening times for the short and long fusion events upon varying the anti-CD3ε concentrations.

Next we quantified the decay time of Syb2 pHuji fluorescence by doing a single exponential fit again using “IGOR Professional” and then the tau value of this curve was calculated, with tau being the time taken for 67% of decrease in fluorescence. The results were split into two groups based on the tau values. All short fusion events ($t < 3$ s) had a tau value of less than 1.0 second and the long fusion events ($t > 3$ s) had a tau value of more than > 1.0 second. For the short fusion events the tau value was on average 0.335 ± 0.05 s for the 5 µg/ml anti-CD3ε condition, 0.339 ± 0.04 s for the 10 µg/ml and 0.319 ± 0.04 s for the 20 µg/ml anti-CD3ε conditions (figure 14). The tau value for the long fusion events was 379.97 ± 122.47 s for the 5 µg/ml, 322.95 ± 134.73 s for the 10 µg/ml and 362.04 ± 172.9 s for the 20 µg/ml anti-CD3ε stimulation conditions respectively (figure 15).

As a control the tau values for Granzyme B mTFP fluorescence were also calculated using a single exponential fit done by “IGOR Professional”. As expected, the average tau value of Granzyme B mTFP was significantly smaller and was on average 0.279 ± 0.002 s in comparison to the average tau value of Syb2 pHuji which was on average 0.332 ± 0.003 s. 71 fusion events were analyzed (figure 16, p-value < 0.001).

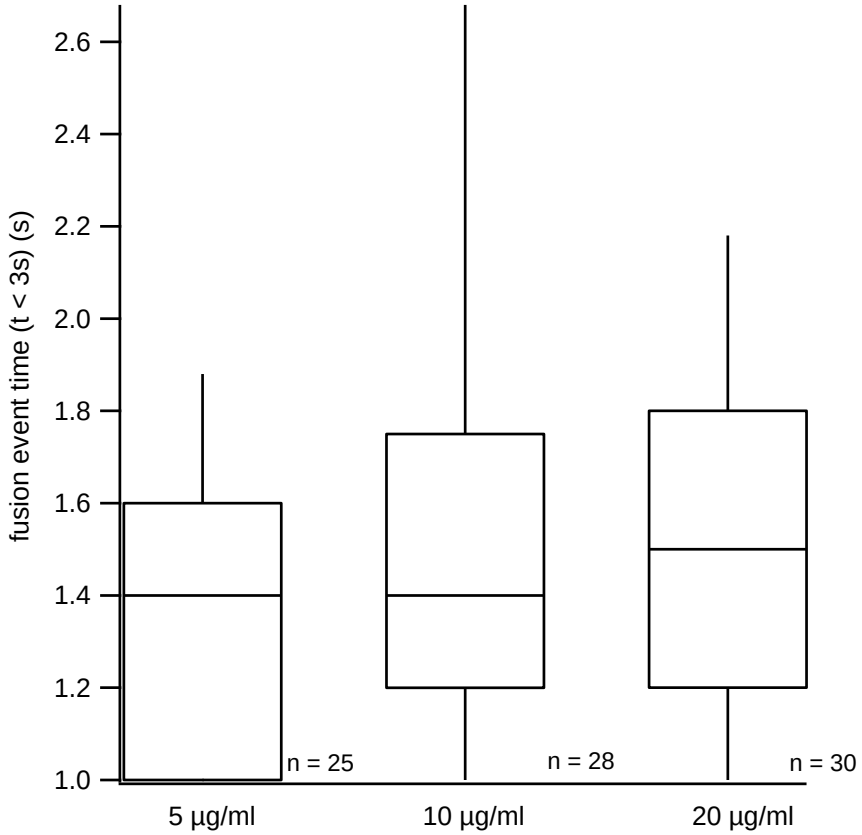

Figure 11 Complete fusion event time for the short fusion events. The complete fusion event time was analyzed as the time elapsed between one end of the base of the bell curve to the other end of the base. All the events where this time was less than 3 s were classified as short fusion events (t < 3 s). n = 25, 28 and 30 for the 5, 10 and 20 µg/ml anti-CD3ε conditions where n is the number of fusion events.

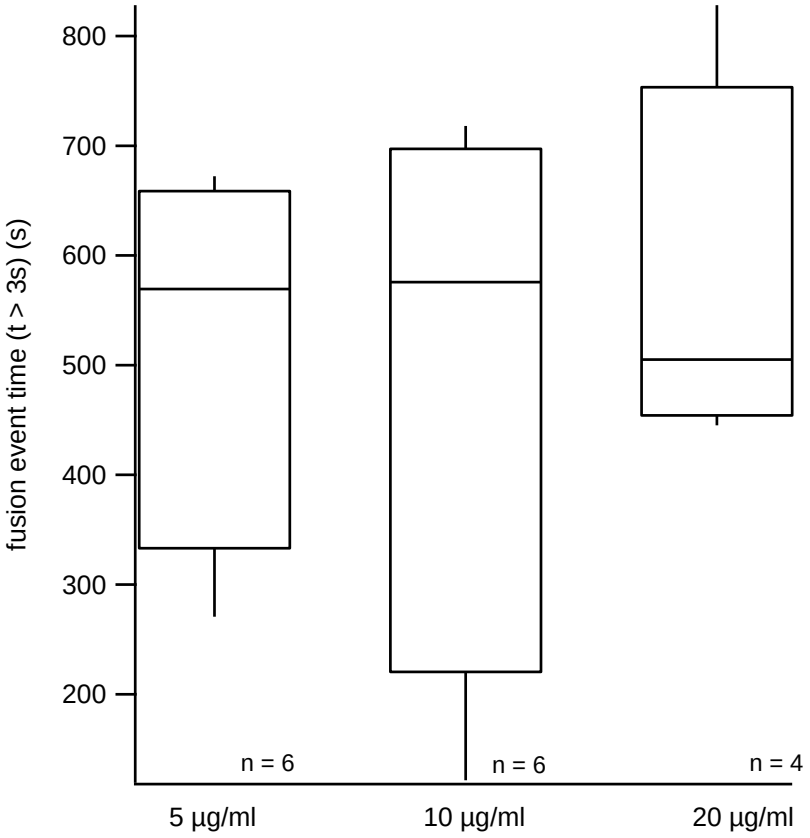

Figure 12 Complete fusion event times for the long fusion events (t > 3s). The complete fusion event time was analyzed as the time elapsed between one end of the base of the bell curve to the other end of the base. All the events where this time was more than 3 s were classified as long fusion events. n = 6, 6 and 4 for the 5, 10 and 20 µg/ml anti-CD3ε conditions where n is the number of fusion events.

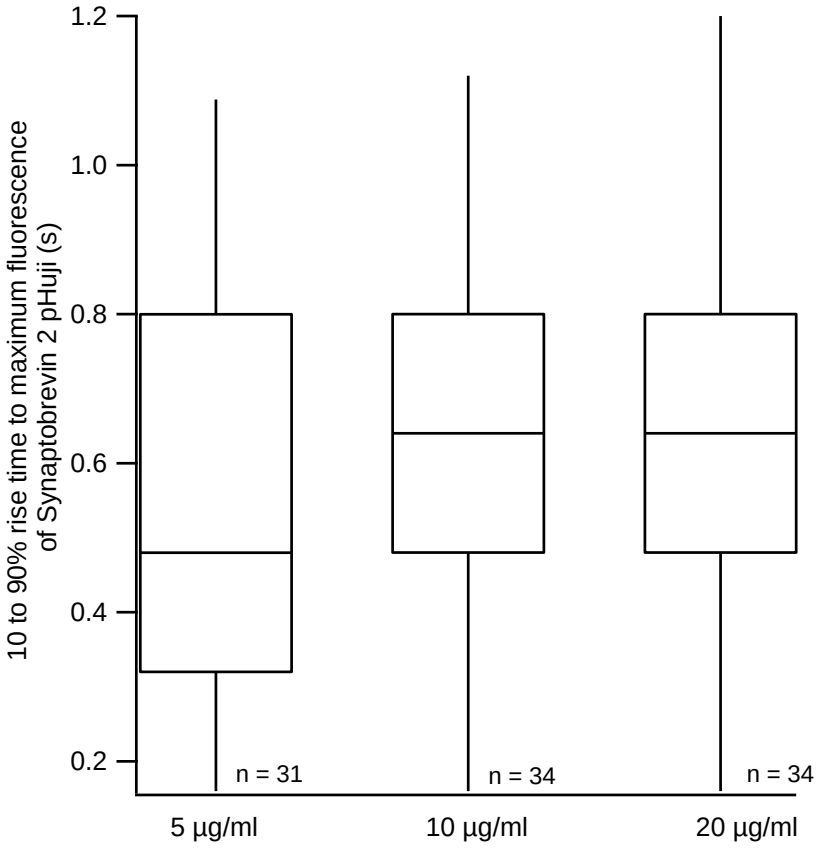

Figure 13 Rise time from 10% to 90% of the Syb2 pHuji fluorescence was not significantly different when the anti-CD3ε concentrations were changed. 31 fusion events for the 5, 34 fusion events for the 10 and 34 fusion events for the 20 µg/ml anti-CD3ε concentrations were analyzed respectively.

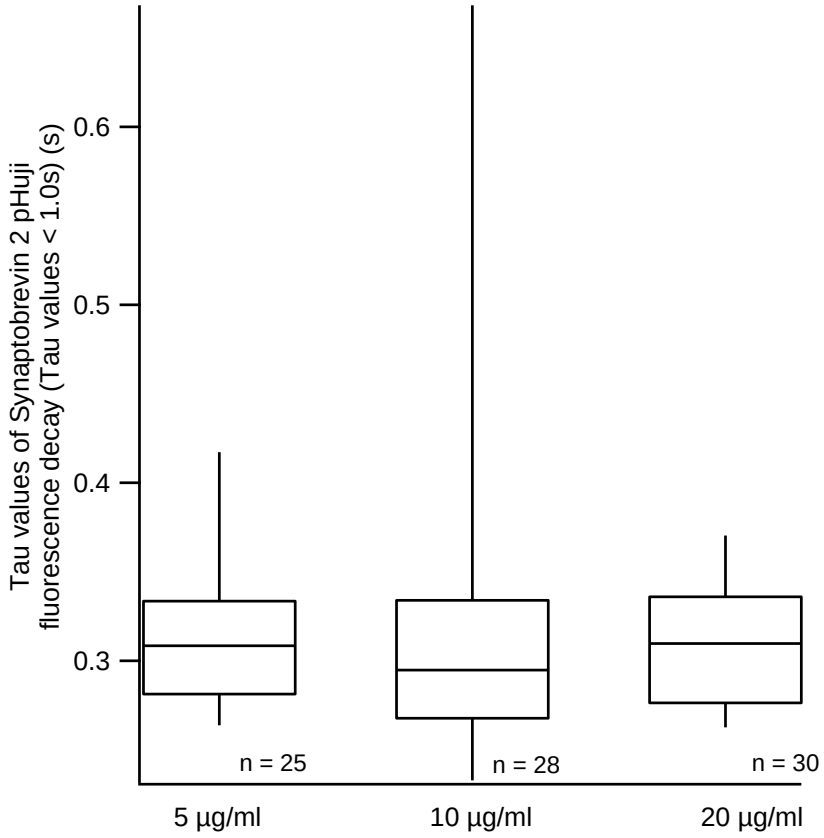

Figure 14 Tau values of Syb2 pHuji fluorescence for the short fusion events which were less than 1 s. 25 fusion events for the 5, 28 fusion events for the 10 and 30 fusion events for the 20 µg/ml anti-CD3ε stimulation were analyzed.

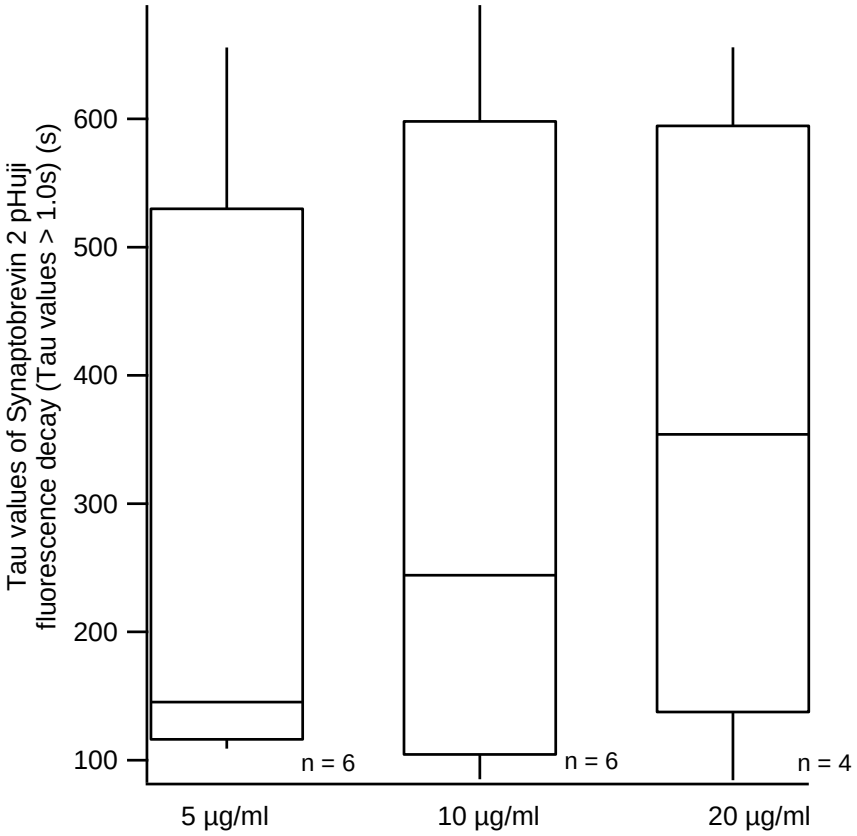

Figure 15 Tau values of Syb2 pHuji fluorescence for the long fusion events which were more than 1 s. 6 fusion events for the 5, 6 fusion events for the 10 and 4 fusion events for the 20 µg/ml anti-CD3ε stimulations were analyzed.

.

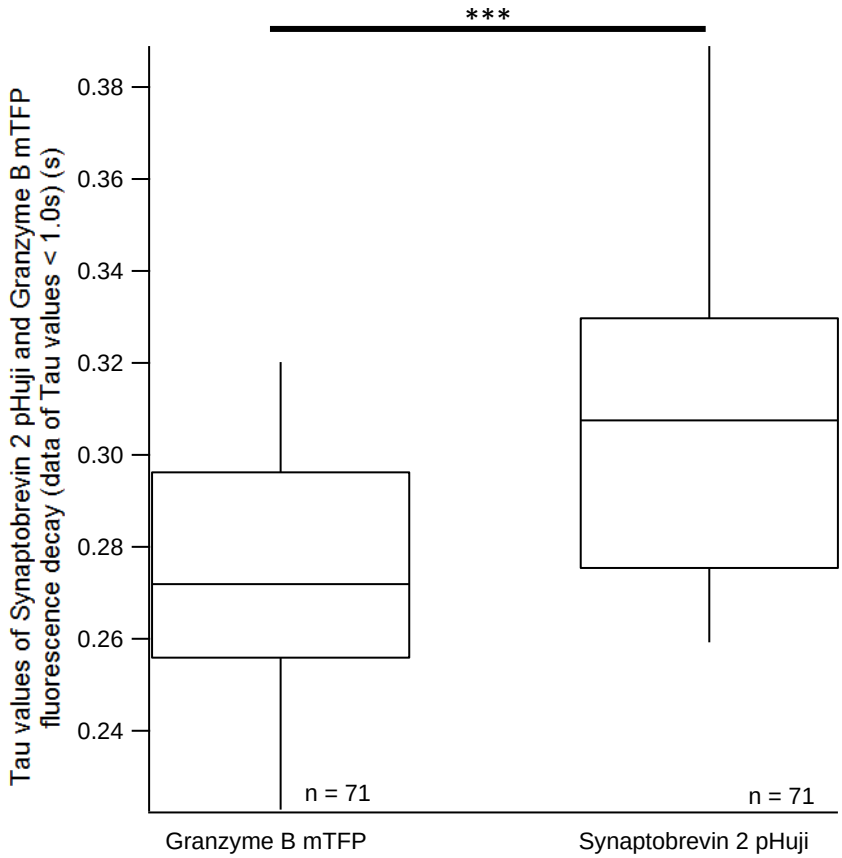

Figure 16 Tau values of Granzyme B mTFP and Syb2 pHuji are significantly different (tau values < 1.0s). Tau values for Granzyme B mTFP and Syb2 pHuji are 0.279 ± 0.0001 s and 0.332 ± 0.001 s. n = 71 fusion events; p-value < 0.001, Mann-Whitney-U-test.

As another control experiment to verify whether the entire vesicle is disappearing non reacidified into the cytosol following secretion of Granzyme B mTFP we performed sequential TIRF and epifluorescence imaging with a delay of 100 ms. By epifluorescence imaging we can image deeper into the cell. Therefore, we imaged long and short fusion events in TIRF and epifluorescence and could clearly see that in both the short and long fusion events, the fluorescence was disappearing in both the TIRF and epifluorescence images at the same time.

Ten short fusion events and three long fusion events of Syb2 pHuji that were imaged in both epifluorescence and TIRF mode were analyzed from 3 different mice each (figures 17, 18). The result was that in both cases the fluorescence also disappears entirely at the same time as in the TIRF mode, which means that in both types of fusion events the CG is not disappearing as a non-reacidified vesicle into the cytosol following Granzyme B secretion.

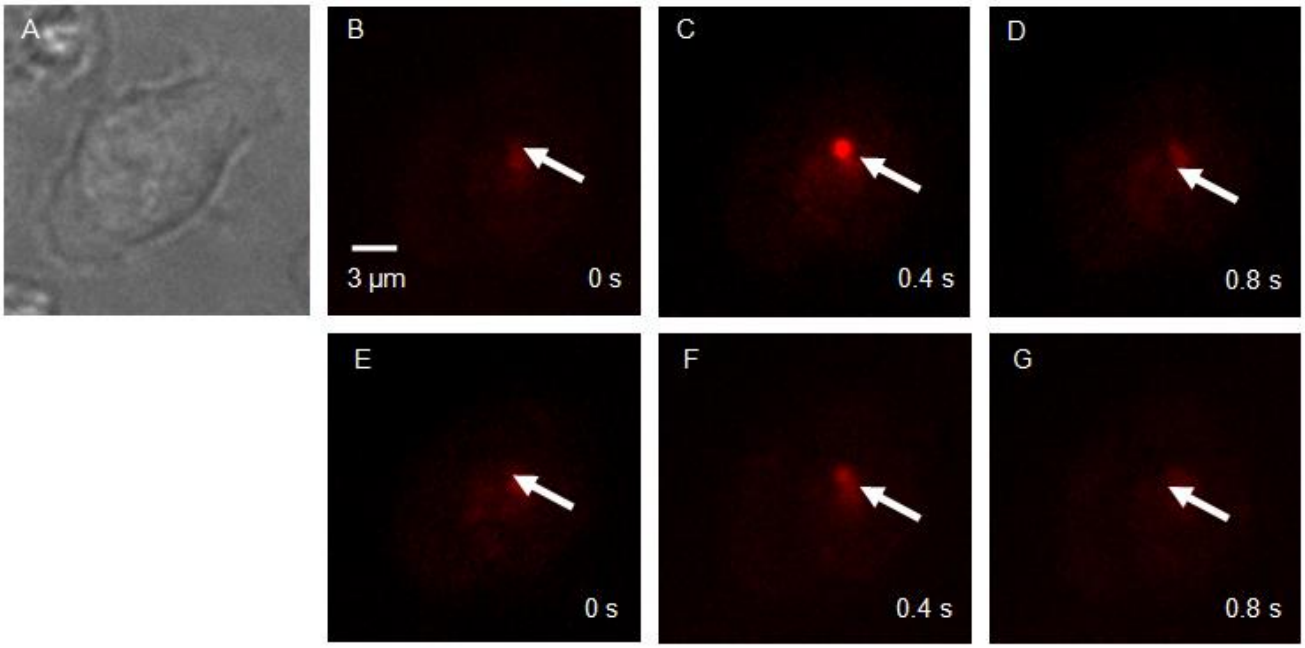

Figure 17 TIRF and epifluorescence snapshots of a murine wildtype CTL transfected with Syb2 pHuji. Image A shows the CTL in brightfield and images B to D are TIRF images and images E to G are the epifluorescence images of the same short fusion event. The Syb2 pHuji fluorescence is also disappearing in the epifluorescence mode in a short fusion event.

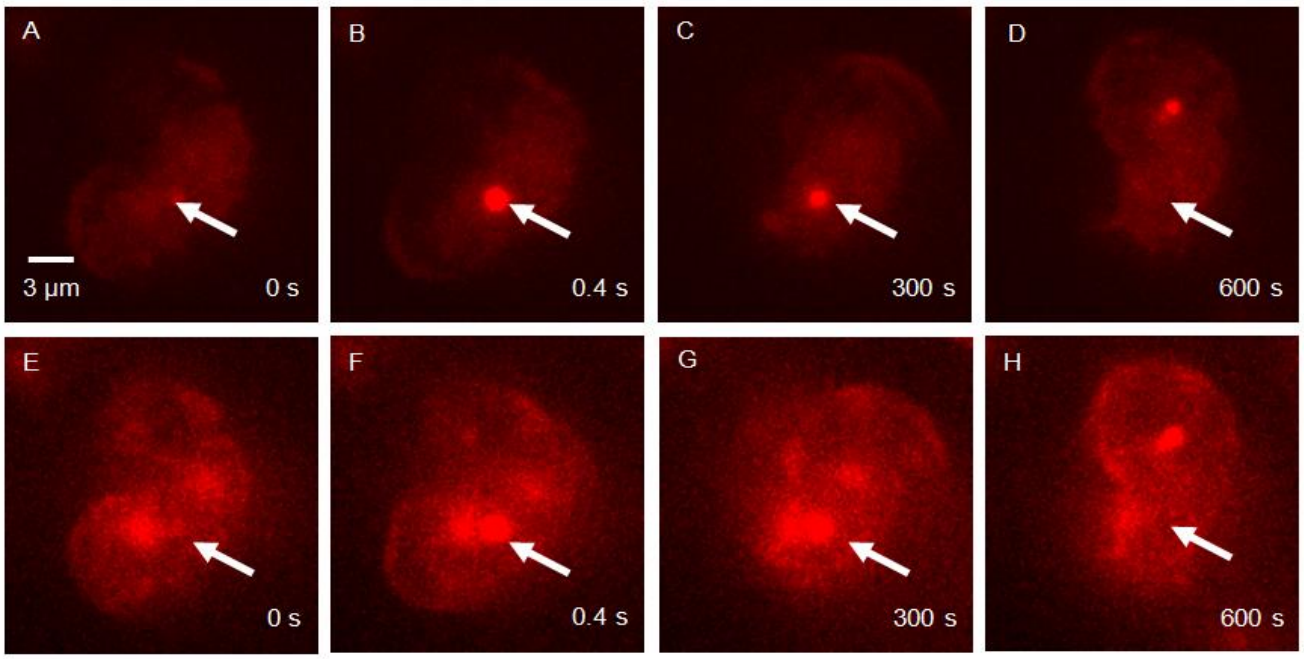

Figure 18 TIRF and epifluorescence snapshots of a murine wildtype CTL transfected with Syb2 pHuji. Images A to D show a long fusion event imaged sequentially in TIRF mode and images E to H show the images of the same fusion in epifluorescence mode. The fluorescence of Syb2 pHuji disappears in both the TIRF and epifluorescence mode simultaneously.

To clarify if in terms of a short fusion event (tau value < 1.0 s) the Syb2 pHuji is diffusing laterally into the plasma membrane two different types of analysis were done:

The first one was to merge 15 timelapse TIRF images of Syb2 pHuji fluorophore and the Granzyme B mTFP that cover 5 timepoints before and 10 timepoints after secretion of Granzyme B mTFP. The merged image was then analyzed by the program “ImageJ” by the line plot function in which we could analyze the fluorescence from the center of the fusion event up to the peripheral areas (figure 19). The fluorescence profile had a typical bell-shaped curve. Then the half width at half maximum value of the bell-shaped curves was calculated in nanometers with the program “IGOR Professional” for Syb2 pHuji and Granzyme B mTFP respectively. The result was that on average the half width at half maximum of these curves for Granzyme B mTFP was 2.9 ± 0.03 pixels (464 ± 4.8 nm) and for Syb2 pHuji 3.4 ± 0.06 pixels (544 ± 9.6 nm). Fifty-nine short fusion events were analyzed with this method and a Mann-Whitney-U-test revealed that the values of the half width at half maximum of the curves of Syb2 pHuji and Granzyme B mTFP are significantly different (figure 20, p-value < 0.05). This result implies that Syb2 is diffusing into the plasma membrane and therefore the diffusion speed is lower than that for Granzyme B which is diffusing into the extracellular milieu.

In a second type of analysis performed to validate Syb2 pHuji diffusion, the fluorescent bell curves of Syb2 pHuji 100 ms before and 100 ms after Granzyme B mTFP secretion were analyzed and compared to see if there would be an increase in the half width of the bell curve after secretion which would be indicative of lateral diffusion. Again, the line plot function of ImageJ was used to generate fluorescent bell-shaped curves of Syb2 pHuji fluorescence 100 ms before and after secretion. The half width at half maximum values of the curves were calculated by IGOR professional program. Sixty nine short fusion events were analyzed and the average half width at half maximum 100 ms before Granzyme B mTFP secretion was 473.6 ± 18.05 nm and 100 ms after the secretion it was 565.79 ± 21.66 nm. A Mann-Whitney-U-test was used to compare the two populations of data and revealed that they were significantly different from one another (figure 21, p-value < 0.01).

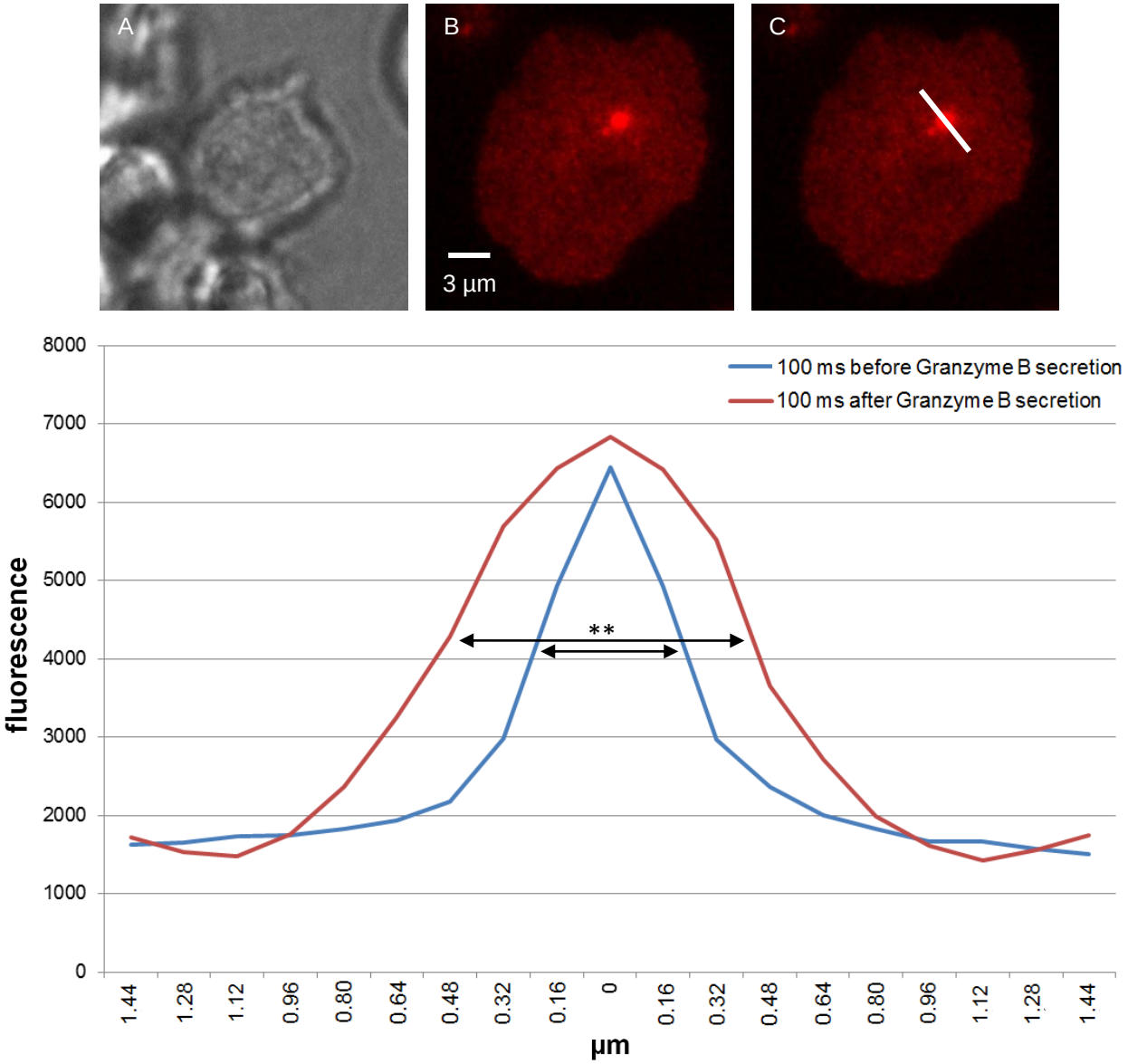

Figure 19 Line-plot analysis of fusion events. Image A shows the brightfield picture of a CTL. Images B and C show TIRF images of the Syb2 pHuji fluorescence in CTLs 100 ms before and after Granzyme B secretion. In image C the white line drawn through the CG shows the position of the line plot analysis in ImageJ. The chart below shows the results of a line plot analysis of Syb2 pHuji 100 ms before Granzyme B secretion (blue) and 100 ms after Granzyme B secretion (red). The x-axis shows the distance from the center of the fusion event in µm and the y-axis shows the fluorescence of Syb2 pHuji. The half width at half maximum for the Syb2 pHuji bell curve is larger 100ms after Granzyme B secretion (p-value < 0.01, Mann-Whitney-U-test).

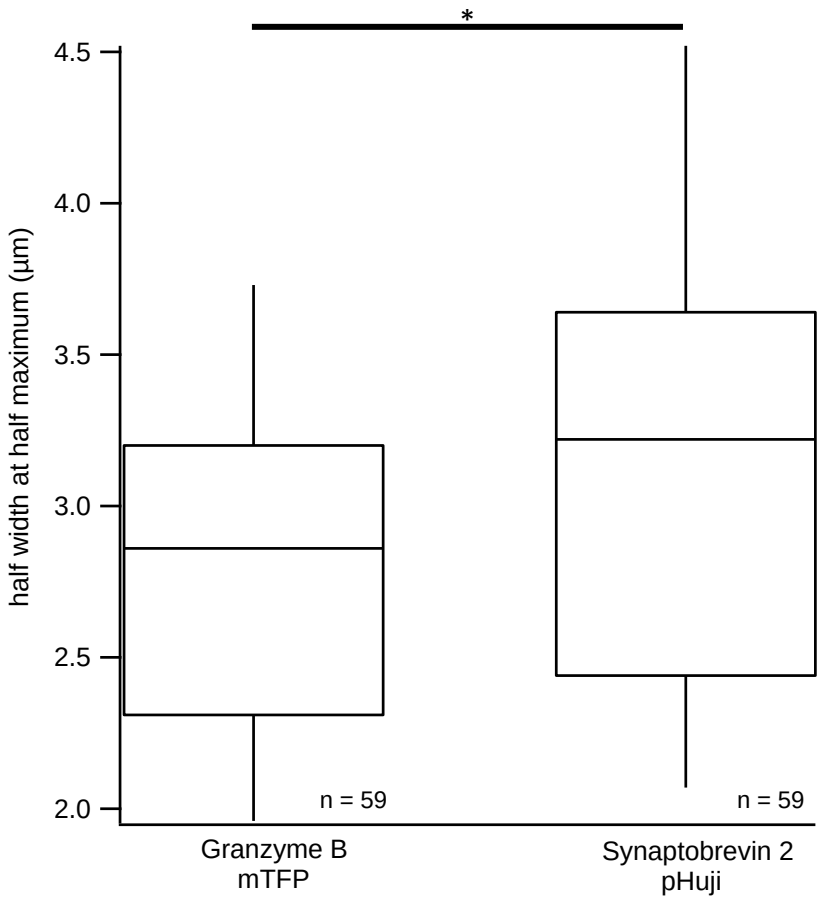

Figure 20 Differences in half width at half maximum between Granzyme B mTFP and Syb2 pHuji. The half width at half maximum values for Granzyme B mTFP and Syb2 pHuji fluorescence bell curves from a short fusion event (tau value < 1.0 s) obtained from a merged image that spans 15 time points (5 before and 10 after Granzyme B secretion). p-value < 0.05; Mann-Whitney-U-test. 59 fusion events were analyzed.

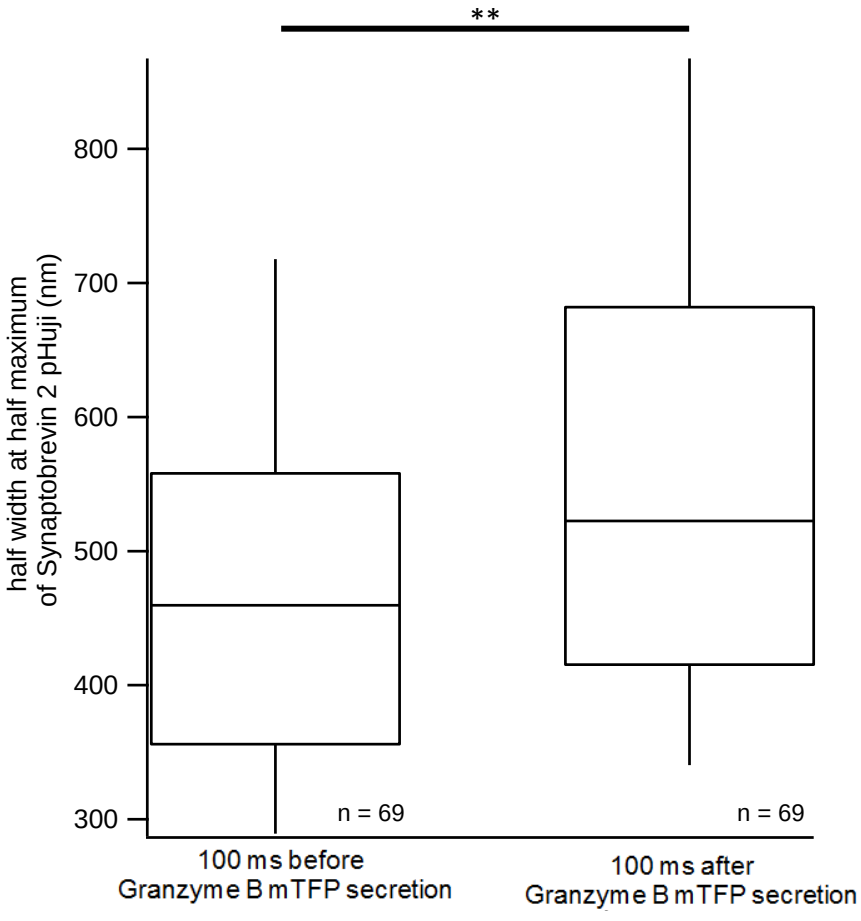

Figure 21 Differences in half width at half maximum of Syb2 pHuji 100 ms before and after Granzyme B secretion. This box plot shows the half width at half maximum values of Syb2 pHuji 100 ms before and 100 ms after Granzyme B mTFP secretion, the result was highly significant below the 0.01 level by the Mann-Whitney-U-test. 69 fusion events were analyzed in this way.

5.2 IS formation of murine CTLs with varied stimulus on the TCR

We varied the strength of the TCR stimulus by varying anti-CD3ε concentrations on the lipid bilayer and aimed to systematically analyze the subsequent effects on various parameters pertaining to IS formation and stability. The idea behind this project was to identify differences in IS formation in CTLs upon varying the strength of TCR stimulus. CTLs that have been activated for 7 or 8 days with anti-CD3/ anti-CD28 coated beads and IL-2 were made to overexpress lifeact mRFP and CD3ε TFP and imaged on lipid bilayers containing 5, 10 and 20 µg/ml anti-CD3ε for 15 min by TIRF microscopy.

Lifeact, a 17-amino-acid peptide, which stains filamentous actin (F-actin), does not interfere with actin dynamics in vivo and in vitro and when coupled with a fluorophore such as RFP or GFP can be used for visualizing actin dynamics [84]. We used lifeact coupled with mRFP as a marker for the dSMAC as it is one of the major components in this zone of the IS. CD3ε TFP was used to mark surface and recycling TCRs that eventually polarize to the cSMAC.

Typical IS formation by CTLs on anti-CD3ε and ICAM containing lipid bilayers is depicted below (figure 22).

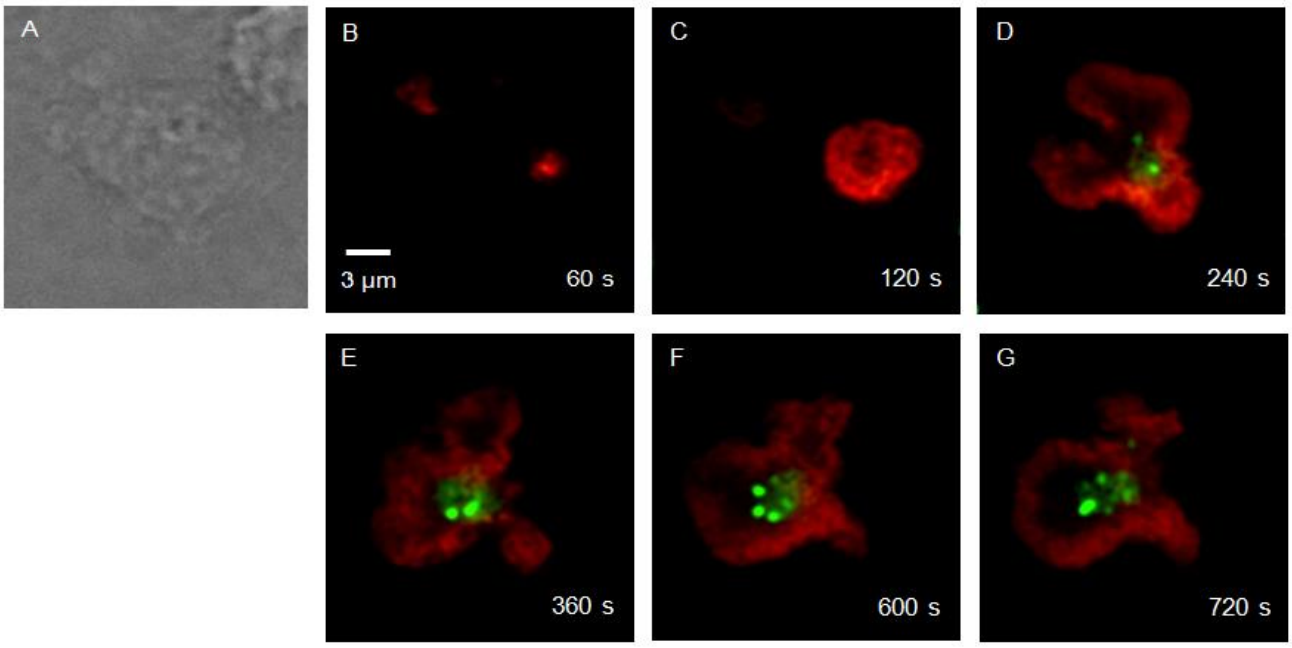

Figure 22 IS formation visualized in a murine wildtype CTL expressing lifeact mRFP and CD3ε TFP. TIRFM snapshots of a CTL forming an IS on lipid bilayers containing anti-CD3ε and ICAM at the indicated time points after cell addition. The red fluorescence is lifeact mRFP and the green is CD3ε TFP. Actin clearance from the center and formation of a ring is seen along with accumulation of CD3ε TFP clusters.

Parameters such as latency of adhesion, dwell times and maximum area spread on the IS were analyzed for 30 CTLs prepared from 6 different mice for each concentration of anti-CD3ε on the lipid bilayer over an acquisition time of 15 min. Thresholds were set manually to the images to distinguish fluorescence from noise and were verified by the line plot function of the program "ImageJ". Dwell time was defined as the time duration in which the fluorescent CD3ε TFP vesicle or the actin ring remained in the TIRF field. The latency of cell adhesion was calculated by the difference in the time when the first cell adhered with an area of ~3 µm² to the lipid bilayer after the addition of the cells into the lipid bilayer chamber (t = 0). This time was on average for the 10 µg/ml anti-CD3ε 45.47 ± 5.47 s, for 20 µg/ml 134.03 ± 7.3 s and for 5 µg/ml 296.37 ± 12.78 s. Statistical significance was tested by a one-way ANOVA test which demonstrated that the datasets are significantly different from another (p-value < 0.001) (figure 23). Next we analyzed the latency of full actin ring formation following adherence of the cell to the bilayer. With the 5 µg/ml condition the latency was 102.21 ± 5.47 s, for the 10 µg/ml condition it was 105.63 ± 10.04 s and for the 20 µg/ml condition it was 10.73 ± 8.21 s. A one-way ANOVA test revealed no significant differences among the data sets (figure 24). Next, the timepoint of the first visible CD3ε TFP aggregate after the first sign of a fully formed dSMAC ring (t = 0) was on average 77.23 ± 9.1 s for the 5 µg/ml condition, 85.61 ± 7.1 s for the 10 µg/ml condition and 92.48 ± 7.66 s for the 20 µg/ml condition. A one-way ANOVA test revealed no significant differences among the data sets (figure 25). Furthermore, the number of CD3ε TFP aggregates per cell were on average 4.27 ± 0.36 for the 5, 5.83 ± 0.18 for the 10 and 5.9 ± 0.23 for the 20 µg/ml anti-CD3ε concentrations respectively (figure 26). The average area of a CD3ε TFP aggregate was 0.84 µm² ± 0.06 for the 5 µg/ml, 1.48 µm² ± 0.06 for the 10 µg/ml and 1.25 µm² ± 0.05 for the 20 µg/ml (figure 27). Both the size and the number of CD3ε TFP clusters formed in CTLs stimulated with either 5, 10 or 20 µg/ml anti-CD3ε significantly increase with increasing anti-CD3ε concentrations. Next we analyzed the dwell time of a CD3ε TFP cluster which on average for the 5 µg/ml condition was 99.69 ± 5.3 s, for the 10 µg/ml was 154.13 ± 7.55 s and for the 20 µg/ml anti-CD3ε stimulation was 106.7 ± 4.55 s. A one-way ANOVA test showed that the data sets are statistically different from another (figure 28). The area of the dSMAC increases with increasing concentrations of anti-CD3ε and was on average for the 5 µg/ml condition 116.97 ± 12.8 µm², for the 10 µg/ml condition 133.13 ± 5.48 µm² and for the 20 µg/ml condition 137.86 ± 10.95 µm, but a one-way ANOVA test revealed no significant differences among the data sets (figure 29). The dwell time of the actin ring also increased with increasing concentrations and was on average 266.56 ± 11.6 s for the 5 µg/ml condition, 325.3 ± 4.6 s for the 10 µg/ml condition and 332.36 ± 7.1 s for the 20 µg/ml condition. A one-way ANOVA test showed that cells adhering and forming an IS with 5 µg/ml anti-CD3ε have a significantly lower actin ring dwell time than the cells forming an IS with 10 and 20 µg/ml anti-CD3ε (figure

30). Furthermore, the maximum pSMAC and cSMAC size were analyzed and the average was for the 5 µg/ml condition 55.38 ± 3.6 µm², for the 10 µg/ml 88.1 ± 7.3 µm² and for the 20 µg/ml 78.81 ± 5.47 µm². The p+cSMAC area in CTLs forming an IS with 5µg/ml were significantly lower than those formed in CTLs stimulated with 10 or 20 µg/ml anti-CD3ε (figure 31, p-value < 0.01). In addition to that, the ratio between the dSMAC and the pSMAC/cSMAC size was calculated and on average it was for the 5 µg/ml 3.46 ± 0.27, for the 10 µg/ml 2.38 ± 0.18 and for the 20 µg/ml 3.07 ± 0.15. A one-way ANOVA test revealed that between 5 µg/ml to 10 µg/ml the result was below the 0.01 value significantly different (figure 32). Apart from that, the center of mass of each cell was calculated every 200 ms for the entire acquisition period. With this data the speed of movement in 200 ms could be generated because the x and y-axis change every 200 ms could be re-shaped into lines of a right triangle from the hypotenuse calculated to give the speed of movement of the CTL every 200 ms. The value obtained was multiplied by 5 to get the speed of movement per second. Our result showed that cell mobility on 5 µg/ml anti-CD3ε bilayers was 0.284 ± 0.035 µm/s, on 10 µg/ml anti-CD3ε bilayers was 0.251 ± 0.027 µm/s and on 20 µg/ml anti-CD3ε bilayers was 0.167 ± 0.018 µm/s. A one-way ANOVA test showed that the cells stimulated with 5 µg/ml anti-CD3ε showed significantly more movement when compared to 20 µg/ml anti-CD3ε stimulations (figure 33, p-value < 0.05).

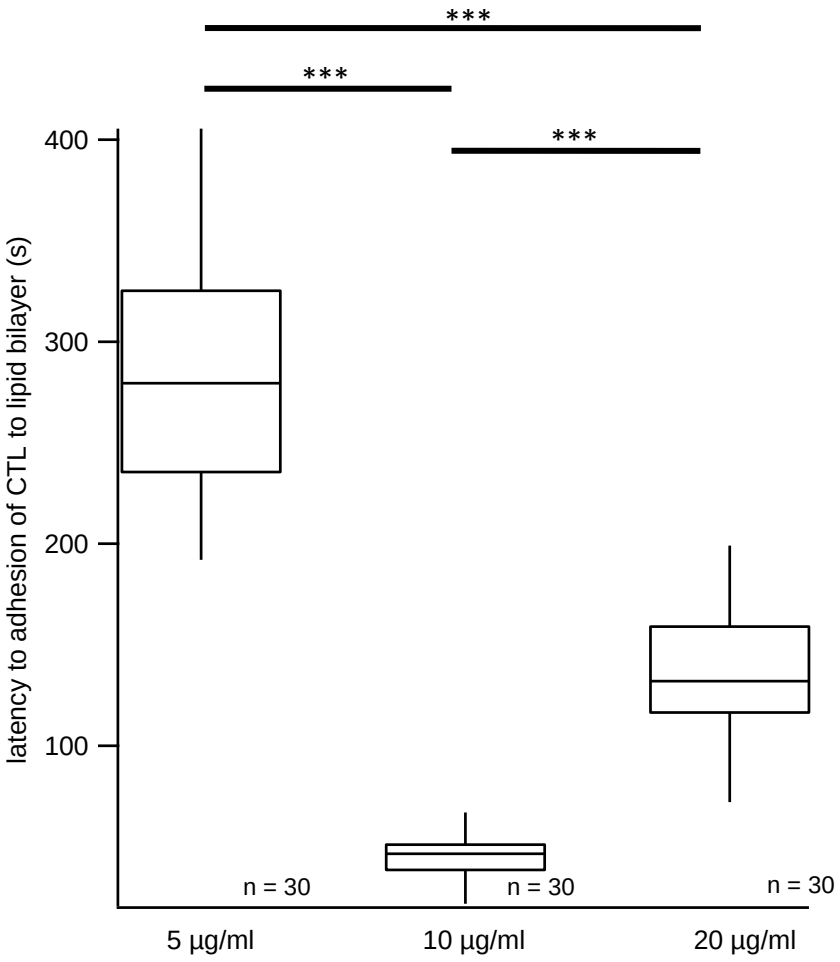

Figure 23 Latency to adhesion of the CTL to lipid bilayer varies depending on the anti-CD3ε antibody concentration. The latency of adhesion of the CTL to the lipid bilayer is significantly changed with changing anti-CD3ε antibody concentrations. 30 cells were analyzed for each concentration.

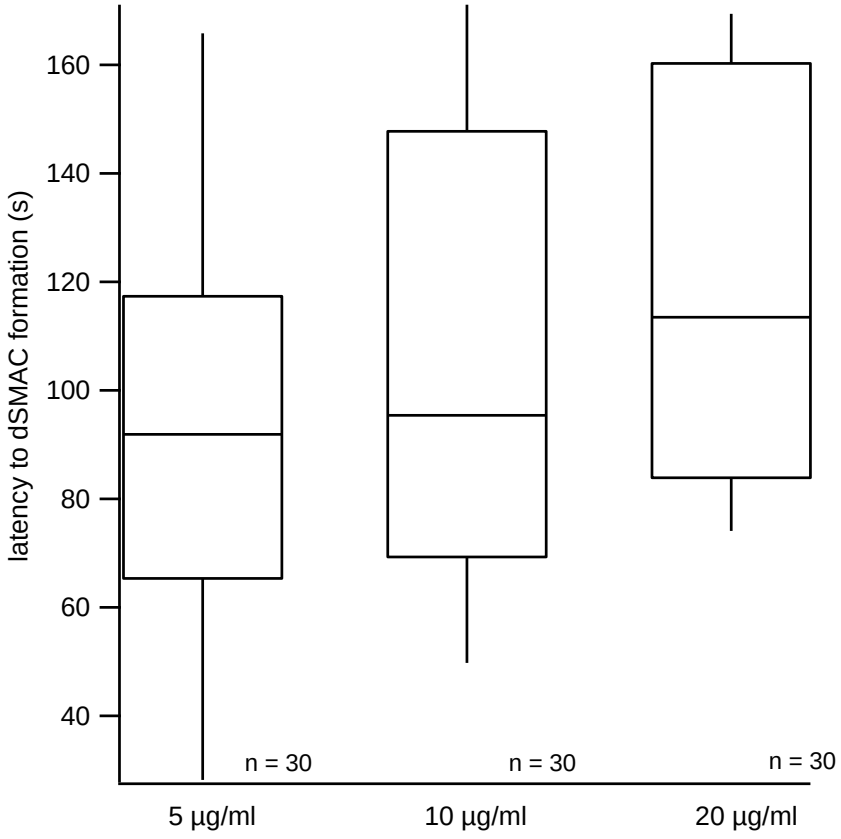

Figure 24 Latency to dSMAC formation normalized to cell adhesion. The latency to dSMAC formation after cell adhesion to the lipid bilayer is not changed with varying anti-CD3ε antibody concentrations. 30 cells were analyzed for each concentration.

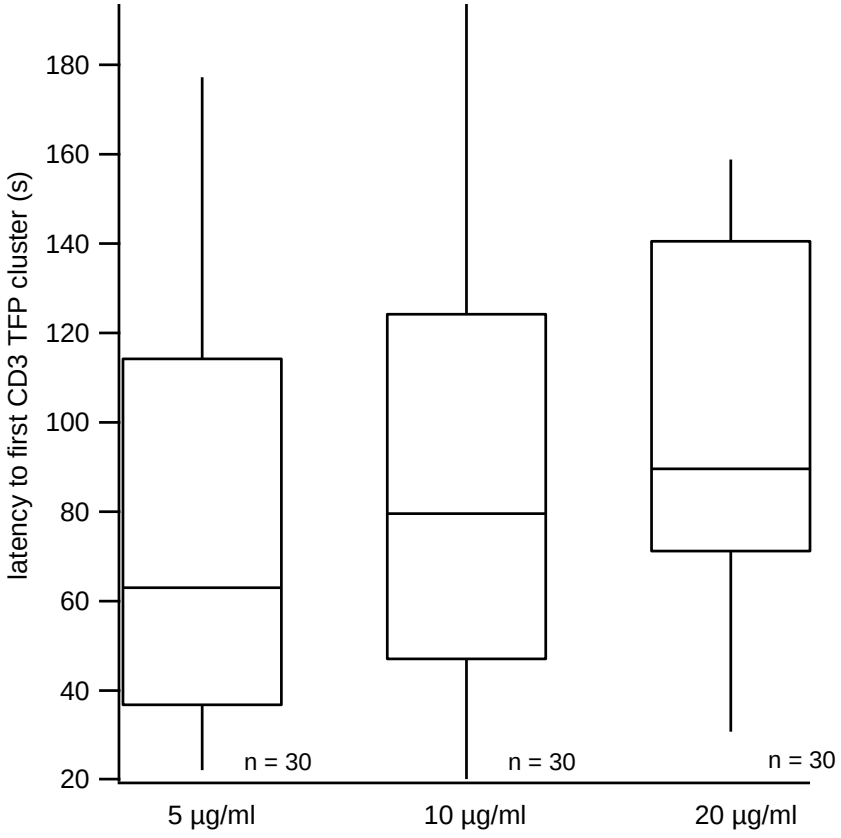

Figure 25 Latency to first CD3ε TFP cluster following cell adhesion. The latency to the first CD3ε TFP cluster following cell adhesion to the bilayer is unchanged with varying anti-CD3ε antibody concentrations. 30 cells were analyzed for each concentration.

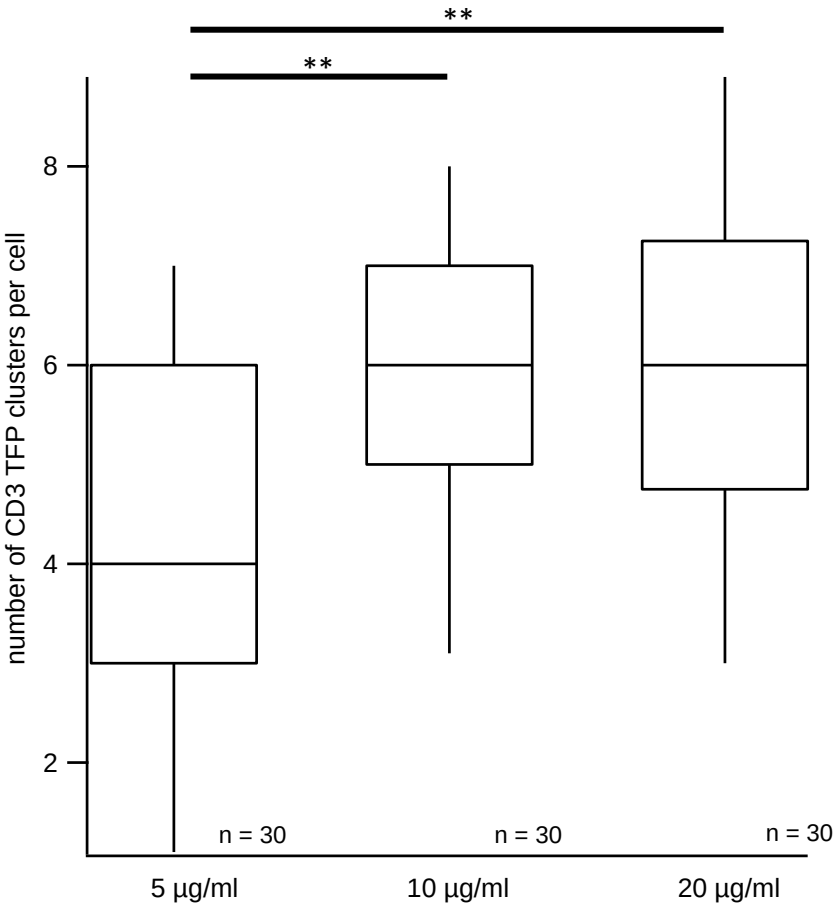

Figure 26 Number of CD3ε TFP clusters per cell increased with increasing anti-CD3ε antibody concentrations. The number of CD3ε TFP clusters per cell significantly changes upon varying anti-CD3ε antibody concentrations. 30 cells were analyzed for every concentration.

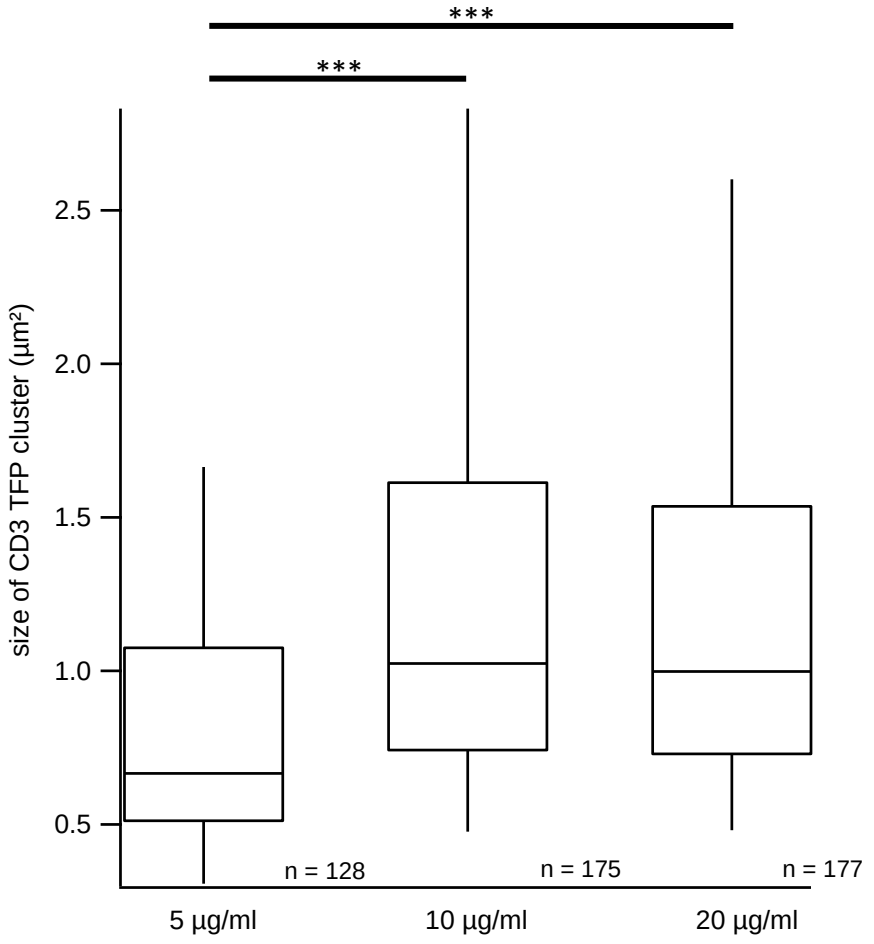

Figure 27 Area of CD3ε TFP clusters changes significantly upon changing anti-CD3ε antibody concentrations. 128 CD3ε TFP cluster were analyzed for the 5 µg/ml anti-CD3ε condition, 175 for the 10 and 177 for the 20 µg/ml anti-CD3ε conditions respectively.

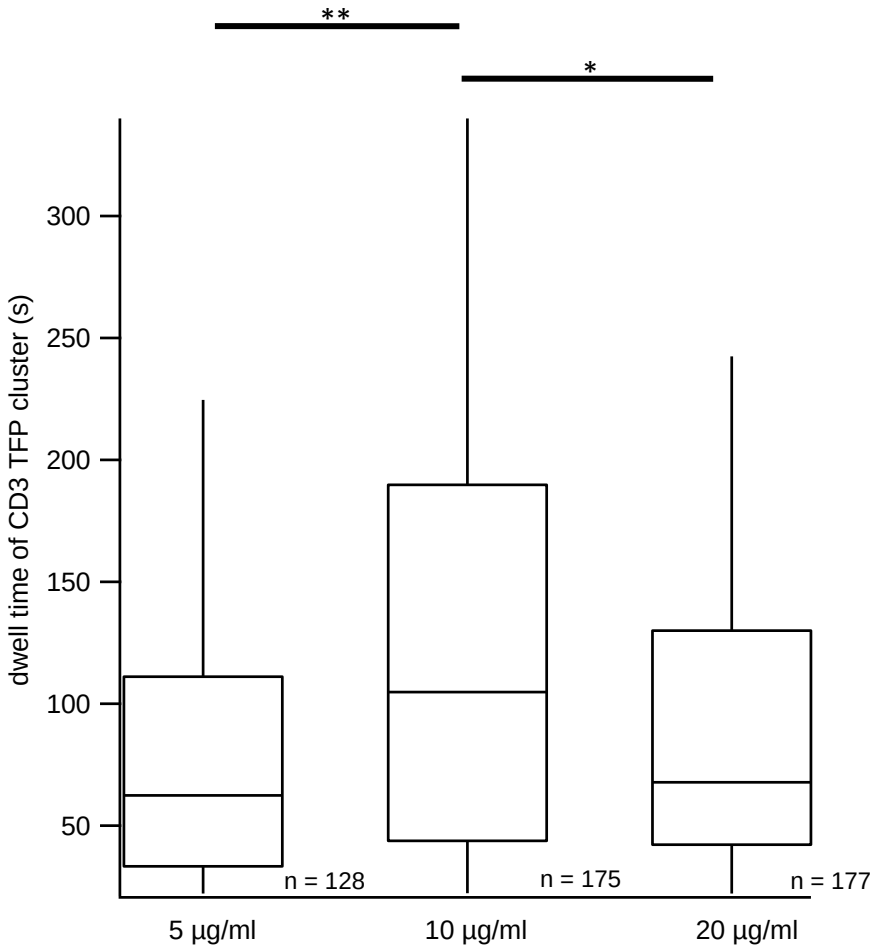

Figure 28 Dwell time of CD3ε TFP clusters in the cSMAC required an optimum stimulus on the TCR. The dwell time of the CD3ε TFP clusters changes significantly with changing concentrations and is the maximum in CTLs stimulated with 10 µg/ml anti-CD3ε antibody. 128 CD3ε TFP cluster were analyzed for the 5, 175 for the 10 and 177 for the 20 µg/ml anti-CD3ε stimulation conditions.

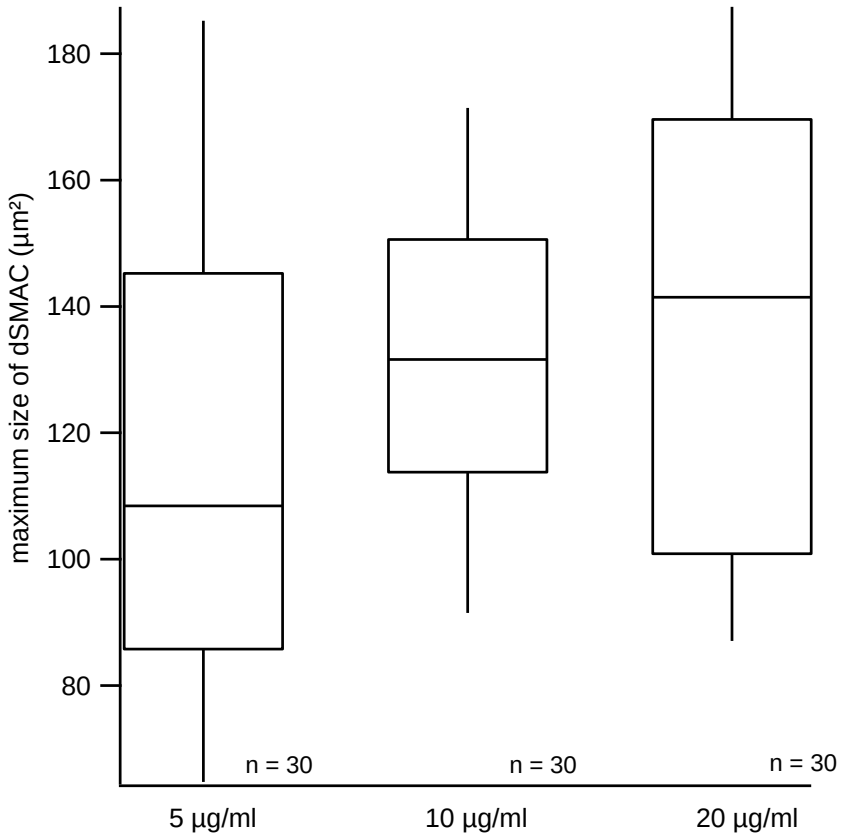

Figure 29 Varying anti-CD3ε antibody concentrations has no significant influence on the size of the dSMAC. 30 cells were analyzed for each concentration.

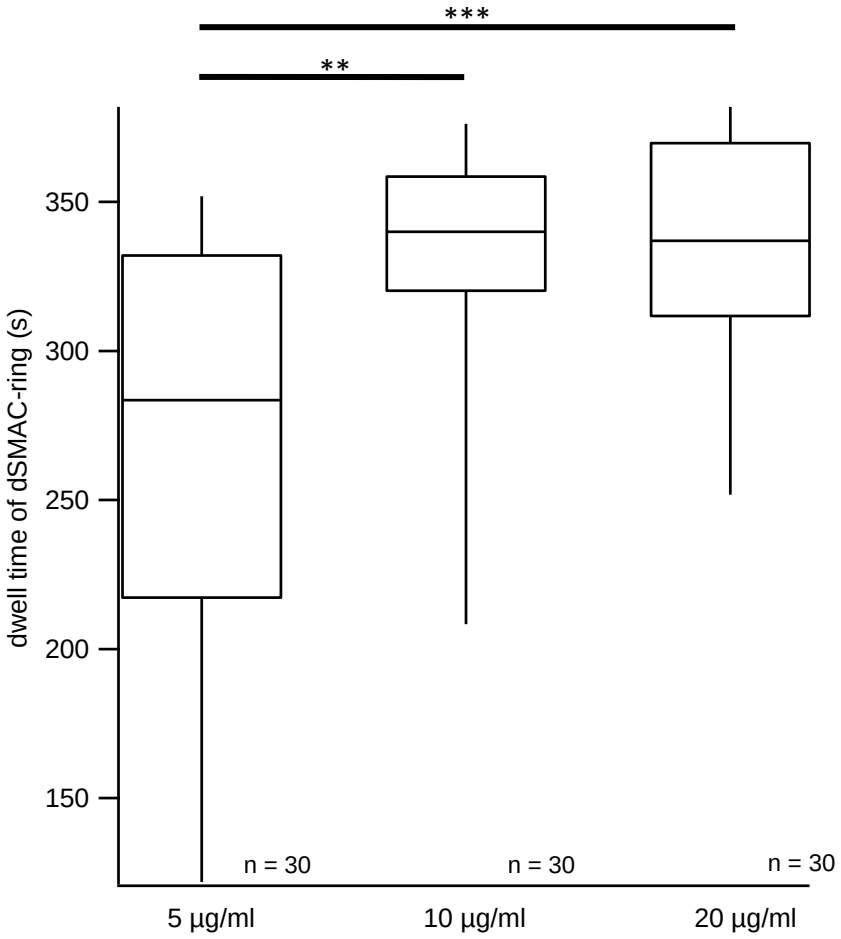

Figure 30 Dwell time of dSMAC ring normalized to adhesion increases with increasing anti-CD3ε antibody concentrations. The dwell time of the dSMAC ring changes with increasing anti-CD3ε antibody concentrations. 30 cells were analyzed for each concentration

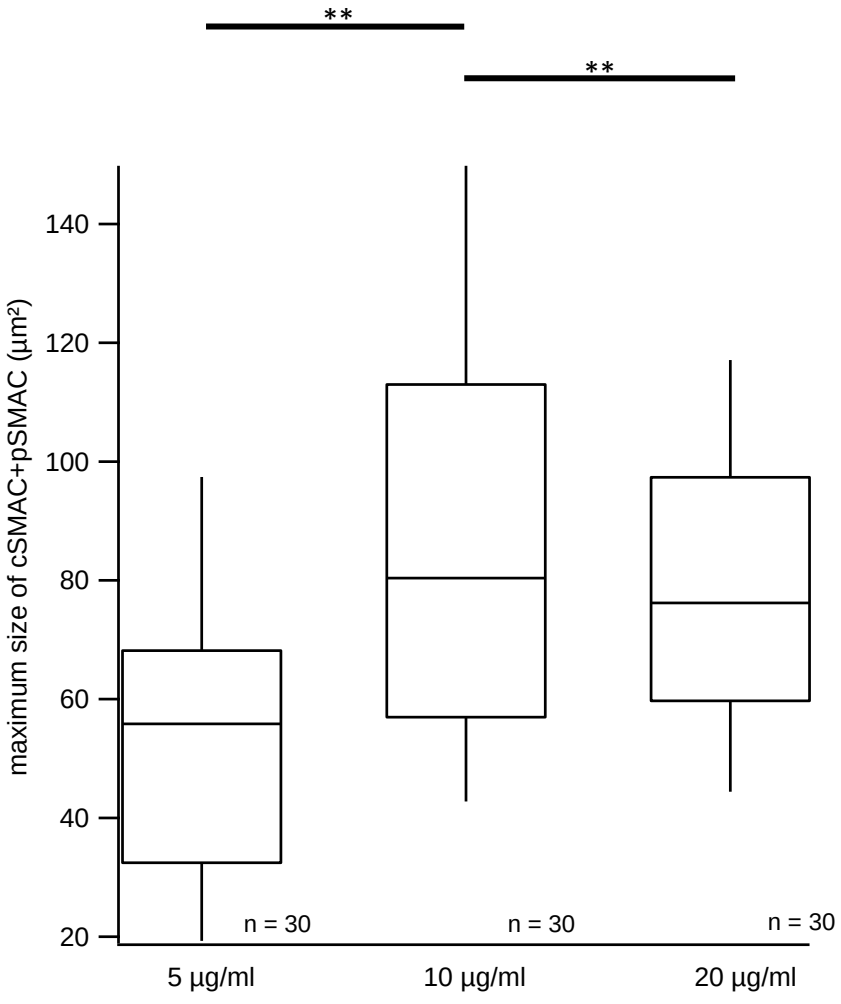

Figure 31 The combined cSMAC+pSMAC size required an optimum stimulus. The size of the actin free area was maximal with 10 µg/ml anti-CD3ε. 30 cells for each concentration were analyzed.

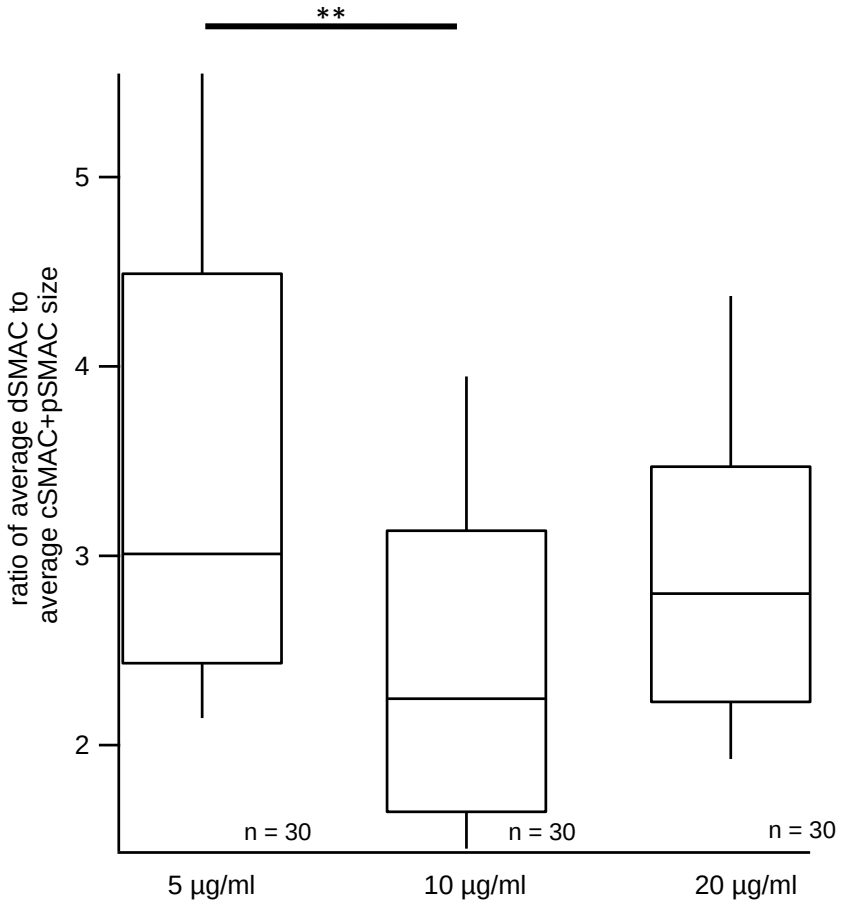

Figure 32 Ratio between dSMAC to cSMAC+pSMAC seems to depend on an optimum anti-CD3ε antibody concentration. The ratio between the average dSMAC size compared to the average cSMAC + pSMAC size is the largest with the 10 µg/ml anti-CD3ε stimulation. 30 cells were analyzed for each concentration.

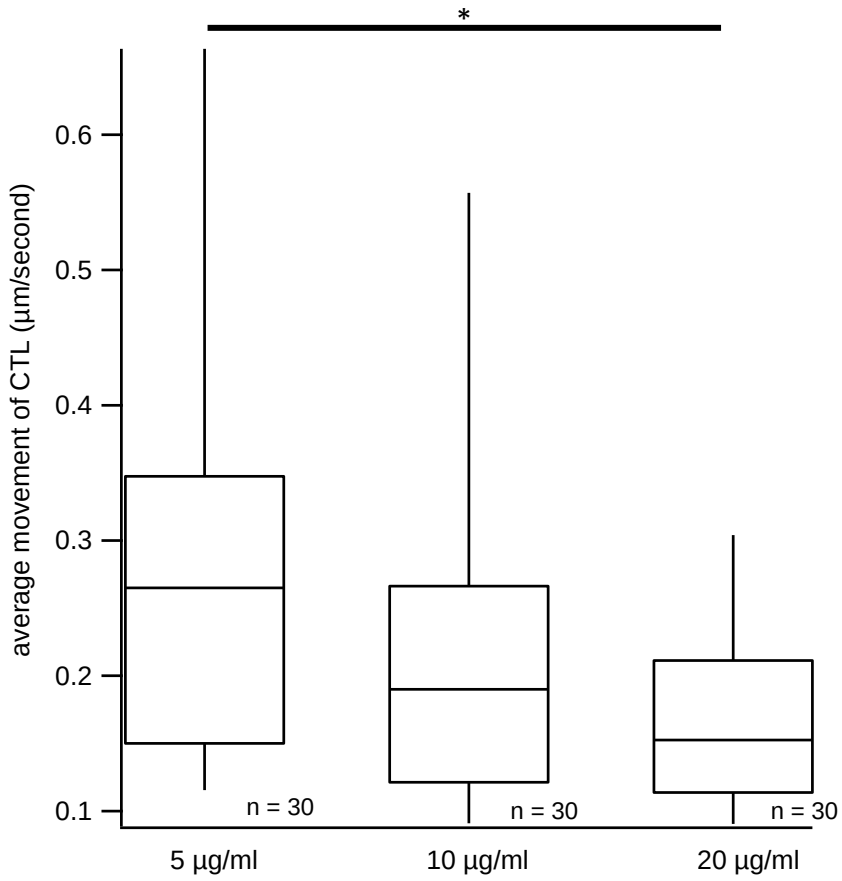

Figure 33 Average movement of CTL. The average movement of the CTL in µm/s is significantly higher in cells stimulated with lower anti-CD3ε antibody concentrations. 30 cells for each concentration were analyzed

5.3 Differences in behavior of Granzyme B mTFP knock-in CTLs due to variation in the strength of stimulus of the TCR in murine CTLs

In this study the strength of stimulus on the TCR was varied by preparing lipid bilayers containing different concentrations of anti-CD3ε antibodies and the behaviour of CTLs related to effector function was analyzed thereafter. Granzyme B mTFP knock-in CTLs were used as their cytotoxic granules were endogenously fluorescently labeled and therefore could be imaged by TIRFM.

A fusion event of a CG was defined as an event where the Granzyme B mTFP fluorescence would decrease at least 50% within 200 ms and the fluorescence would completely disappear within 400 ms (figure 34).

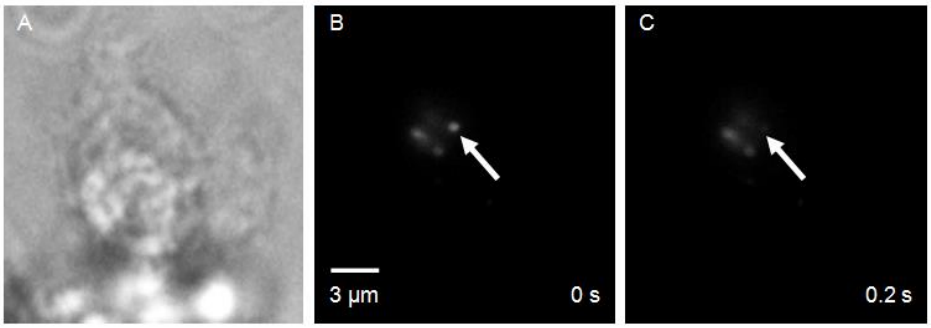

Figure 34 TIRFM snapshots of a knock-in Granzyme B mTFP CTL on lipid bilayer. An exemplary fusion event of a Granzyme B containing vesicle. The entire fluorescence of Granzyme B mTFP disappears within 200 ms (image B and C).

For the 5, 10 and 20 anti-CD3ε concentrations 366, 127 and 255 cells were analyzed respectively out of 30 different mice. The highest secretion rate of CTLs was seen with the 10 µg/ml anti-CD3ε concentration and was 38.6%. In contrast only 18.8% and 13.9% of the cells secreted with the 20 and 5 µg/ml anti-CD3ε. Correspondingly the highest number of secretion events per cell was also seen with the 10 µg/ml anti-CD3ε and was 3.04 ± 0.09. On the contrary only 1.24 ± 0.02 and 2.04 ± 0.04 fusion events per cell were seen with the 5 and 20 µg/ml anti-CD3ε respectively. The number of fusion events per cell on lipid bilayers significantly differed with varying anti-CD3ε concentrations with a p-value of less than 0.001 (figures 36, 37). Next we analyzed, the latency of the adherence of the cells to the bilayer containing the different concentrations of anti-CD3ε and found that the adherence time was significantly shorter with the 10 µg/ml anti-CD3ε and was on average 45.93 ± 3.68 s in comparison to the 5 and the 20 conditions where the latency of adherence was 279.49 ± 4.91 s and 141.58 ± 7.23 s (figure 35). A one-way ANOVA test demonstrated significant

differences in the latency of adherence of the CTLs to the bilayers with a tendency similar to results obtained with lifeact mRFP and CD3ε TFP (figure 23).

Interestingly, the latency of CG secretion after cell adhesion is not significantly different between the 5, 10 and 20 µg/ml anti-CD3ε concentrations. The latency of secretion following cell adherence was on average 321.43 ± 24.63 s for 5 µg/ml, 284.69 ± 54.77 s for 10 µg/ml and for 311.22 ± 28.86 s 20 µg/ml (figure 38).

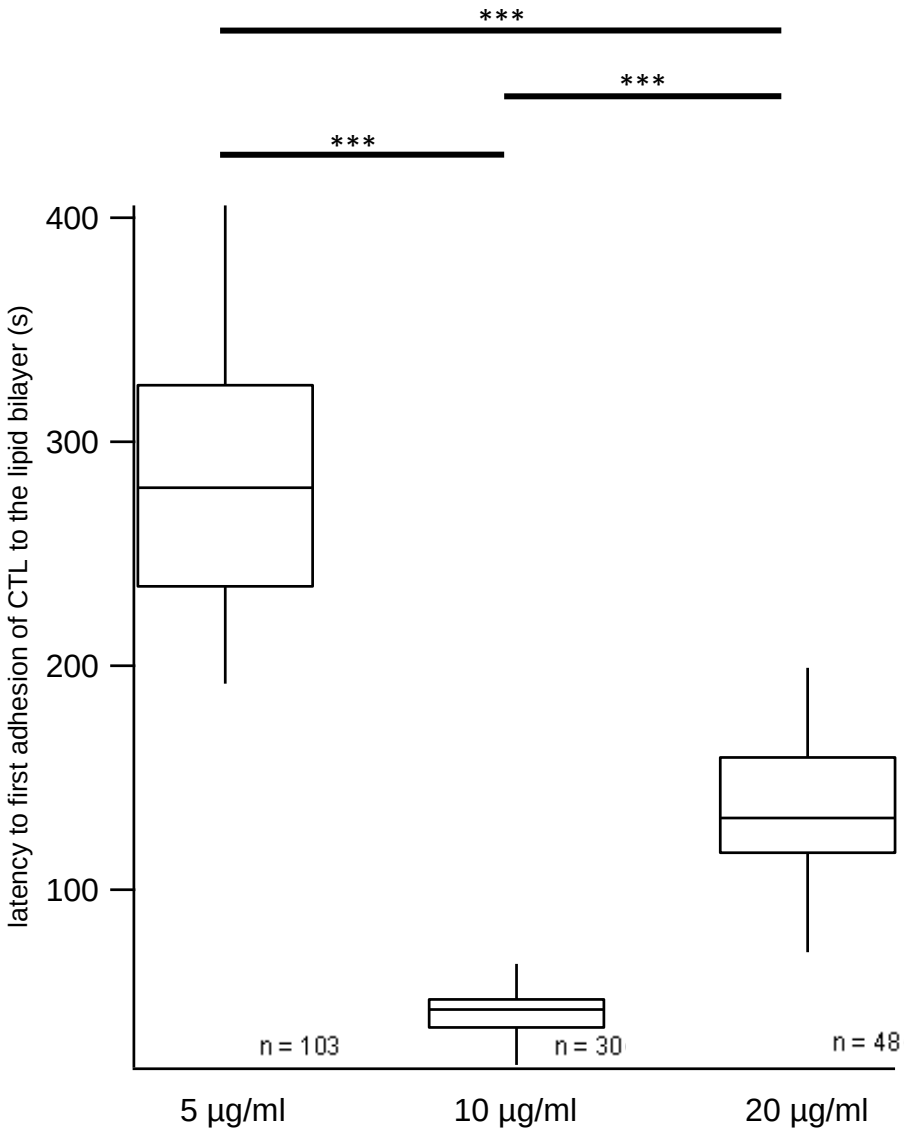

Figure 35 Latency to adhesion time of CTL to bilayer containing 5, 10 or 20 µg/ml anti-CD3ε. The latency to adhesion of the first cell to the lipid bilayer containing different anti-CD3ε concentrations. "n" is the number of cells that where analyzed. 103 cells with 5 µg/ml, 30 cells with 10 µg/ml and 48 cells with 20 µg/ml were analyzed.

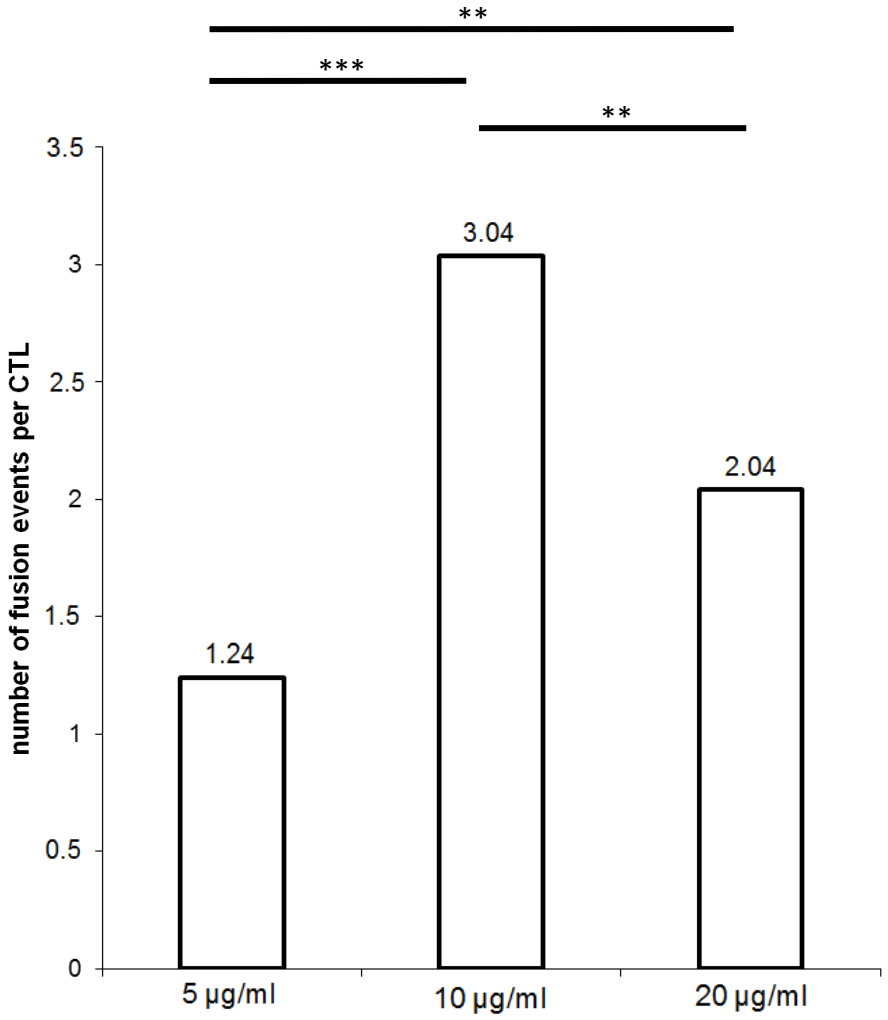

Figure 36 Average number of fusion events under varying anti-CD3ε antibody concentration. On average 1.24 ± 0.02 fusion events per CTL were seen with 5 µg/ml anti-CD3ε antibody, 3.04 ± 0.09 with 10 µg/ml and 2.04 ± 0.04 with 20 µg/ml anti-CD3ε antibody concentration.

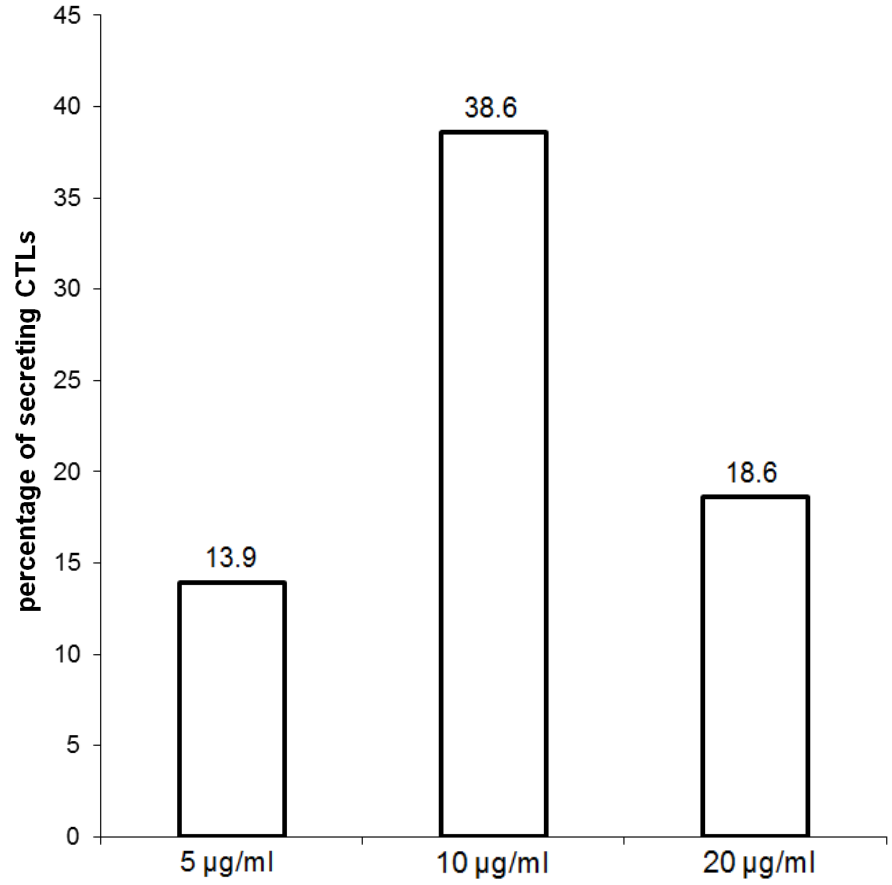

Figure 37 Percentage of secreting CTLs varying anti-CD3ε concentrations. 13.9%, 38.6% and 18.6% of the CTLs that adhered to the lipid bilayer secreted Granzyme B when stimulated by 5, 10 or 20 µg/ml anti-CD3ε.

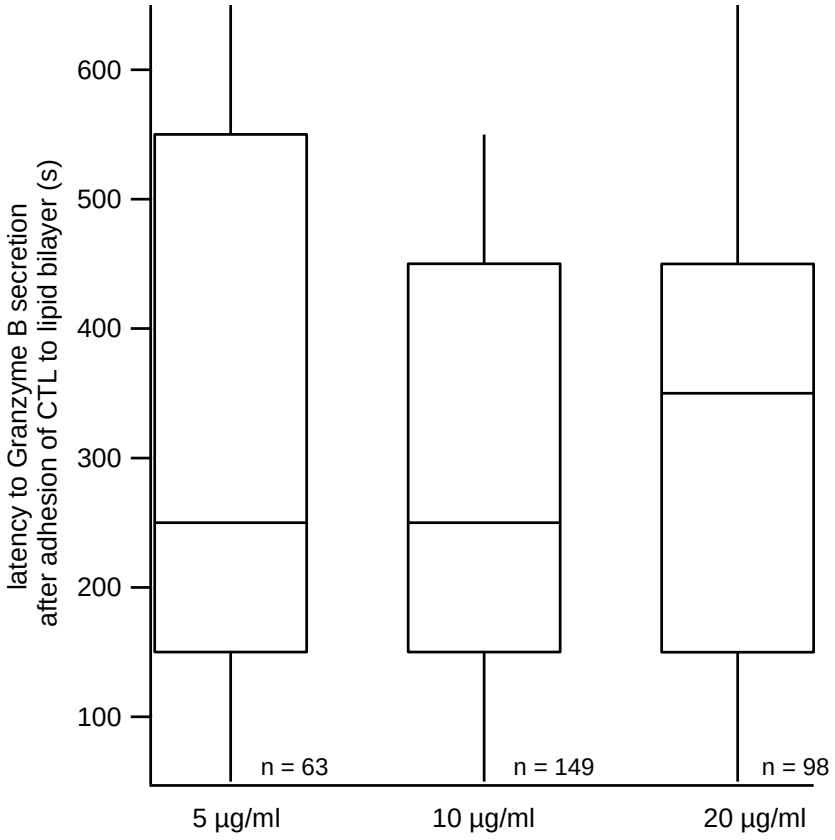

Figure 38 Latency to Granzyme B secretion events normalized to cell adhesion to the lipid bilayer. The latency to CG fusion events after CTL adherence to the lipid bilayer. 63 fusion events for the 5 µg/ml, 149 fusion events for the 10 µg/ml and 98 fusion events for the 20 µg/ml were analyzed. There was no significance difference in the latency of CG secretion following cell adherence.

5.4 Clathrin is transported to the IS by cytotoxic granules in murine CTLs

Clathrin is a protein that is involved in multiple membrane traffic cargo. In addition to that, the role of clathrin in terms of endocytosis is already well established, however where the clathrin molecules are coming from is not yet known. Since endocytosis of CGs is a clathrin dependent process [13], one intriguing question remains to be answered about the localization of clathrin before and after CG exocytosis. For that purpose we overexpressed the light chain of clathrin as a fusion protein with mcherry (ClathrinLC mcherry) in Granzyme B mTFP knock-in mice and observed the behavior of the two proteins before and after IS formation using TIRF microscopy (figure 39).

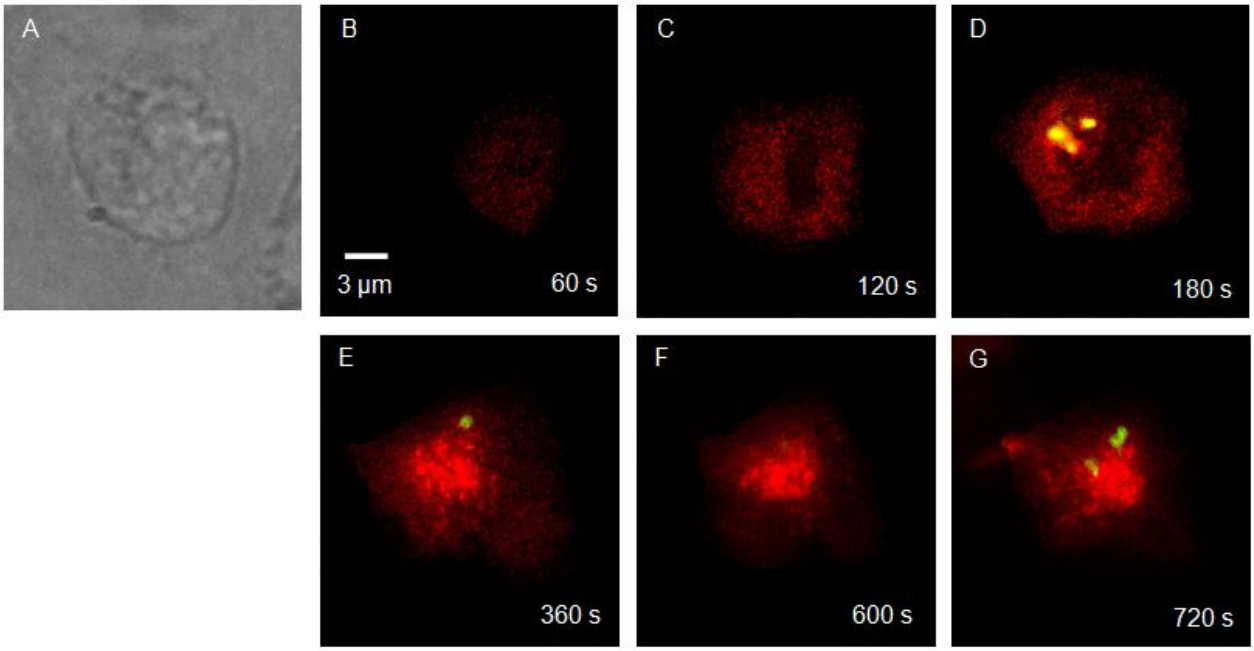

Figure 39 TIRFM snapshots of an activated CTL from a Granzyme B mTFP knock-in mouse expressing ClathrinLC mcherry. Image A is the brightfield picture of the CTL. Images B to G show the different stages of adhesion of the CTL to the lipid bilayer. Images B and C show that within 2 min after adhesion of the CTL to the lipid bilayer, the ClathrinLC mcherry forms a ring. Image D shows co-localization of clathrin with CGs. Image E-G show that in the cSMAC a massive ClathrinLC mcherry cluster is formed which stays until the end of the movie. Also, a lot of small peripheral ClathrinLC mcherry clusters appear in the pSMAC and dSMAC area. Red: ClathrinLC mcherry; Green: Granzyme B mTFP; Yellow: implies co-localization.

A co-localization analysis between clathrin and Granzyme B was done for 62 CGs that fused using the program ImageJ which confirmed that ClathrinLC mcherry is co-localizing with CGs. Some clathrin molecules were already localized at the plasma membrane at the beginning of the adhesion process of the CTL towards the lipid bilayer. We analyzed whether more

clathrin molecules are transported towards the IS via CGs. For that purpose, the fluorescence intensity of ClathrinLC mcherry co-localizing with CGs was compared with the fluorescence intensity of clathrin already residing in the plasma membrane. It turns out that on average the fluorescence intensity of ClathrinLC mcherry present on CGs was 2927.69 ± 254 and that present on the plasma membrane was 343.28 ± 18.3 (figure 40, p-value < 0.001). This result implies that on average ten times more clathrin is present per unit area on CGs in comparison to the plasma membrane.

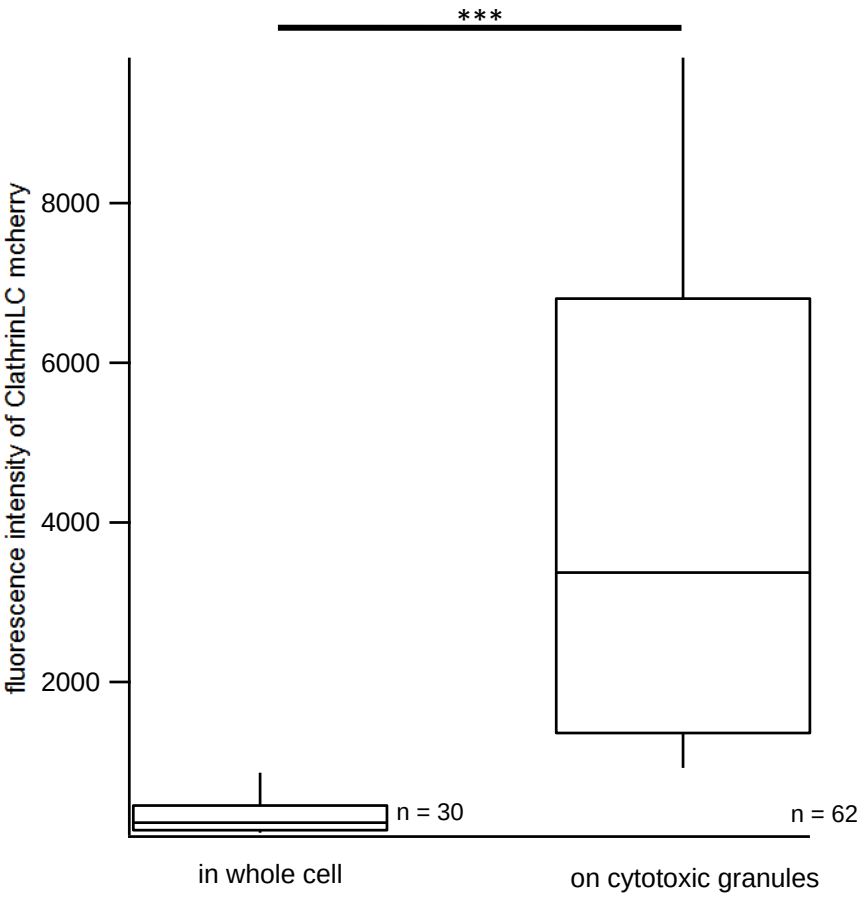

Figure 40 Fluorescence intensity of ClathrinLC mcherry is significantly higher on CGs in comparison to the plasma membrane. Fluorescence intensities of ClathrinLC mcherry in the plasma membrane compared to CGs are significantly different. This was the result of 62 analyzed cytotoxic granules from 30 cells; p-value < 0.001, Mann-Whitney-U-test.

Since TIRFM has a good resolution in z but an insufficient resolution in x,y, we performed high resolution Structured Illumination Microscopy (SIM). Granzyme B mTFP knock-in CTLs were transfected with ClathrinLC mcherry and after 7 min of incubation on either a poly-ornithine coated or an anti-CD3ε antibody coated glass coverslip, cells were fixed in 4% PFA solution, washed and mounted for imaging. After processing the images with ZEN (Olympus), an automated co-localization analysis was done using the JACoP plugin in ImageJ (figure 41). Cells coated on poly-ornithine coated coverslips were used as a control in which no IS formation is triggered. In contrast, cells coated on anti-CD3ε coated coverslips form a functional IS leading to CG release. A higher degree of co-localization between clathrin and Granzyme already in poly-ornithine coated coverslips in comparison to anti-CD3ε coated coverslips would strongly indicate that the clathrin is localizing on CGs before fusion. 15 CTLs from three different mice were analyzed.

The Pearson's correlation coefficient between ClathrinLC mcherry and Granzyme B mTFP in CTLs on poly-ornithine coated coverslips was on average 0.56 ± 0.01 and on anti-CD3ε antibody coated coverslips 0.21 ± 0.05 (figure 42, p-value < 0.001). The Mander's overlap coefficient of ClathrinLC mcherry with Granzyme B mTFP in CTLs on poly-ornithine coated coverslips was 0.486 ± 0.01 and on anti-CD3ε antibody coated coverslips was 0.22 ± 0.04 (figure 43, p-value < 0.001). In addition to that, the Mander's overlap coefficient of Granzyme B mTFP with ClathrinLC mcherry in CTLs on poly-ornithine coated coverslips was 0.536 ± 0.04 and on anti-CD3ε antibody coated coverslips was 0.04 ± 0.01 (figure 44, p-value < 0.001). Therefore, ClathrinLC mcherry appears to be co-localized with CGs before coming to the IS where it appears to be present at a higher concentration than the plasma membrane.

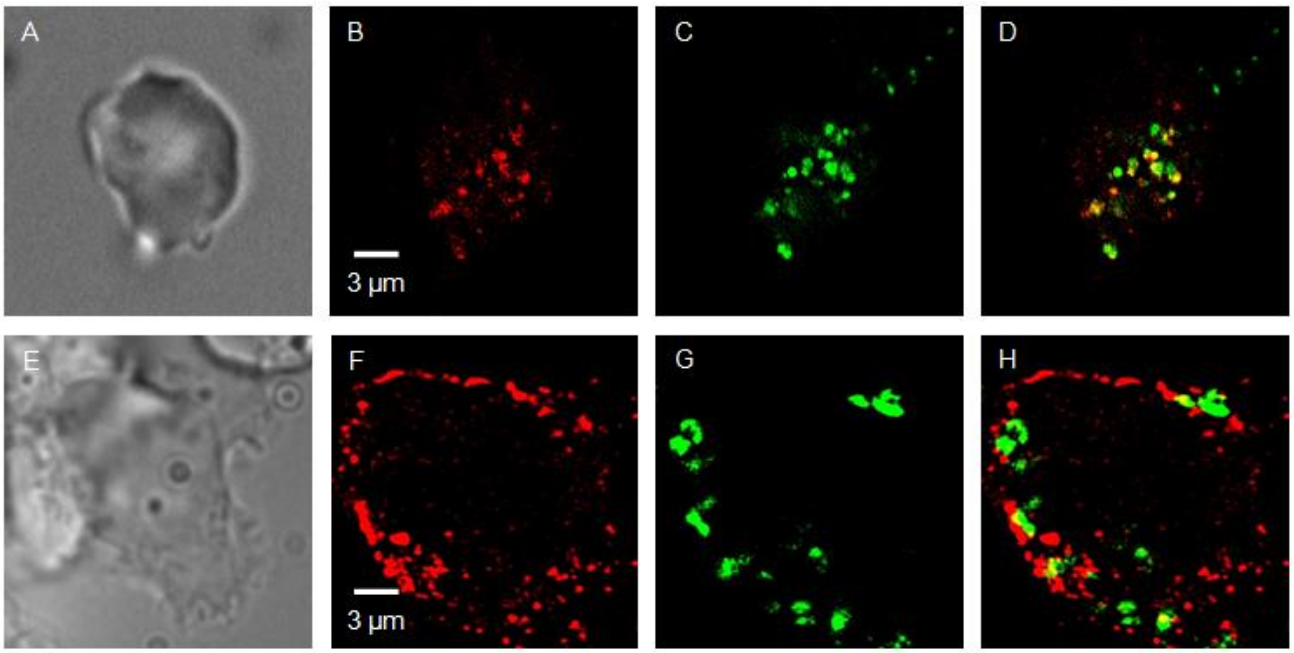

Figure 41 SIM snapshots of Granzyme B mTFP and ClathrinLC mcherry in resting and stimulated CTLs. SIM image snapshots of a CTL adhered to a poly-ornithine coated glass coverslip (images B-D) or anti-CD3ε antibody coated glass coverslip (images F-H). Red: ClathrinLC mcherry; Green: Granzyme B mTFP; Yellow: implies co-localization. A and E are corresponding brightfield images

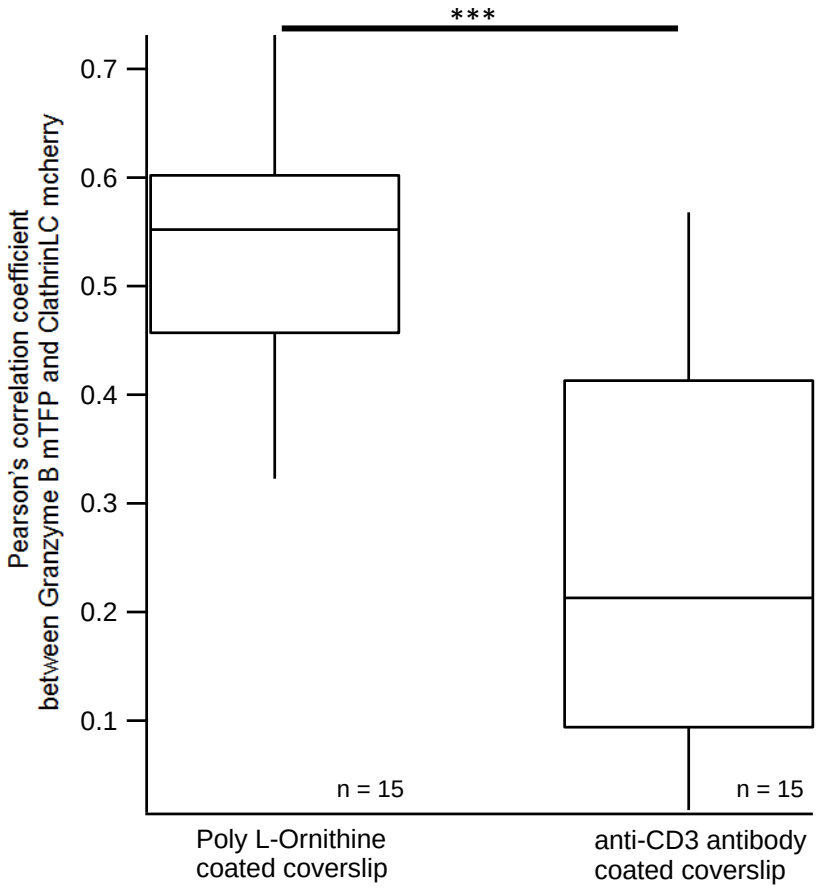

Figure 42 Co-localization analysis of ClathrinLC mcherry and Granzyme B mTFP in resting and activated CTLs represented as Pearson's correlation coefficient. Pearson's correlation coefficients of Granzyme B mTFP and ClathrinLC mcherry in CTLs adhered on poly-ornithine or anti-CD3ε antibody coated glass coverslips analyzed for 15 cells each; p-value < 0.001, Mann-Whitney-U-test.

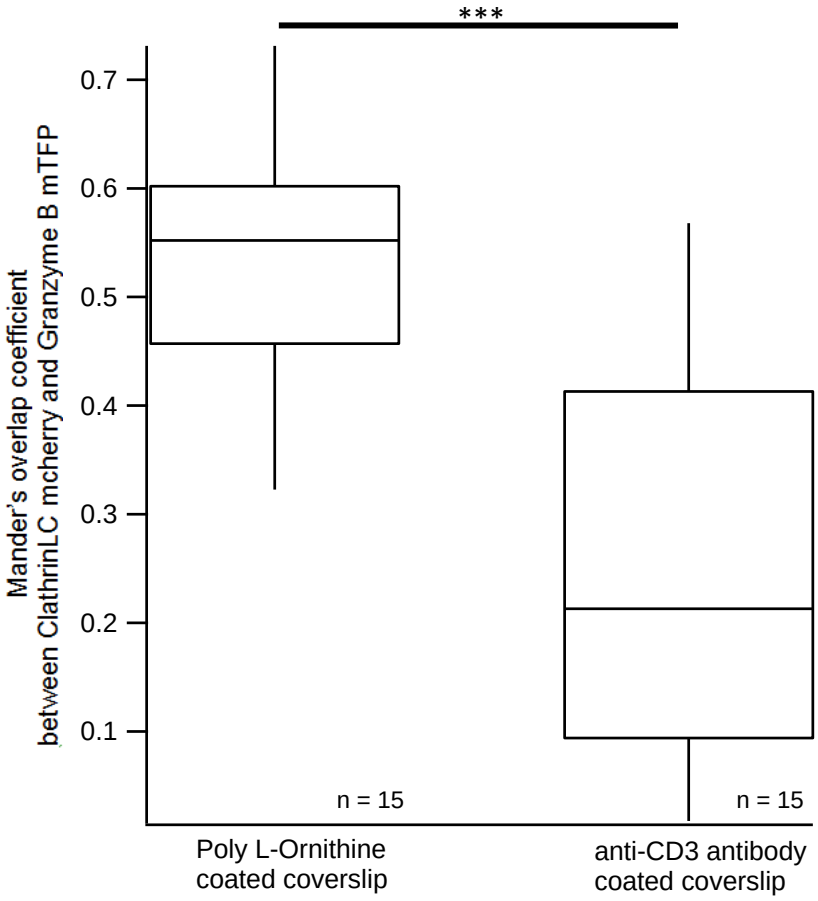

Figure 43 Mander's overlap coefficient of ClathrinLC mcherry and Granzyme B mTFP. Mander's overlap coefficients of ClathrinLC mcherry and Granzyme B mTFP in CTLs adhered on either poly-ornithine or anti-CD3ε antibody coated glass coverslips. CTLs were fixed in 4% PFA and imaged by high resolution SIM. 15 cells were analyzed each; p-value < 0.001, Mann-Whitney-U-test.

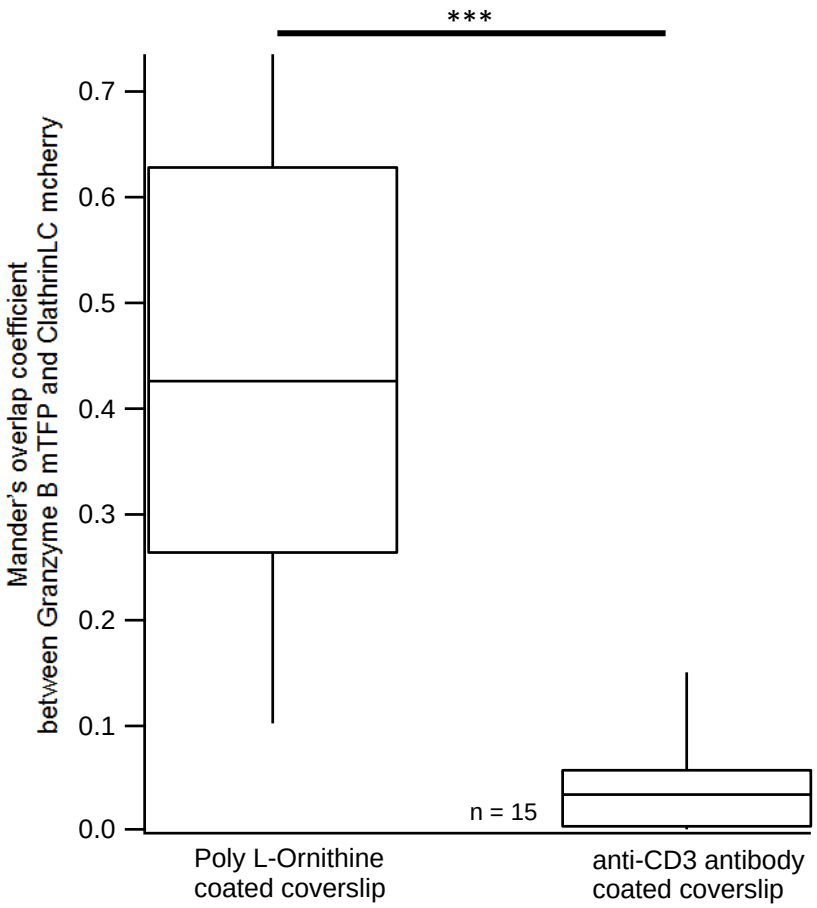

Figure 44 Mander's overlap coefficient of Granzyme B mTFP and ClathrinLC mcherry. Mander's overlap coefficients of Granzyme B mTFP and ClathrinLC mcherry in CTLs adhered on either poly-ornithine or anti-CD3ε antibody coated glass coverslips. CTLs were fixed in 4% PFA and imaged by high resolution SIM. 15 cells were analyzed each; p-value < 0.001, Mann-Whitney-U-test.

Murine day 7 and day 8 activated wildtype CTLs were transfected with lifeact eGFP and ClathrinLC mcherry and added on lipid bilayers containing 10 µg/ml anti-CD3ε and imaged with TIRF microscopy. Within the first min of CTL adhesion to the lipid bilayer the ClathrinLC mcherry and lifeact mRFP were excluded out of the center into the periphery to form a ring (figure 45).

30 cells from 6 different mice were included in the co-localization analysis. The result was that the average area of ClathrinLC mcherry fluorescence over the whole IS was 118.46 ± 2.8 µm² and for lifeact eGFP 93.09 ± 3.6 µm² (figure 46, p-value < 0.01). This result means that ClathrinLC mcherry and lifeact eGFP are not completely co-localizing, because ClathrinLC mcherry is also localized in the pSMAC and cSMAC areas (the average size of ClathrinLC mcherry fluorescence in this area was 25.36 ± 1.8 µm²).

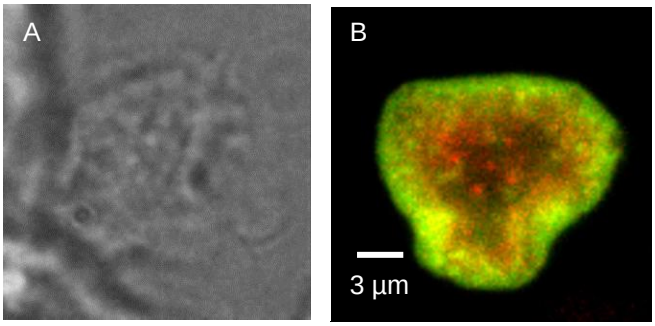

Figure 45 Co-localization of clathrin and F-actin in the first 2 min of cell adhesion to lipid bilayer. TIRFM snapshots of ClathrinLC-mcherry (red) and lifeact eGFP (green) at the IS 2 min after cell adhesion. Yellow implies co-localization.

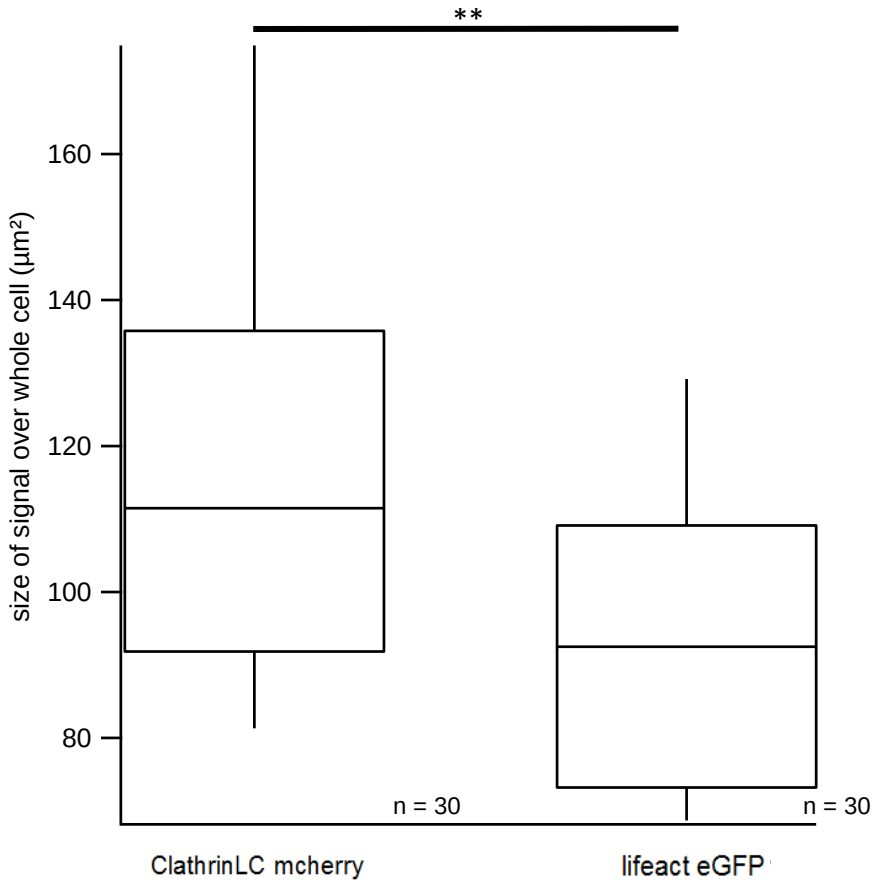

Figure 46 Area of ClathrinLC mcherry fluorescence and lifeact eGFP fluorescence. The maximum area of the ClathrinLC mcherry in the first 2 min is significantly larger compared to the area of the lifeact eGFP fluorescence in the whole cell; p-value < 0.01, Mann-Whitney-U-test, n = 30 cells.

Furthermore, 6 to 8 min following adhesion of the CTLs to the lipid bilayer, ClathrinLC mTFP forms a massive cluster at the cSMAC of the IS. To verify if this was a center for endocytosis and recycling we co-transfected the cells with the recycling endosome marker Rab11a-mcherry and found that there was co-localization between Rab11a-mcherry and the central clathrin-mTFP fluorescence (figure 47). These results are preliminary as only three cells were analyzed and therefore will need further proof to verify if the observed co-localization between ClathrinLC TFP cluster in the center with Rab11a-mcherry is also the site of MTOC docking.

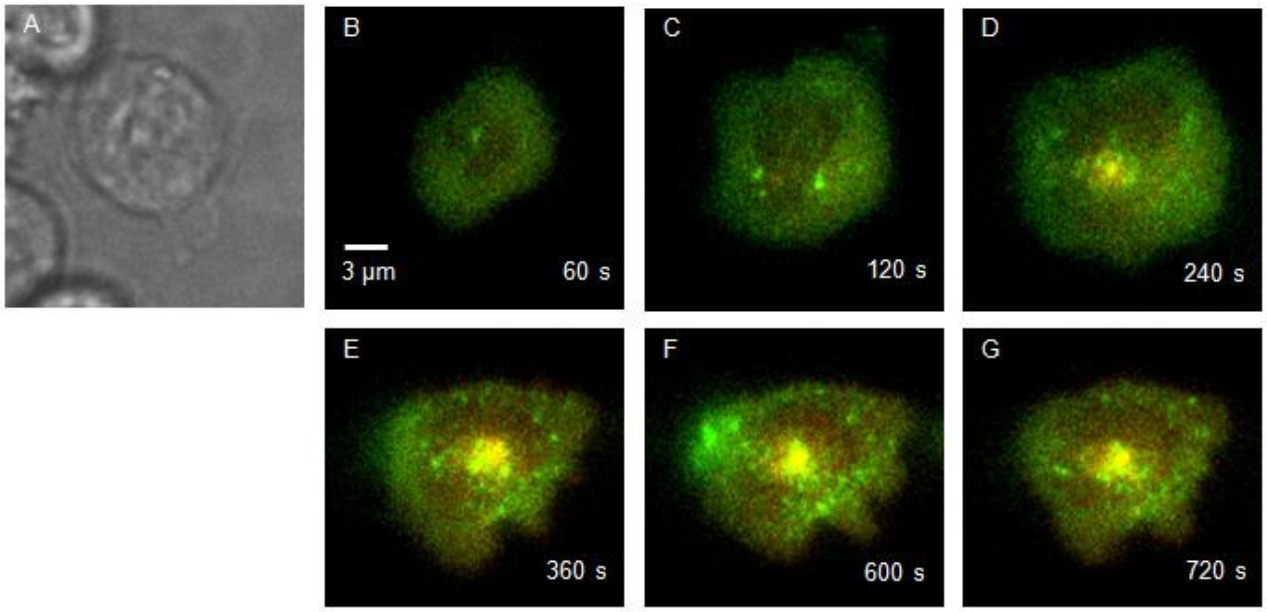

Figure 47 TIRFM snapshots of a murine wildtype CTL expressing ClathrinLC TFP and Rab11a-mcherry at the IS. TIRFM snapshots showing that within 6 min following adhesion of the CTL to the lipid bilayer there is visual co-localization or proximity between Rab11a-mcherry (red) and central ClathrinLC-TFP cluster (green); Yellow: implies co-localization between both fluorophores.

6 Discussion

For this thesis TIRF and SIM microscopy were used to visualize the behavior of CTLs on lipid bilayers that imitate a target cell by containing ICAM and biotinylated anti-CD3ε antibodies. Differing concentrations of anti-CD3ε antibody were used to study possible effects of varying TCR stimulus strengths on the modes of IS formation and CG fusion. Additionally, the localization of clathrin during IS formation was investigated. To address these scientific points, CTLs from C57BL/6 wildtype and/or Granzyme B mTFP knock-in mice were activated for 7 to 8 days and were made to overexpress various proteins of interest such as Syb2, clathrin, Rab11a or actin coupled to either pH-dependent or independent fluorophores depending on the pertaining question and imaged using high resolution fluorescence microscopy.

We observed under our experimental conditions two different types of Syb2 pHuji behavior upon CG fusion that are seemingly stimulus independent. Interestingly, various stages of IS formation starting from the early actin clearance up to the fusion of CGs show different dependencies to the TCR stimulus. An optimum stimulus seems to be required for the stability and maximum CG fusion efficiency necessary for maximum effector function. Since endocytosis of Syb2 is a clathrin mediated process we investigated the localization of clathrin and interestingly observed three different localizations during different stages of IS formation. All together our data demonstrate the effects of varying TCR stimuli on specific stages of IS formation leading up to CG fusion.

6.1 Synaptobrevin 2 pHuji exhibits two types of behavior upon exocytosis of cytotoxic granules at the IS

Granzyme B reliably marks cytotoxic granules in CTLs [103] and Syb2 has been shown to be the v-SNARE required for CG exocytosis [67]. In neurons and neuroendocrine cells Syb2 exhibits only fast endocytosis (which lasts for 1.8 s) with a low stimulus and fast and slow endocytosis (which lasts for 20 s) with a high stimulus on the plasma membrane [104]. Since Syb2 is the major v-SNARE in cytotoxic granules of murine CTLs we asked whether stimulus induced modes of exo-endocytosis also exist in murine CTLs. To address this scientific question CTLs were added to lipid bilayers containing different concentrations of anti-CD3$^{\varepsilon}$ antibody namely 5, 10 and 20 µg/ml. CTLs from Granzyme B mTFP knock-in mice were transfected with Syb2 pHuji to visualize simultaneously the lumen and membrane of cytotoxic granules. pHuji, is a pH-dependent fluorophore and therefore the fluorescence is quenched in an acidic environment, however, upon fusion pore opening the fluorophore is exposed to neutral pH resulting in fluorescence dequenching which is visualized by a large fold increase in fluorescence.

We investigated with the help of the Syb2 pHuji construct that two different types of behavior of Syb2 exist upon exocytosis of cytotoxic granules at the IS and these behaviors were independent of the concentration of anti-CD3$^{\varepsilon}$ antibody on the lipid bilayer. In the first type of behavior the fluorescence of Syb2 pHuji disappears within 3 seconds after Granzyme B mTFP secretion (figures 7 and 9), we call these short fusion events. Control experiments allowed us to clarify that in a short fusion event (tau value < 1.0 s) the Syb2 pHuji is diffusing laterally into the plasma membrane after the release of Granzyme B mTFP (figures 17, 19, 20 and 21). In the second type of behavior Syb2 pHuji remains at the same place of Granzyme B mTFP secretion and the fluorescence disappears slowly within or sometimes more than 5 min after Granzyme B mTFP secretion (figures 8 and 10), we call these long fusion events. The timing of the long fusion events are in concordance with unpublished results from Rettig et al. which show that endocytosis of Syb2 lasts sometimes more than 5 min. Syb2 mRFP knock-in CTLs were made to adhere and form an IS with a fluorescently labeled anti-mRFP antibody which was added to the extracellular medium. They could observe that the anti-RFP 488 signal of the CGs appears and remains in 74.4 % of the cases in the range from 11.6 s to 548.6 s and in 29.6 % of the cases more than 548.6 seconds, which is according to the time required for endocytosis indicative of clathrin being involved in Syb2 endocytosis in the long fusion event mode of this study [102]. Furthermore, the long fusion event of Syb2 pHuji showed a significant increase of 51.7 ± 0.7 % (p-value < 0.001, n = 17) in fluorescence and 75.1 ± 0.6 % (p-value < 0.001, n = 17) in diameter (figure 49) for

123.8 ± 2.6 s after the secretion of Granzyme B mTFP and only after this process the fluorescence of Syb2 pHuji would disappear completely in the TIRF field. Figure 48 shows TIRF snapshots of a Granzyme B mTFP knock-in CTL transfected with Syb2 pHuji. This CTL exhibits at first short fusion events and afterwards a long fusion event which is the typical temporal order of the two fusion event types.

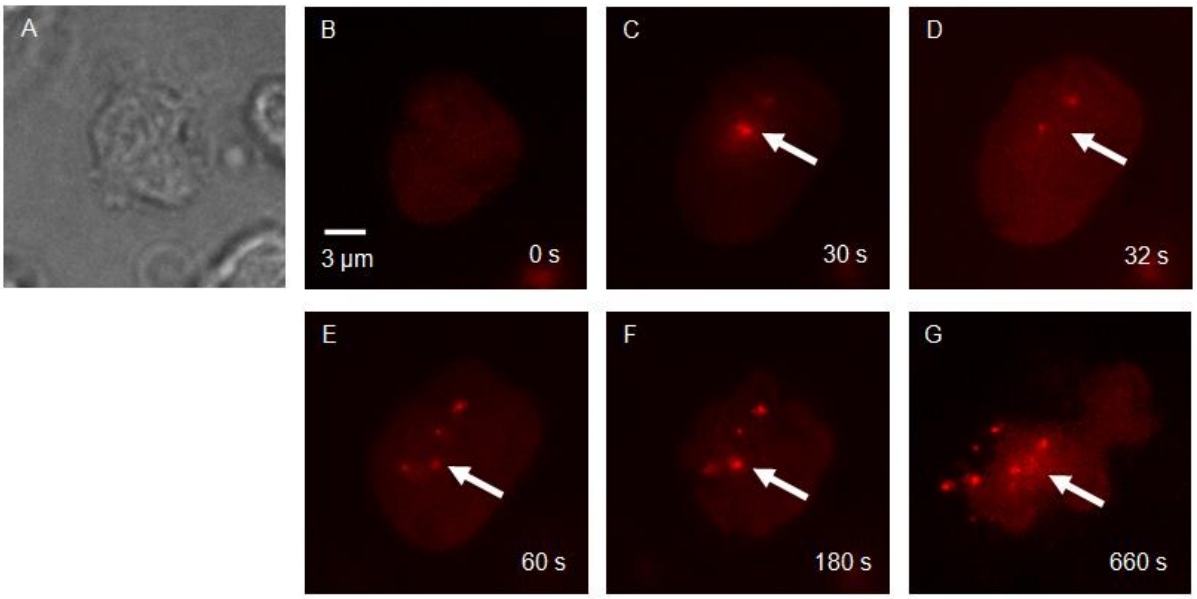

Figure 48 TIRFM snapshots of a knock-in Granzyme B mTFP CTL expressing Syb2 pHuji. TIRFM snapshots of an exemplary CTL showing typically at first short fusion events of Syb2 pHuji (images B-D) and afterwards a long fusion event at the IS (images E-G); Red: Syb2 pHuji fluorescence.

This phenomenon might indicate that Syb2 pHuji molecules from short fusion events and possibly other Syb2 molecules located in the plasma membrane diffuse to the same position at the plasma membrane where the long fusion event occurs and they are all endocytosed together at the same place. The result might mean that Syb2 is diffusing into the plasma membrane after CG fusion in 80 % of the observed short fusion events and in the other 20 % of long fusion events a hotspot of endocytosis is generated after cargo release at the same position in the plasma membrane which would explain the increase in fluorescence and diameter of Syb2 pHuji in this hotspot of endocytosis which is followed by the complete disappearance of the Syb2 pHuji fluorescence within 5 min or more. In general, a slow increase in fluorescence in TIRFM could also be interpreted as a fluorophore moving closer to the objective, however, the temporal order of short and long fusion events allude to the above hypothesis as short fusion events occur before long fusion events in this study (figure 48).

Nevertheless, we observed also some CTLs that exhibited only short fusion events which could mean that CTLs basically exhibit long fusion events if the concentration of Syb2 molecules in the plasma membrane exceeds a particular limit and the CTLs need to endocytose this protein again. The fact that CTLs which showed long fusion events in this study exhibited significantly more short fusion events (2.9 ± 0.16 short fusion events per cell) compared to the CTLs which did not exhibit long fusion events (1.6 ± 0.04 short fusion events per cell) (p-value < 0.05, n = 49 cells) alludes to the above hypothesis.

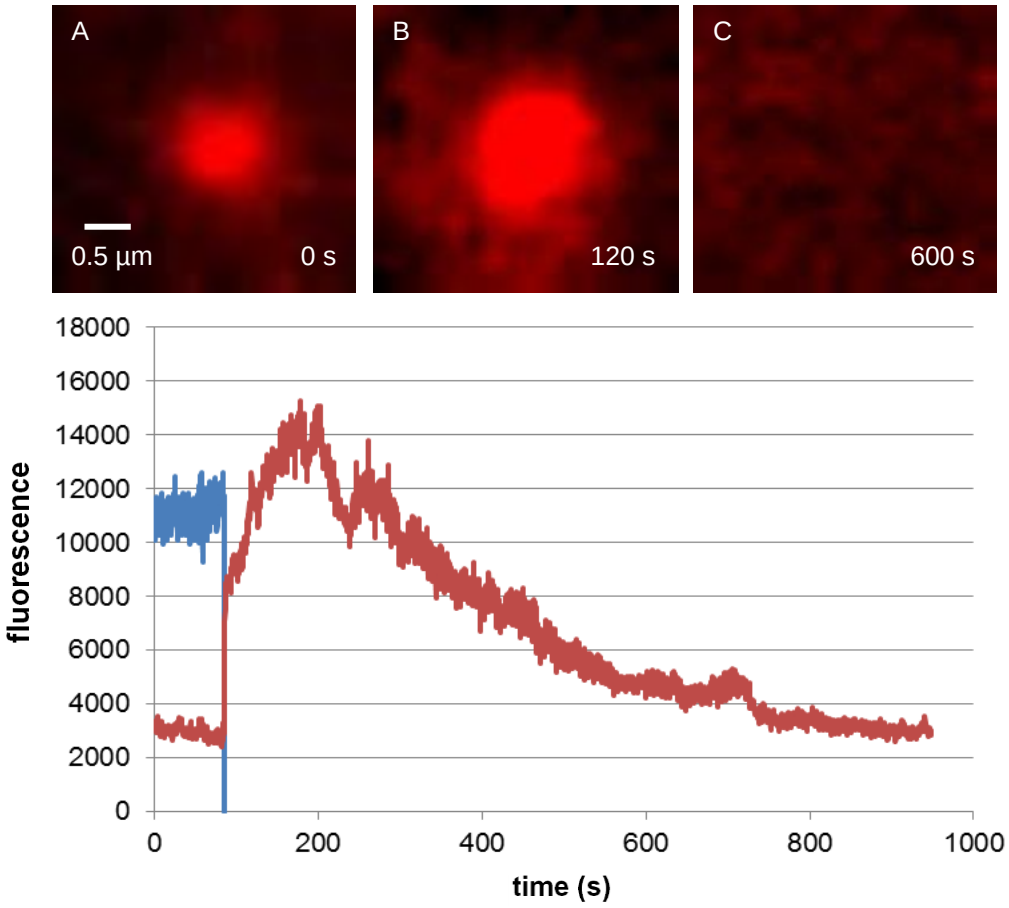

Figure 49 TIRFM snapshots of an exemplary CG expressing Syb2 pHuji in a long fusion event. TIRFM snapshots of an exemplary long fusion event of Syb2 pHuji expressing CG which is significantly increasing in diameter and fluorescence for 123.8 ± 10.9 s and after that the fluorescence would disappear completely in the TIRF field (images A-C); Red: Syb2 pHuji fluorescence. The chart shows that after the Granzyme B mTFP signal disappears completely within 400 ms, Syb2 pHuji displays a sudden increase followed by a slow increase of 51.7 ± 2.8 % for 123.8 ± 10.9 s and after the fluorescence reached its zenith the signal would disappear within 5 min in a long fusion event. Blue: Granzyme B mTFP fluorescence; Red: Syb2 pHuji fluorescence.

Different modes of vesicle fusion have been reported in the literature namely full-collapse fusion, kiss-and-run and compound exocytosis [41,44]. However, the amount of cargo released into the extracellular milieu depends on the fusion event type. During compound-exocytosis there is release of huge compound vesicles [44] and in a full-collapse fusion the complete content of a vesicle is released [46]. In a kiss-and-run mode of fusion the fusion pore opens and closes quickly and therefore just allows the content to partially release, before the vesicle is retrieved into the cytoplasm again [101]. To clarify if the two different types of CG fusion reported in this study exhibit varied amounts of content release, we analyzed the diameter of the Granzyme B mTFP fluorescence, namely 468 ± 1.3 nm in the short fusion events (n = 69) and 515.5 ± 2.3 nm in the long fusion events (n = 10). Although a Mann-Whitney-U-test revealed a significant difference between these two data sets (p-value < 0.05), this result is invalidated by the pixel size of 160 nm in the TIRFM setup used in this study and thus, the difference between the two groups of data is beyond the resolution limit of the setup corresponding to a quarter of a pixel of difference. Nevertheless, this result suggests that a long fusion event marginally releases more cargo compared to a short fusion event. However, in both the reported fusion event types the criteria of a full-collapse fusion hold true as the cargo is completely released and the vesicle membrane is coalescing with the plasma membrane upon fusion. Our results are in concordance with the results of Martina et al. which show that CTLs exhibit modified full-collapse fusion [65].

In conclusion, this study suggests that CTLs exhibit two different types of CG fusion independent of the strength of the TCR stimulus, additionally, delivering almost the same amount of cargo and exhibit only the mode of full-collapse fusion. However, neurons and neuroendocrine cells exhibit stimulus dependent modes of exo-endocytosis of vesicles [104]. These different modes of exo-endocytosis in neurons are important to maintain the huge variability of signals in the CNS [41] and allude to the complex system of synaptic signaling in the CNS. In contrast to neurons, CTLs only eliminate mutagenic or virus infected cells and do not require subtle synaptic signaling for this process as CTLs operate autonomously [2]. Furthermore, neurons profit from different modes of exo-endocytosis such as the kiss-and-run mode especially during times of intense stimulation, as it is retrieved back into the cytosol after release and prevents in this way an exhaustion of vesicles, morphological changes in the nerve terminal and an overload of proteins in the plasma membrane [105]. Although CTLs require endocytosis of CG membrane proteins such as Syb2 for multiple target cell killing, representing an event of intense stimulation, clathrin and dynamin dependent modes of endocytosis, which can last for several minutes, suffice to maintain their function and thus, CTLs might not require rapid retrieval of vesicle occurring in a kiss-and-run mode of exo-endocytosis [13].

6.2 Differences in IS formation of murine CTLs with a varied stimulus on TCR in lipid bilayer TIRF

In this study we show that the different steps of IS formation are differently dependent on the strength of the TCR stimulus. By providing three different anti-CD3ε antibody concentrations but constant ICAM concentrations on lipid bilayers the strength of stimulus on the TCR was varied to unleash CG fusion in CTLs. With the TIRFM setup we demonstrate that some stages of IS formation exhibit a bell-shaped dependency to the strength of TCR stimulus, whereas others show a linear increase or decrease depending on the stimulus strength. However, we ascertain in this study that with an optimum TCR stimulus consisting of 10 µg/ml anti-CD3ε antibody in the lipid bilayers CTLs display the shortest latency time for adhesion to lipid bilayers, the longest dwell time of CD3ε TFP clusters and maximum efficiency in CG fusion.

It has been reported that stronger TCR stimuli lead to an increased CTL mediated cytotoxicity and cytokine release [51]. However, our TIRFM data demonstrate that CTLs require an optimum trigger on the TCR to exhibit maximum secretion of CGs (figure 36). Furthermore, CTLs exhibit a bell-shaped calcium dependency for perforin mediated killing with an optimum intracellular calcium concentration between 122 and 334 nM and an extracellular calcium concentration between 23 and 625 µM [109]. Under our experimental conditions we demonstrate that CTLs exhibit less CG secretion beyond an optimum stimulus of 10 µg/ml anti-CD3ε antibody, which could be correlated to the bell-shaped calcium dependency. However, as there is no dose dependent effect between the strength of the stimulus on the TCR and CG fusion our results could also imply that there may be an unknown check point system in CTLs that avoids a dose dependent effect between strength of stimulus on the TCR and the secretion of CGs. This checkpoint system prevents CTLs from secreting all of their CG pool to just one target although the stimulus on the TCR is disproportionately large, because in the absence of CGs newly detected targets by the CTLs will not be killed until new CGs are synthesized [13]. Thus, a hyperactivity of inhibitory signals inside CTLs could explain the lower CG secretion efficiency with 20 compared to 10 µg/ml anti-CD3ε antibody.

We demonstrate in this study that increasing the trigger on the TCR results in a linear increase in the size and number of average CD3ε TFP clusters (figures 26 and 27). However, only with an optimal concentration of anti-CD3ε antibody do the CD3ε TFP clusters reside the longest at the IS as quantified by their dwell time (figure 28). Thus, the size and dwell time of CD3ε TFP clusters are differently dependent on the strength of the TCR stimulus. Reports prove that constant TCR signaling is required for the maintenance of the IS and full effector

function of näive T helper cells [48]. CTLs stimulated with an optimum intermediate TCR of 10 µg/ml anti-CD3ε antibody exhibit a significant increase in the dwell time of CD3ε TFP at the IS which may have positive effects on the downstream signaling pathway and provide these CTLs with the maximum CG fusion efficiency.

We observe that the latency of the actin ring formation is not affected by the strength of the TCR stimulus (figure 24). Considering that the central clearance of actin is a critical step in IS formation influencing the timing of CG release [87], this could explain why varied anti-CD3ε antibody concentrations have no impact on the latency of Granzyme B secretion following adhesion of the CTL to the bilayers (figure 38). However, Dock2 is required for the polymerization of actin in CTLs and in its absence leads to a miniaturized IS [60]. In this study we demonstrate that the area of the actin ring at the IS is not affected by different TCR stimulus strengths (figure 29), thus, we propose that the stimulus strength on the TCR has no influence on the PIP3 and Dock2. This explains why we also do not find a significant difference in the latency of actin ring formation following adhesion upon changing anti-CD3ε concentrations. However, the size of the actin free area was found to correlate with the size of the CD3ε TFP clusters (figure 27 and 31) and on a molecular level, this could indicate that the actin free area is adjusted by the amount of signaling molecules present in the cSMAC because the CTLs stimulated with 10 µg/ml anti-CD3ε exhibited the largest actin free area (named cSMAC+pSMAC area in results) and CD3ε TFP clusters compared to CTLs stimulated with 5 and 20 µg/ml anti-CD3ε. This could be explained by the increased CG secretion rate seen with 10 µg/ml anti-CD3ε compared to the other two concentrations (figure 36), which leads to more CG membrane proteins to be present at the IS, since the CG membrane coalesces into the plasma membrane upon fusion. Our results demonstrate that the dwell time of the actin ring and CD3ε TFP show different dependencies on the strength of TCR stimulus. This may be due to altered activity of LAT, since it is not necessary for the kinetics of IS formation but for the maintenance of a stable cytotoxic synapse in CTLs [77].

The T cells that adhered to stimulatory bilayers containing either 5, 10 or 20 µg/ml anti-CD3ε antibody demonstrated a significant increase in movement with decreasing anti-CD3ε concentrations (figure 33). Since a stable adhesion between CTLs and target cells is required for optimum effector function of CTLs [4,95], this may explain why cells stimulated with 5 µg/ml anti-CD3ε exhibit lower fusion efficiency and less fusion events per cell. However, the cells stimulated with 20 µg/ml anti-CD3ε antibody display less movement but in contrast, exhibit reduced fusion efficiency. We conclude that the reduced movement of CTLs during synapse formation is a consequence of increased TCR stimulus strengths and may lead to exhaustion of CTLs exhibiting diminished T cell effector function. In cancers and chronic infections CTL exhaustion has been reported and develops due to extended antigen

exposure [45,74]. Since in vivo CTL exhaustion is a very complex process involving proteins such as PD-L1 and SIRPα [74], it is implausible to provoke exhaustion under our experimental setting where we only altered the strength of TCR stimulus by varied anti-CD3ε antibody concentrations. However, new mechanistic insights into the exhaustion process might reveal new targets for cancer immunotherapy [43].

6.3 Clathrin is transported to the IS by cytotoxic granules in murine CTLs

Clathrin is a major endocytic protein that is involved in the endocytosis of several receptor proteins and it is also required for the endocytosis of CGs in CTLs [13,61,71]. The role of clathrin in terms of endocytosis is already well established, however the localization of clathrin before and after IS formation is not yet known. Different localizations of clathrin have been reported, for example clathrin is detected in the Golgi complex of human fibrosarcoma cells and in the plasma membrane of CTLs before it is involved in endocytic pathways [50,73]. Furthermore, in Jurkat T cells clathrin molecules are needed for the polymerization of actin at the IS and are provided by MVBs [10].

In this study, Granzyme B mTFP knock-in mouse CTLs were transfected with clathrin light chain fused to mcherry (ClathrinLC mcherry) to visualize the localization of clathrin during IS formation and CG fusion. We observed three different localizations of clathrin. The first localization appears to be in the plasma membrane which gets cleared from the cSMAC. The second is on CGs and interestingly CGs appear to transport clathrin towards the IS. ClathrinLC mcherry co-localized with CGs has a ten times higher fluorescence intensity than in the plasma membrane implying a higher concentration of clathrin on CGs (figure 40). It has been reported that clathrin is located on MVBs [10] and since MVBs are able to fuse with lysosomes this may explain our findings where we see co-localization between clathrin and CGs [30,63,81].

Our data could mean two things – clathrin needed for endocytic events occurring early on in the IS formation process are already in the plasma membrane but however do not suffice for the endocytic process of CG membrane proteins and therefore there is more transport of clathrin by CGs which deliver the clathrin to the membrane upon exocytosis. This results in the third localization of clathrin seen after CG fusion – clusters at the IS which may be hotspots of endocytosis. To verify if these were centers for endocytosis and recycling we co-transfected the CTLs with the recycling endosome marker Rab11a-mcherry. We found that there was co-localization between Rab11a-mcherry and the central ClathrinLC TFP fluorescence cluster (figure 47) implying that the cluster of ClathrinLC TFP fluorescence could be a hub for endocytosis and recycling of CG membrane proteins. Of course one experiment to do would be to investigate whether these big clusters of ClathrinLC TFP appear only after CG fusion. The co-localization between ClathrinLC mcherry and Granzyme B mTFP was also analyzed by high resolution structured illumination microscopy in cells that were made to adhere to poly-ornithine coated coverslips (resting CTLs) or anti-CD3$^{\varepsilon}$ coated coverslips to trigger an IS and CG fusion (figure 41). The resting cells exhibited a significantly higher degree of co-localization. The Pearson's correlation coefficient between ClathrinLC

mcherry and Granzyme B mTFP in CTLs on poly-ornithine coated coverslips was on average 0.56 ± 0.01 and on anti-CD3ε antibody coated coverslips 0.21 ± 0.05 (figure 42). In addition to that, the Mander's overlap coefficient of Granzyme B mTFP with ClathrinLC mcherry in CTLs on poly-ornithine coated coverslips was 0.536 ± 0.04 and on anti-CD3ε antibody coated coverslips 0.04 ± 0.01 (figure 44). Both parameters show a significantly higher degree of co-localization between ClathrinLC mcherry and Granzyme B mTFP in poly-ornithine coated coverslips when compared to anti-CD3ε antibody coated coverslips. The lack of fusion of CGs on poly-ornithine coated coverslips could explain the higher degree of co-localization observed between ClathrinLC mcherry and Granzyme B mTFP in contrast to that observed on anti-CD3ε coated coverslips. On anti-CD3ε coated coverslips, fusion of cytotoxic granules occurs resulting in the release of Granzyme B mTFP, ClathrinLC mcherry however is not released and possibly forms clusters on the plasma membrane. This might be the reason why we observe less co-localization between ClathrinLC mcherry and Granzyme B mTFP on anti-CD3ε coated coverslips. Actually, our results support the hypothesis of clathrin being localized on fusogenic cytotoxic granules. In CTLs co-electroporated with lifeact eGFP and ClathrinLC mcherry we observed that within the first two min of IS formation they appear to co-localize. However, after the initial clearance of actin and clathrin from the central cSMAC zone, the clathrin and lifeact eGFP do not completely co-localize at later time points (figure 45). Imaging of clathrin fused to a pH sensitive fluorophore such as pHuji could further validate the pre-existence of clathrin already in the plasma membrane before CG polarization at the IS and also the delivery of clathrin to the plasma membrane upon CG exocytosis.

7 References

1. Acuto O, Michel F (2003) CD28-mediated co-stimulation: a quantitative support for TCR signalling. Nat Rev Immunol 3:939–951

2. Alzheimer C, Averbeck B, Benndorf K (2013) Physiologie: mit 543 Abbildungen und 88 Tabellen. 6. Auflage edition. Elsevier, Urban & Fischer, München

3. Andrés-Delgado L, Antón OM, Alonso MA (2013) Centrosome polarization in T cells: a task for formins. Front Immunol 4:191

4. Anikeeva N, Somersalo K, Sims TN, Thomas VK, Dustin ML, Sykulev Y (2005) Distinct role of lymphocyte function-associated antigen-1 in mediating effective cytolytic activity by cytotoxic T lymphocytes. Proc Natl Acad Sci USA 102:6437–6442

5. Beal AM, Anikeeva N, Varma R, Cameron TO, Vasiliver-Shamis G, Norris PJ, Dustin ML, Sykulev Y (2009) Kinetics of early T cell receptor signaling regulate the pathway of lytic granule delivery to the secretory domain. Immunity 31:632–642

6. Blott EJ, Griffiths GM (2002) Secretory lysosomes. Nat Rev Mol Cell Biol 3:122–131

7. Boucrot E, Ferreira APA, Almeida-Souza L, Debard S, Vallis Y, Howard G, Bertot L, Sauvonnet N, McMahon HT (2015) Endophilin marks and controls a clathrin-independent endocytic pathway. Nature 517:460–465

8. Boyman O, Sprent J (2012) The role of interleukin-2 during homeostasis and activation of the immune system. Nat Rev Immunol 12:180–190

9. Bucci C, Parton RG, Mather IH, Stunnenberg H, Simons K, Hoflack B, Zerial M (1992) The small GTPase rab5 functions as a regulatory factor in the early endocytic pathway. Cell 70:715–728

10. Calabia-Linares C, Robles-Valero J, de la Fuente H, Perez-Martinez M, Martín-Cofreces N, Alfonso-Pérez M, Gutierrez-Vázquez C, Mittelbrunn M, Ibiza S, Urbano-Olmos FR, Aguado-Ballano C, Sánchez-Sorzano CO, Sanchez-Madrid F, Veiga E (2011) Endosomal clathrin drives actin accumulation at the immunological synapse. J Cell Sci 124:820–830

11. Campi G, Varma R, Dustin ML (2005) Actin and agonist MHC-peptide complex-dependent T cell receptor microclusters as scaffolds for signaling. J Exp Med 202:1031–1036

12. Cantrell DA (2002) T-cell antigen receptor signal transduction. Immunology 105:369–374

13. Chang H-F, Bzeih H, Schirra C, Chitirala P, Halimani M, Cordat E, Krause E, Rettig J, Pattu V (2016) Endocytosis of Cytotoxic Granules Is Essential for Multiple Killing of Target Cells by T Lymphocytes. J Immunol 197:2473–2484

14. Chang H-F, Bzeih H, Chitirala P, Ravichandran K, Sleiman M, Krause E, Hahn U, Pattu V, Rettig J (2017) Preparing the lethal hit: interplay between exo- and endocytic pathways in cytotoxic T lymphocytes. Cell Mol Life Sci 74:399–408

15. Chang H-F, Mannebach S, Beck A, Ravichandran K, Krause E, Frohnweiler K, Fecher-Trost C, Schirra C, Pattu V, Flockerzi V, Rettig J (2018) Cytotoxic granule endocytosis depends on the Flower protein. J Cell Biol 217:667–683

16. Chitirala P, Ravichandran K, Galgano D, Sleiman M, Krause E, Bryceson YT, Rettig J (2019) Cytotoxic Granule Exocytosis From Human Cytotoxic T Lymphocytes Is Mediated by VAMP7. Front Immunol 10:1855

17. Christoforidis S, McBride HM, Burgoyne RD, Zerial M (1999) The Rab5 effector EEA1 is a core component of endosome docking. Nature 397:621–625

18. Combs J, Kim SJ, Tan S, Ligon LA, Holzbaur ELF, Kuhn J, Poenie M (2006) Recruitment of dynein to the Jurkat immunological synapse. Proc Natl Acad Sci USA 103:14883–14888

19. Das V, Nal B, Dujeancourt A, Thoulouze M-I, Galli T, Roux P, Dautry-Varsat A, Alcover A (2004) Activation-induced polarized recycling targets T cell antigen receptors to the immunological synapse; involvement of SNARE complexes. Immunity 20:577–588

20. de Saint Basile G, Ménasché G, Fischer A (2010) Molecular mechanisms of biogenesis and exocytosis of cytotoxic granules. Nat Rev Immunol 10:568–579

21. Delprato A, Merithew E, Lambright DG (2004) Structure, exchange determinants, and family-wide rab specificity of the tandem helical bundle and Vps9 domains of Rabex-5. Cell 118:607–617

22. Dhein J, Walczak H, Bäumler C, Debatin KM, Krammer PH (1995) Autocrine T-cell suicide mediated by APO-1/(Fas/CD95). Nature 373:438–441

23. Dudenhöffer-Pfeifer M, Schirra C, Pattu V, Halimani M, Maier-Peuschel M, Marshall MR, Matti U, Becherer U, Dirks J, Jung M, Lipp P, Hoth M, Sester M, Krause E, Rettig J (2013) Different Munc13 isoforms function as priming factors in lytic granule release from murine cytotoxic T lymphocytes. Traffic 14:798–809

24. Fasshauer D, Otto H, Eliason WK, Jahn R, Brünger AT (1997) Structural changes are associated with soluble N-ethylmaleimide-sensitive fusion protein attachment protein receptor complex formation. J Biol Chem 272:28036–28041

25. Ferguson SM, De Camilli P (2012) Dynamin, a membrane-remodelling GTPase. Nat Rev Mol Cell Biol 13:75–88

26. Ford MGJ, Mills IG, Peter BJ, Vallis Y, Praefcke GJK, Evans PR, McMahon HT (2002) Curvature of clathrin-coated pits driven by epsin. Nature 419:361–366

27. Forgac M (1998) Structure, function and regulation of the vacuolar (H+)-ATPases. FEBS Lett 440:258–263

28. Freiberg BA, Kupfer H, Maslanik W, Delli J, Kappler J, Zaller DM, Kupfer A (2002) Staging and resetting T cell activation in SMACs. Nat Immunol 3:911–917

29. Fukuda M (1991) Lysosomal membrane glycoproteins. Structure, biosynthesis, and intracellular trafficking. J Biol Chem 266:21327–21330

30. Futter CE, Pearse A, Hewlett LJ, Hopkins CR (1996) Multivesicular endosomes containing internalized EGF-EGF receptor complexes mature and then fuse directly with lysosomes. J Cell Biol 132:1011–1023

31. Geiger B, Rosen D, Berke G (1982) Spatial relationships of microtubule-organizing centers and the contact area of cytotoxic T lymphocytes and target cells. J Cell Biol 95:137–143

32. Gil D, Schamel WWA, Montoya M, Sánchez-Madrid F, Alarcón B (2002) Recruitment of Nck by CD3 epsilon reveals a ligand-induced conformational change essential for T cell receptor signaling and synapse formation. Cell 109:901–912

33. Gomez TS, Billadeau DD (2008) T cell activation and the cytoskeleton: you can’t have one without the other. Adv Immunol 97:1–64

34. Gorman JA, Babich A, Dick CJ, Schoon RA, Koenig A, Gomez TS, Burkhardt JK, Billadeau DD (2012) The cytoskeletal adaptor protein IQGAP1 regulates TCR-mediated signaling and filamentous actin dynamics. J Immunol 188:6135–6144

35. Grakoui A, Bromley SK, Sumen C, Davis MM, Shaw AS, Allen PM, Dustin ML (1999) The immunological synapse: a molecular machine controlling T cell activation. Science 285:221–227

36. Gruenberg J, Stenmark H (2004) The biogenesis of multivesicular endosomes. Nat Rev Mol Cell Biol 5:317–323

37. Hales CM, Vaerman J-P, Goldenring JR (2002) Rab11 family interacting protein 2 associates with Myosin Vb and regulates plasma membrane recycling. J Biol Chem 277:50415–50421

38. Halimani M, Pattu V, Marshall MR, Chang HF, Matti U, Jung M, Becherer U, Krause E, Hoth M, Schwarz EC, Rettig J (2014) Syntaxin11 serves as a t-SNARE for the fusion of lytic granules in human cytotoxic T lymphocytes. Eur J Immunol 44:573–584

39. Han GA, Malintan NT, Saw NMN, Li L, Han L, Meunier FA, Collins BM, Sugita S (2011) Munc18-1 domain-1 controls vesicle docking and secretion by interacting with syntaxin-1 and chaperoning it to the plasma membrane. Mol Biol Cell 22:4134–4149

40. Hanson PI, Roth R, Morisaki H, Jahn R, Heuser JE (1997) Structure and conformational changes in NSF and its membrane receptor complexes visualized by quick-freeze/deep-etch electron microscopy. Cell 90:523–535

41. Harata NC, Aravanis AM, Tsien RW (2006) Kiss-and-run and full-collapse fusion as modes of exo-endocytosis in neurosecretion. J Neurochem 97:1546–1570

42. Harris DT, Kranz DM (2016) Adoptive T Cell Therapies: A Comparison of T Cell Receptors and Chimeric Antigen Receptors. Trends Pharmacol Sci 37:220–230

43. Hashimoto M, Kamphorst AO, Im SJ, Kissick HT, Pillai RN, Ramalingam SS, Araki K, Ahmed R (2018) CD8 T Cell Exhaustion in Chronic Infection and Cancer: Opportunities for Interventions. Annu Rev Med 69:301–318

44. He L, Xue L, Xu J, McNeil BD, Bai L, Melicoff E, Adachi R, Wu L-G (2009) Compound vesicle fusion increases quantal size and potentiates synaptic transmission. Nature 459:93–97

45. He Q-F, Xu Y, Li J, Huang Z-M, Li X-H, Wang X (2019) CD8+ T-cell exhaustion in cancer: mechanisms and new area for cancer immunotherapy. Brief Funct Genomics 18:99–106

46. Heuser JE, Reese TS (1981) Structural changes after transmitter release at the frog neuromuscular junction. J Cell Biol 88:564–580

47. Huotari J, Helenius A (2011) Endosome maturation. EMBO J 30:3481–3500

48. Huppa JB, Gleimer M, Sumen C, Davis MM (2003) Continuous T cell receptor signaling required for synapse maintenance and full effector potential. Nat Immunol 4:749–755

49. Jahn R, Scheller RH (2006) SNAREs--engines for membrane fusion. Nat Rev Mol Cell Biol 7:631–643

50. Jaiswal JK, Rivera VM, Simon SM (2009) Exocytosis of post-Golgi vesicles is regulated by components of the endocytic machinery. Cell 137:1308–1319

51. Jenkins MR, Tsun A, Stinchcombe JC, Griffiths GM (2009) The strength of T cell receptor signal controls the polarization of cytotoxic machinery to the immunological synapse. Immunity 31:621–631

52. Kane LP, Lin J, Weiss A (2000) Signal transduction by the TCR for antigen. Curr Opin Immunol 12:242–249

53. Kataoka T, Takaku K, Magae J, Shinohara N, Takayama H, Kondo S, Nagai K (1994) Acidification is essential for maintaining the structure and function of lytic granules of CTL. Effect of concanamycin A, an inhibitor of vacuolar type H(+)-ATPase, on CTL-mediated cytotoxicity. J Immunol 153:3938–3947

54. Kelly BT, Graham SC, Liska N, Dannhauser PN, Höning S, Ungewickell EJ, Owen DJ (2014) Clathrin adaptors. AP2 controls clathrin polymerization with a membrane-activated switch. Science 345:459–463

55. Kirchhausen T, Harrison SC (1981) Protein organization in clathrin trimers. Cell 23:755–761

56. Kirchhausen T, Owen D, Harrison SC (2014) Molecular structure, function, and dynamics of clathrin-mediated membrane traffic. Cold Spring Harb Perspect Biol 6:a016725

57. Koretzky GA, Abtahian F, Silverman MA (2006) SLP76 and SLP65: complex regulation of signalling in lymphocytes and beyond. Nat Rev Immunol 6:67–78

58. Kurisu S, Takenawa T (2009) The WASP and WAVE family proteins. Genome Biol 10:226

59. Lafourcade C, Sobo K, Kieffer-Jaquinod S, Garin J, van der Goot FG (2008) Regulation of the V-ATPase along the endocytic pathway occurs through reversible subunit association and membrane localization. PLoS ONE 3:e2758

60. Le Floc'h A, Tanaka Y, Bantilan NS, Voisinne G, Altan-Bonnet G, Fukui Y, Huse M (2013) Annular PIP3 accumulation controls actin architecture and modulates cytotoxicity at the immunological synapse. J Exp Med 210:2721–2737

61. Le Roy C, Wrana JL (2005) Clathrin- and non-clathrin-mediated endocytic regulation of cell signalling. Nat Rev Mol Cell Biol 6:112–126

62. Lin RC, Scheller RH (1997) Structural organization of the synaptic exocytosis core complex. Neuron 19:1087–1094

63. Luzio JP, Gray SR, Bright NA (2010) Endosome-lysosome fusion. Biochem Soc Trans 38:1413–1416

64. Malek TR, Bayer AL (2004) Tolerance, not immunity, crucially depends on IL-2. Nat Rev Immunol 4:665–674

65. Martina JA, Wu XS, Catalfamo M, Sakamoto T, Yi C, Hammer JA (2011) Imaging of lytic granule exocytosis in CD8+ cytotoxic T lymphocytes reveals a modified form of full fusion. Cell Immunol 271:267–279

66. Masson D, Tschopp J (1987) A family of serine esterases in lytic granules of cytolytic T lymphocytes. Cell 49:679–685

67. Matti U, Pattu V, Halimani M, Schirra C, Krause E, Liu Y, Weins L, Chang HF, Guzman R, Olausson J, Freichel M, Schmitz F, Pasche M, Becherer U, Bruns D, Rettig J (2013) Synaptobrevin2 is the v-SNARE required for cytotoxic T-lymphocyte lytic granule fusion. Nat Commun 4:1439

68. Maxfield FR, Yamashiro DJ (1987) Endosome acidification and the pathways of receptor-mediated endocytosis. Adv Exp Med Biol 225:189–198

69. Maxfield FR, McGraw TE (2004) Endocytic recycling. Nat Rev Mol Cell Biol 5:121–132

70. Mayor S, Presley JF, Maxfield FR (1993) Sorting of membrane components from endosomes and subsequent recycling to the cell surface occurs by a bulk flow process. J Cell Biol 121:1257–1269

71. McMahon HT, Boucrot E (2011) Molecular mechanism and physiological functions of clathrin-mediated endocytosis. Nat Rev Mol Cell Biol 12:517–533

72. Monks CR, Freiberg BA, Kupfer H, Sciaky N, Kupfer A (1998) Three-dimensional segregation of supramolecular activation clusters in T cells. Nature 395:82–86

73. Murk JL a. N, Humbel BM, Ziese U, Griffith JM, Posthuma G, Slot JW, Koster AJ, Verkleij AJ, Geuze HJ, Kleijmeer MJ (2003) Endosomal compartmentalization in three dimensions: implications for membrane fusion. Proc Natl Acad Sci USA 100:13332–13337

74. Myers LM, Tal MC, Torrez Dulgeroff LB, Carmody AB, Messer RJ, Gulati G, Yiu YY, Staron MM, Angel CL, Sinha R, Markovic M, Pham EA, Fram B, Ahmed A, Newman AM, Glenn JS, Davis MM, Kaech SM, Weissman IL, Hasenkrug KJ (2019) A functional subset of CD8+ T cells during chronic exhaustion is defined by SIRPα expression. Nat Commun 10:794

75. Oh-hora M, Rao A (2008) Calcium signaling in lymphocytes. Curr Opin Immunol 20:250–258

76. Okkenhaug K, Ali K, Vanhaesebroeck B (2007) Antigen receptor signalling: a distinctive role for the p110delta isoform of PI3K. Trends Immunol 28:80–87

77. Ou-Yang C, Zhu M, Fuller DM, Sullivan SA, Chuck MI, Ogden S, Li Q-J, Zhang W (2012) Role of LAT in the granule-mediated cytotoxicity of CD8 T cells. Mol Cell Biol 32:2674–2684

78. Pearse BM (1987) Clathrin and coated vesicles. EMBO J 6:2507–2512

79. Peters PJ, Geuze HJ, Van der Donk HA, Slot JW, Griffith JM, Stam NJ, Clevers HC, Borst J (1989) Molecules relevant for T cell-target cell interaction are present in cytolytic granules of human T lymphocytes. Eur J Immunol 19:1469–1475

80. Peters PJ, Borst J, Oorschot V, Fukuda M, Krähenbühl O, Tschopp J, Slot JW, Geuze HJ (1991) Cytotoxic T lymphocyte granules are secretory lysosomes, containing both perforin and granzymes. J Exp Med 173:1099–1109

81. Piper RC, Katzmann DJ (2007) Biogenesis and function of multivesicular bodies. Annu Rev Cell Dev Biol 23:519–547

82. Podack ER, Hengartner H (1989) Structure of perforin and its role in cytolysis. Year Immunol 6:245–261

83. Potter TA, Grebe K, Freiberg B, Kupfer A (2001) Formation of supramolecular activation clusters on fresh ex vivo CD8+ T cells after engagement of the T cell antigen receptor and CD8 by antigen-presenting cells. Proc Natl Acad Sci USA 98:12624–12629

84. Riedl J, Crevenna AH, Kessenbrock K, Yu JH, Neukirchen D, Bista M, Bradke F, Jenne D, Holak TA, Werb Z, Sixt M, Wedlich-Soldner R (2008) Lifeact: a versatile marker to visualize F-actin. Nat Methods 5:605–607

85. Rink J, Ghigo E, Kalaidzidis Y, Zerial M (2005) Rab conversion as a mechanism of progression from early to late endosomes. Cell 122:735–749

86. Ritter AT, Angus KL, Griffiths GM (2013) The role of the cytoskeleton at the immunological synapse. Immunol Rev 256:107–117

87. Ritter AT, Asano Y, Stinchcombe JC, Dieckmann NMG, Chen B-C, Gawden-Bone C, van Engelenburg S, Legant W, Gao L, Davidson MW, Betzig E, Lippincott-Schwartz J, Griffiths GM (2015) Actin depletion initiates events leading to granule secretion at the immunological synapse. Immunity 42:864–876

88. Rizo J, Südhof TC (2002) Snares and Munc18 in synaptic vesicle fusion. Nat Rev Neurosci 3:641–653

89. Ross SH, Cantrell DA (2018) Signaling and Function of Interleukin-2 in T Lymphocytes. Annu Rev Immunol 36:411–433

90. Ryser JE, Rungger-Brändle E, Chaponnier C, Gabbiani G, Vassalli P (1982) The area of attachment of cytotoxic T lymphocytes to their target cells shows high motility and polarization of actin, but not myosin. J Immunol 128:1159–1162

91. Sassa T, Harada S, Ogawa H, Rand JB, Maruyama IN, Hosono R (1999) Regulation of the UNC-18-Caenorhabditis elegans syntaxin complex by UNC-13. J Neurosci 19:4772–4777

92. Shi L, Mai S, Israels S, Browne K, Trapani JA, Greenberg AH (1997) Granzyme B (GraB) autonomously crosses the cell membrane and perforin initiates apoptosis and GraB nuclear localization. J Exp Med 185:855–866

93. Söllner T, Whiteheart SW, Brunner M, Erdjument-Bromage H, Geromanos S, Tempst P, Rothman JE (1993) SNAP receptors implicated in vesicle targeting and fusion. Nature 362:318–324

94. Sørensen JB, Wiederhold K, Müller EM, Milosevic I, Nagy G, de Groot BL, Grubmüller H, Fasshauer D (2006) Sequential N- to C-terminal SNARE complex assembly drives priming and fusion of secretory vesicles. EMBO J 25:955–966

95. Stinchcombe JC, Bossi G, Booth S, Griffiths GM (2001) The immunological synapse of CTL contains a secretory domain and membrane bridges. Immunity 15:751–761

96. Stinchcombe JC, Majorovits E, Bossi G, Fuller S, Griffiths GM (2006) Centrosome polarization delivers secretory granules to the immunological synapse. Nature 443:462–465

97. Szymczak AL, Workman CJ, Gil D, Dilioglou S, Vignali KM, Palmer E, Vignali DAA (2005) The CD3epsilon proline-rich sequence, and its interaction with Nck, is not required for T cell development and function. J Immunol 175:270–275

98. van der Bliek AM, Meyerowitz EM (1991) Dynamin-like protein encoded by the Drosophila shibire gene associated with vesicular traffic. Nature 351:411–414

99. Vanlandingham PA, Barmchi MP, Royer S, Green R, Bao H, Reist N, Zhang B (2014) AP180 couples protein retrieval to clathrin-mediated endocytosis of synaptic vesicles. Traffic 15:433–450

100. Varma R, Campi G, Yokosuka T, Saito T, Dustin ML (2006) T cell receptor-proximal signals are sustained in peripheral microclusters and terminated in the central supramolecular activation cluster. Immunity 25:117–127

101. Wang C-T, Lu J-C, Bai J, Chang PY, Martin TFJ, Chapman ER, Jackson MB (2003) Different domains of synaptotagmin control the choice between kiss-and-run and full fusion. Nature 424:943–947

102. Watanabe S, Boucrot E (2017) Fast and ultrafast endocytosis. Curr Opin Cell Biol 47:64–71

103. Waterhouse NJ, Sedelies KA, Clarke CJ (2004) Granzyme B; the chalk-mark of a cytotoxic lymphocyte. J Transl Med 2:36

104. Wu L-G, Hamid E, Shin W, Chiang H-C (2014) Exocytosis and endocytosis: modes, functions, and coupling mechanisms. Annu Rev Physiol 76:301–331

105. Wu X-S, Wu L-G (2009) Rapid endocytosis does not recycle vesicles within the readily releasable pool. J Neurosci 29:11038–11042

106. Wucherpfennig KW, Gagnon E, Call MJ, Huseby ES, Call ME (2010) Structural biology of the T-cell receptor: insights into receptor assembly, ligand recognition, and initiation of signaling. Cold Spring Harb Perspect Biol 2:a005140

107. Yamashiro DJ, Tycko B, Fluss SR, Maxfield FR (1984) Segregation of transferrin to a mildly acidic (pH 6.5) para-Golgi compartment in the recycling pathway. Cell 37:789–800

108. Yamashiro DJ, Maxfield FR (1987) Acidification of morphologically distinct endosomes in mutant and wild-type Chinese hamster ovary cells. J Cell Biol 105:2723–2733

109. Zhou X, Friedmann KS, Lyrmann H, Zhou Y, Schoppmeyer R, Knörck A, Mang S, Hoxha C, Angenendt A, Backes CS, Mangerich C, Zhao R, Cappello S, Schwär G, Hässig C, Neef M, Bufe B, Zufall F, Kruse K, Niemeyer BA, Lis A, Qu B, Kummerow C, Schwarz EC, Hoth M (2018) A calcium optimum for cytotoxic T lymphocyte and natural killer cell cytotoxicity. J Physiol (Lond) 596:2681–2698

8 Acknowledgements

First of all, I would like to give my deepest gratitude to Prof. Dr. Jens Rettig for guidance and a lot of support during the years of my medical doctor thesis.

I want to extend my thanks to Dr. Varsha Pattu for the great idea of my thesis work. I would further like to give many thanks to PD Dr. Ute Becherer for her outstanding help with any problem. I appreciate the help of PD Dr. Elmar Krause and Dr. David Stevens for much input in my projects. My essential thanks go to the technicians for excellent technical support Margarete Klose, Tamara Paul, Anja Ludes and Katrin Sandmeier. Further thanks to Praneeth Chitirala, who generated some of my DNA constructs and the primers for the Granzyme B mTFP knock-in mouse and Paloma Marzlow, Ruth Juraschitz, Keerthana Chitirala and Lukas Knobe for helpful discussions in the lab about science.

I also sincerely appreciate the „Studienstiftung des Deutschen Volkes“ for their help as I am receiving a scholarship of them.

I thank my mum, my dad, my grandmother, Egbert, Maximilian and my friends for their support and Michelle, thank you for everything.

In May 2019 I presented the results of this study at the Symposium on “Hemophagocytic lymphohistiocytosis” in Paris at the institute “imagine“ (Institut des Maladies Génétiques).

9 Publication

Estl M, Blatt P, Li X, Becherer U, Chang HF, Rettig J, Pattu V. Various Stages of Immune Synapse Formation Are Differently Dependent on the Strength of the TCR Stimulus. Int J Mol Sci. 2020 Apr 2;21(7):E2475. doi: 10.3390/ijms21072475. PMID: 32252488.